REVIEWS OF TOPICAL PROBLEMS

Nonlinear effects in the ionosphere

Physics – Uspekhi **50** (11) 1091 – 1121 (2007)

REVIEWS OF TOPICAL PROBLEMS PACS numbers: 41.20.Jb, **52.35. – g**, 52.40.Db, **94.20. – y**

Nonlinear effects in the ionosphere*

A V Gurevich

DOI: 10.1070/PU2007v050n11ABEH006212

Contents

Abstract. The review is based on a report presented by the author at the RAS Physical Sciences Division's session in honor of Vitaly L Ginzburg's 90th birthday. It examines the current status of theoretical and experimental research on nonlinear phenomena arising when a powerful radio wave propagates in the ionosphere. The focus is on the modification of the ionosphere under the resonance excitation of natural plasma oscillations by radio waves. The upper-hybrid resonance gives rise to strong upper- and lower-hybrid plasma waves; excites strongly elongated ionospheric irregularities, and induces artificial ionospheric radio emission. Nonlinear processes are found to undergo complete transformation near double resonances, when the upper-hybrid frequency is close to a multiple of the electron gyromagnetic frequency. In the neighborhood of the Langmuir resonance, intense plasma waves and ion-sound waves are excited, electrons are effectively accelerated, and an artificial glow of the ionosphere appears.

A V Gurevich P N Lebedev Physical Institute,
Russian Academy of Sciences,
Leninskii prosp. 53, 119991 Moscow, Russian Federation
Tel. (7-499) 132 64 14. E-mail: alex@lpi.ru

Received 13 June 2007, revised 8 August 2007
Uspekhi Fizicheskikh Nauk **177** (11) 1145 – 1177 (2007)
DOI: 10.3367/UFNr.0177.200711a.1145
Translated by Yu V Morozov; edited by A Radzig

1. Introduction

The ionosphere is the plasma layer in the upper atmosphere at altitudes between 60 and 1000 km (Fig. 1a). Ionospheric plasma is created by solar UV radiation. The plasma layer is as thick as several hundred kilometers. Maximum plasma concentration is reached in the so-called F-layer at an altitude of roughly 300 km. It amounts to approximately 10^6 electrons per cubic centimeter in the daytime but drops to 3×10^5 cm^{-3} at night. The maximum concentration of electrons in the ionosphere depends on the latitude and slightly varies during the 11-year solar activity cycle. The E- and D-layers lying below the F-layer contain only 10^3 cm^{-3} and even 10^2 cm^{-3} electrons. Sometimes, electron concentration and its inhomogeneous structure in the E-layer increase considerably; in such cases, it is referred to as the sporadic E_s-layer. The D-layer exists only in the daytime and disappears at night.

The concentration of the neutral plasma component (i.e., the air) in the ionosphere varies from approximately 10^{16} cm^{-3} at an altitude of 50 – 60 km to 10^9 cm^{-3} at 300 km. It further decreases with altitude, where the plasma gradually approaches the completely ionized state. The

*This review is based on the report under the same title presented at the joint scientific session of the Physical Sciences Division, RAS and the Scientific Council of P N Lebedev Physical Institute celebrating the 90th birthday of Academician V L Ginzburg, October 4, 2006 [see *Phys. Usp.* **50** (5) 529 (2007)]. (*Note by the Editorial Board.*)

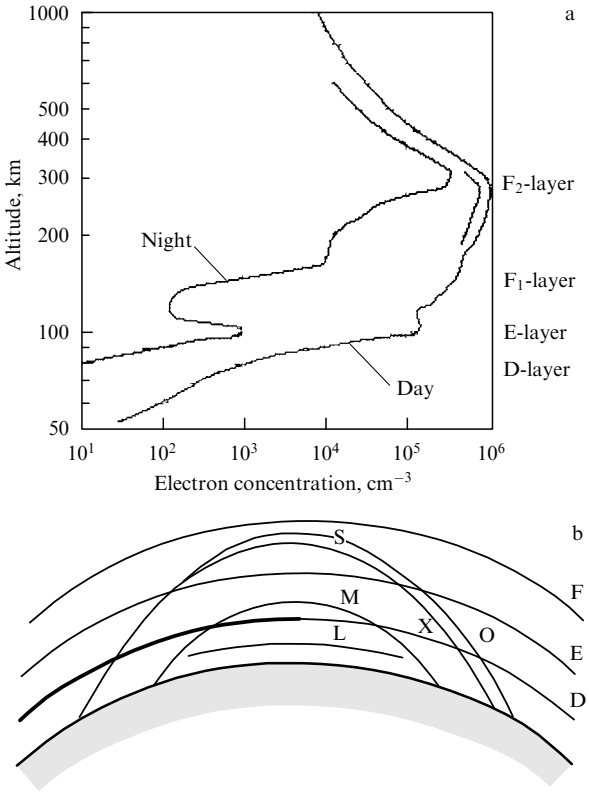

Figure 1. (a) Altitude (z) distribution of ionospheric plasma concentration. Maximum plasma concentration N_{max} occurs in the upper F-layer at $z \approx 300$ km: $N_{max} \approx 10^6$ cm^{-3} in daylight, and $N_{max} \approx 3 \times 10^5$ cm^{-3} at night. The E- and D-layers are located at 60 – 100 km. The lower D-layer (60 – 80 km) exists only in the daytime. (b) Characteristic trajectories of radio wave propagation. O and X are ordinary and extraordinary waves with respect to polarization, respectively; S — short radio waves ($10 \leqslant \lambda < 200$ m, frequency $30 \geqslant f \geqslant 1.5$ MHz, cyclic frequency $2 \times 10^8 \geqslant \omega \geqslant 10^7$ s^{-1}); M — medium radio waves ($200 \leqslant \lambda \leqslant 2000$ m, $1.5 \geqslant f \geqslant 0.15$ MHz, $10^7 \geqslant \omega \geqslant 10^6$ s^{-1}), and L — long radio waves ($2000 \leqslant \lambda \leqslant 20{,}000$ m, $0.15 \geqslant f \geqslant 0.015$ MHz, $10^6 \geqslant \omega \geqslant 10^5$ s^{-1}).

ionosphere smoothly turns into the magnetosphere at altitudes above 1000 km.

The ionosphere is crucial for *radio wave propagation*. Short radio waves reflect from the F-layer (Fig. 1b) and spread over long distances (up to 2 – 3 thousand kilometers) due to a high altitude of the layer. Long and medium radio waves propagate in the E- and D-layers. The anisotropy of ionospheric plasma due to the Earth's magnetic field accounts for the presence of two radio wave components, ordinary (O-mode) and extraordinary (X-mode). This phenomenon is analogous to birefringence of electromagnetic waves in anisotropic crystals [1 – 3].

The absorption of radio waves resulting from collisions between electrons and neutral molecules occurs largely in the low-lying layers (60 – 100 km) where neutral particle concentration is especially high and, consequently, the frequency of electron – neutral collisions is also strongly elevated (Fig. 1b). Absorption sharply decreases during the nighttime by virtue of electron disappearance in the D-layer via recombination.

Nonlinear phenomena. As the electron concentration in the ionosphere is low, rather strong local disturbance of electron distribution becomes possible through a relatively weak impact. It is this fact that underlies experimental physical investigations of ionospheric plasma using radio wave action. Such studies were first undertaken in the USSR in 1961, and in the USA in 1970.

Today, five facilities for this purpose are operated throughout the world, viz. Sura (Vasil'sursk) in Russia; Tromsö (Northern Norway) and SPEAR (Svalbard, Spitsbergen) in Europe, and HAARP and HIPAS (Alaska) in the USA. [1]

There are many broadcasting and other radio stations on the Earth equal to or more powerful than these. The difference is that radio waves emitted by facilities designed to affect the ionosphere are focused almost vertically to enable them to reach the resonance region in the vicinity of electron concentration maximum in the F-layer. Efficiency of radio wave action is due to the coincidence of the disturbing wave frequency and the frequencies of natural plasma oscillations. The result is strong excitation of natural electron plasma oscillations and the development of plasma turbulence responsible for the heating of electron plasma, its structurization, generation of artificial radio emission, electron acceleration, and a number of other interesting physical phenomena in the resonance region.

A remarkable feature of the plasma in a magnetic field is the variety of wave types, as opposed to a single one (acoustic waves) in ordinary liquids and gases. These are

- plasma waves or longitudinal oscillations of the hot electron plasma component;
- ion-acoustic waves or combined longitudinal oscillations of electrons and ions;
- upper-hybrid (UH) plasma waves, i.e., electron oscillations across the magnetic field;
- Bernstein modes related to multiple gyromagnetic resonance,

and other kinds of waves. This diversity accounts for a large number of nonlinear phenomena in the ionospheric plasma, arising from the resonant action of powerful radio waves.

Investigations into physical phenomena in ionospheric plasma affected by radio waves have an almost 40-year history. A large variety of diagnostic tools have been developed to study radio wave-induced plasma disturbances, such as radar sensing systems, multifrequency Doppler measuring complexes, incoherent scattering radars (including the world's most sensitive one at Arecibo), special chambers and telescopes for optical measurements, magnetometers, and other measuring devices. Rockets and artificial satellites are also used to conduct direct observations.

The present publication is designed to overview current studies of the aforementioned problems.

2. Cross modulation

The nonlinear effects of propagating radio waves in ionospheric plasma are apparent even if they are emitted by relatively low-power transmitters.

Cross modulation was the first nonlinear phenomenon discovered by B Tellegen in 1930 [4]. He noticed that the transmission from the powerful Luxembourg radio station could be heard in the background of programs transmitted from other medium-wave stations working at totally different frequencies. Cross modulation is explained by the effect of a powerful radio wave resulting in a slight change in electron

[1] The Sura and Tromsö stations are named after their location; HAARP — High Frequency Active Auroral Research Program; HIPAS — High Power Auroral Simulations, and SPEAR — Space Plasma Exploration by Active Radar.

temperature in the ionosphere on the order of $\Delta T/T \sim 5\,\%$. However, even such a small change affects the electron collision frequency and thereby the absorption intensity of radio waves passing through the perturbed region. Acoustic signals are transmitted when the radio wave amplitude is modulated on the sound frequency $F \sim 1$ kHz. Amplitude modulation of radio waves transmitted by a high-power station on frequency F results in oscillations of electron temperature perturbations ΔT with the same frequency F. In this way, radio waves of other stations, propagating in the perturbed ionospheric region, acquire the modulation with the powerful station via alternating variations of electron temperature ΔT, collision frequency ν_e^F, and absorption rate $\varkappa^F$.

Cross modulation constitutes a nonlinear phenomenon because the waves propagate freely in a linear medium without interfering with one another. In the given instance, it is thermal nonlinearity resulting from electron heating in the powerful wave field. The thermal nonlinearity is realized in the lower part of the ionosphere, i.e., its D- and E-layers. Cross modulation has been the subject of many experimental studies. It is vital to note that as long ago as 1934, Bailey and Martyn [4] elaborated a beautiful elementary kinetic theory fairly well describing the properties of cross modulation. It should be recalled that the ionosphere was poorly known at that time. The theory of Bailey and Martyn not only offered an explanation of the physical nature of this phenomenon but also described in quantitative terms the amplitude and the phase of cross modulation depending on such parameters as modulation frequency, radio frequencies of interacting waves, and (most important) characteristics of ionospheric plasma: electron number density, and collision frequency. The second cross-modulation harmonic was also predicted [6]. All these conjectures were verified by observations and proved an important source of valuable data about the lower ionosphere [7–9]. The complete *kinetic theory* of cross modulation was developed by Ginzburg [10].

Also worthy of note is the Fejer method, which called for studying interactions between very short pulses and thereby localizing the interaction region in order to obtain a more refined information about ionospheric parameters and their altitude distribution [11]. Wave self-action was also described as a change in the wave amplitude under the effect of the wave's own power [12]. It should be emphasized that all nonlinear perturbations were rather small (weak self-action and weak cross modulation). The theory of cross modulation is expounded at greater length in monographs [13, 14].

3. Action of radio waves on the lower ionosphere

3.1 Earlier studies in the USSR

All cross modulation phenomena had the form of weak plasma disturbances in the lower ionosphere. The first attempts to modify the ionosphere by *powerful* radio waves were undertaken in the USSR. It was a completely classified project, even if based on Bailey's ideas. In 1937, Bailey published a work [15] in which he proposed using resonance between a radio wave and electron rotation about a magnetic field with the frequency $f_H = 1.45$ MHz (or cyclic gyromagnetic frequency $\omega_H = 10^7$ rad s^{-1}). Cyclotron acceleration was known to occur when the electric field vector of a radio wave rotated in the same direction as the electrons. Based on this fact, it was hoped to raise the electron energy to some 10–15 eV and thereby to induce a considerable ionospheric glow. It was even suggested using this glow for city lighting.

Bailey proposed obtaining this effect based on relatively low-power stations with $P = 500$ kW and antenna amplification coefficient $G = 100$, so as to reach the effective radiation power $P_{\text{eff}} = PG = 50$ MW. He calculated that such power was sufficient to obtain the above effect, provided a wave reached as high as 130–140 km. This idea was enthusiastically picked up by our Ministry of Communication.[2] They constructed a powerful pulse radio station near Moscow, emitting on a frequency $f = f_H = 1.45$ MHz with a pulse length of 5 ms. Its antenna system guided the wave beam vertically upward to ensure the maximum effect of the electromagnetic field on the ionospheric plasma. The station was commissioned in 1961.[3] Its effective radiation power P_{eff} amounted to 100 MW, i.e., twice that considered sufficient for the purpose by Bailey. Nevertheless, the desired sky glow failed to be obtained. The gifted engineers of the station led by I S Shlyuger noticed that the maximum effect could be obtained by decreasing the pulse length to 0.5 ms. The resultant effective pulse emission power increased 10 times and reached an enormous value of $P_{\text{eff}} = 1$ GW. Even today, such power is unattainable at the existing low-frequency stations. For all that, no appreciable glow could be observed.[4]

The fact is that such a powerful wave experiences so-called self-action. In other words, the high collision frequency of strongly heated electrons in the lower ionosphere (60–80 km) leads to intense self-absorption of the wave under the effect of its own field. As a result, powerful waves do not reach the upper layers (110–140 km). Nonlinear absorption in these experiments was estimated at 30 dB (based on later measurements) — that is, the wave power decreased almost 1000-fold as a result of self-absorption (Fig. 2a, b). A number of additional strong nonlinear effects were recorded. First, other waves propagating in the disturbed region were totally suppressed, as follows from a 1000-fold decrease in their power instead of weak cross modulation (Fig. 2c). Second, the amplitude modulation pattern was totally altered, with the second harmonic being stronger than the first one. Some other phenomena were also observed. However, the results of this top secret project remained unavailable to interested specialists.

Note that the theory of propagation of intense radio waves in the lower ionosphere was developed by the author of this review in 1956–1958 [17]. The theory predicted a number of strong nonlinear effects. As it later turned out, the predictions by the theory fairly well agreed with nonlinear effects observed at the Moscow station [18]. However, a

[2] One of the deputy ministers bearing the now unpopular Tapuriya surname decided to make use of this phenomenon for city lighting and thereby demonstrate intense activity in his department. The former deputy minister Shlyuger (an equally unpopular surname at that time) undertook to accomplish the task and led the construction of a unique station that required the most painstaking efforts.

[3] An immediate result was a visit by people in civvies with dogs within two hours after the trial finished, who arrested and drived away the leading specialists. The reason was the superhigh-power pulses blocked radio communications, including secret government channels. Fortunately, the arrestees were soon released when found not guilty. Later on, each operation of the station was agreed on in advance with relevant authorities.

[4] Many years later (1978), the optical radiation of the Moscow station was recorded by T G Adeishvili [16] with the help of special photodetectors.

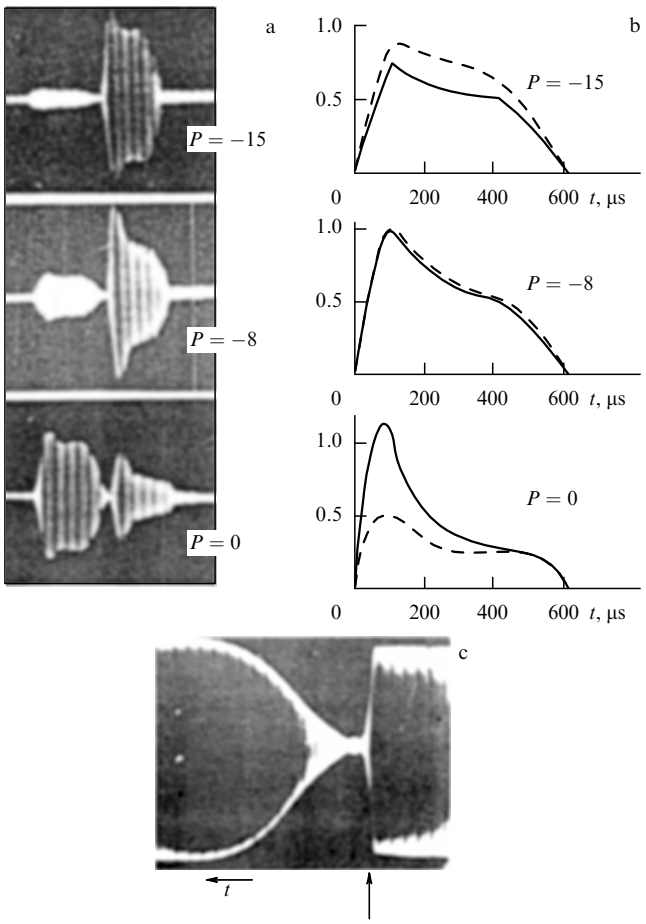

Figure 2. *Strong wave self-action. Nonlinear change in the shape of a strong pulse.* (a) Experimental results. Left: emitted pulse, and right: pulse reflected from the ionosphere (the scale is significantly magnified). Black striations — 100-microsecond time marks; $P = -10\log(W/W_m)$, where W is the emitted pulse power, and $W_m \approx 10^6$ kW. The radio pulse reflected from the ionosphere decays as the power of the emitted pulse increases. (b) Pulse envelope shape: dashed lines — experiment, and solid lines — theory [17, 18]. (c) Disturbance of radio wave envelope ($f = 1.35$ MHz, $\omega = 8.48 \times 10^6$ s^{-1}) by a powerful pulse. Striations — 100-microsecond time marks; pulse length — 500 μs. Onset of the impact is shown by the vertical arrow. Time t runs from right to left. Evidently, the disturbance develops very quickly as a result of the markedly enhanced electron–electron collision frequency in the ionosphere due to a rise in electron temperature T_e. Much slower relaxation depends on the energy loss by heated electrons as they excite rotational levels of air molecules [20].

discussion of these experimental results was out of the question at that time for the reason cited above. One more interesting phenomenon observed at the station is worth mentioning. The passage of a wave through the F-layer resulted in strong self-modulation of the reflected pulse [19]. This effect was probably related not only to direct electron heating by the intense wave field but also to other important physical processes that were later thoroughly examined in F-region modification studies. All these findings remained unknown to the scientific community. The secrecy of priority data obtained in this country at that time explains the lack of demand for them among theorists and experimenters. [5]

[5] The author affiliated with the laboratory of Ya L Al'pert since 1954 came to know about the works at the Moscow station only in 1973 when its observations were declassified. Most of them were published in 1974–1975 [18–20]. By that time, results of American scientists concerning modification of the ionosphere had been widely known.

3.2 Detection effect

In 1974, physicists at the small Zimenki radio station built in the Nishny Novgorod region under the direction of G G Getmantsev observed propagation of the amplitude envelope of a high-frequency signal, arising from the action of a powerful radio wave on the ionosphere [21]. It was a nonlinear effect of detection in the ionosphere of the amplitude-modulated radio signal with the low frequency F: the high-frequency constituent was filtered out and the wave with the low frequency F propagated freely in the Earth–ionosphere waveguide. This effect was theoretically interpreted by Trakhtengerts and Kotik [22] in 1975. The two authors addressed themselves to the stationary electric current J always flowing in the E-layer of the ionosphere. This current results from the interaction between the solar wind plasma flux and the Earth's magnetosphere. As mentioned above, a powerful radio wave whose amplitude is modulated with the low frequency F induces in the ionosphere fluctuations ΔT^F of electron temperature with the modulation frequency F. Similar to the cross modulation case, these disturbances modulate electron collision frequency ν_e^F and, consequently, conductivity σ_e^F of the ionospheric plasma, thereby giving rise to ionospheric current fluctuations with the frequency F. These fluctuations generate low-frequency radiation observed in the Earth–ionosphere waveguide.

Getmantsev immediately called attention to the fact that ionospheric currents in polar regions are much stronger than elsewhere, especially during magnetic storms. This observation provided a rationale for the establishment of a special radio station near Murmansk in 1976 (headed by I N Kapustin and G G Getmantsev). It was soon shown that the detection effect in the ionosphere was strongly heightened in this region (Fig. 3) [23]. Russian physicists proposed the term 'Getmantsev effect' for this phenomenon. Unfortunately, it had not yet won recognition in the West.

Figure 4 exhibits the observational results on detection effect, obtained by Stubbe and co-workers in 1984–1991 at the Tromsö facility [24]. The figure demonstrates the enormous range of modulation frequencies F, from 10^4 to 10^{-3} Hz, i.e., up to a pulsation period of order 1 min. The effects in a frequency range of some 1 kHz resemble cross modulation; they are represented by the peaks in Fig. 4. The peaks collapse at higher modulation frequencies, $F > 3$ kHz, due to interference effects. They likewise fall with decreasing F in a range of $F < 1$ kHz because the wavelength of generated radio waves becomes comparable to the scale of the Earth–ionosphere channel, hampering generation of such low-frequency radio waves. The so-called Schumann resonances occur in the 1–10 Hz frequency range. A radio wave goes around the Earth in a time inverse to the frequency of 8 Hz. Accordingly, the space between the Earth and the ionosphere functions as a resonator with an eigenfrequency of 8 Hz, which is permanently excited by atmospherics (pulses of radio radiation produced by lightnings). A powerful radio station can also contribute to this excitation. The effects at 10^{-3}–10^{-1} Hz shown in Fig. 4 are produced by a different process, namely, alteration of electron concentration under the effect of the radio station. The point is that the recombination coefficient decreases as electron temperature grows, therefore the ionization/recombination balance in the lower ionosphere is disturbed. Hence, there is an increased plasma concentration [13, 14]. Plasma conductivity increases linearly with electron concentration and thus contributes to the enhancement of modulation currents. An enormous rise

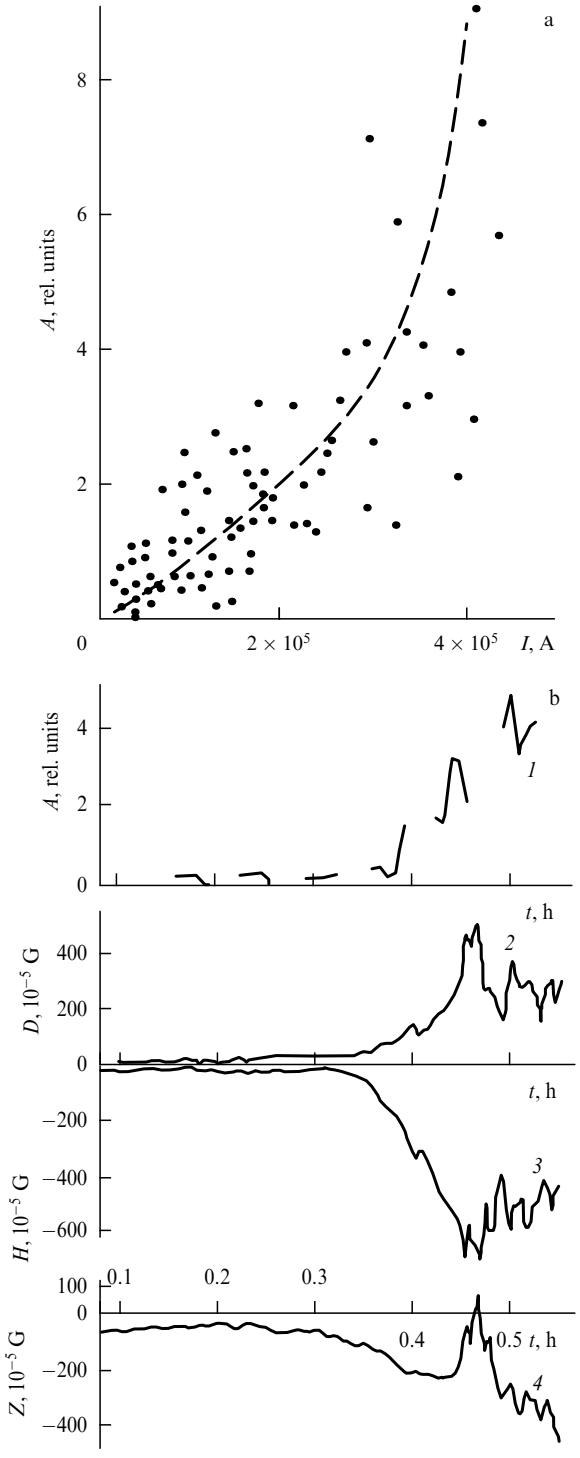

Figure 3. *Detection effect in the polar ionosphere*. (a) Low-frequency radiation amplitude A plotted versus ionospheric current strength I in the auroral jet. The powerful ($P \approx 110$ kW) radio station transmitted at a frequency of $f = 3$ MHz ($\omega \approx 1.9 \times 10^7$ s^{-1}), its antenna had the amplification coefficient $G = 100$; effective power of the disturbing wave was $PG = 10$ MW. Modulation frequency $F = 2.5$ kHz, and modulation depth $\mu = 0.6$. Auroral electrojet current has a maximum at an altitude of 110–130 km. (b) An example of abruptly enhanced low-frequency signal amplitude with a rise in the ionospheric current during a magnetic storm. The powerful station was programmed to switch on and off every 2 min: *1* — amplitude A of the low-frequency signal, *2–4* — variations of disturbance components of the Earth's magnetic field with the time t (Kapustin et al. [23]).

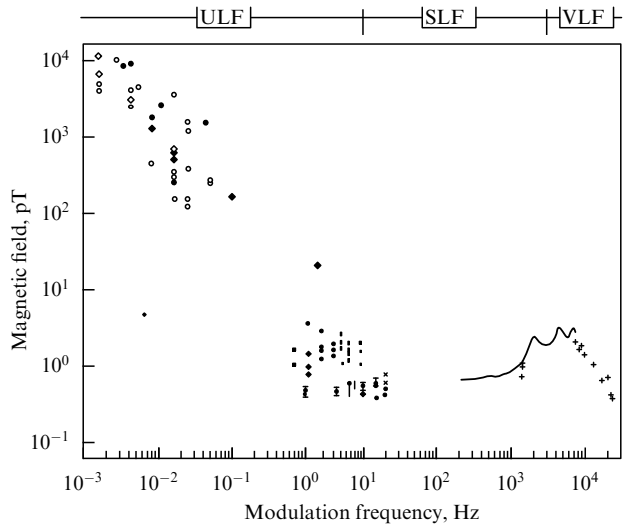

Figure 4. *Detection effect*. Summarized data: amplitudes of the detected signal measured at the Tromsö station (Barr, Stubbe, 1991).

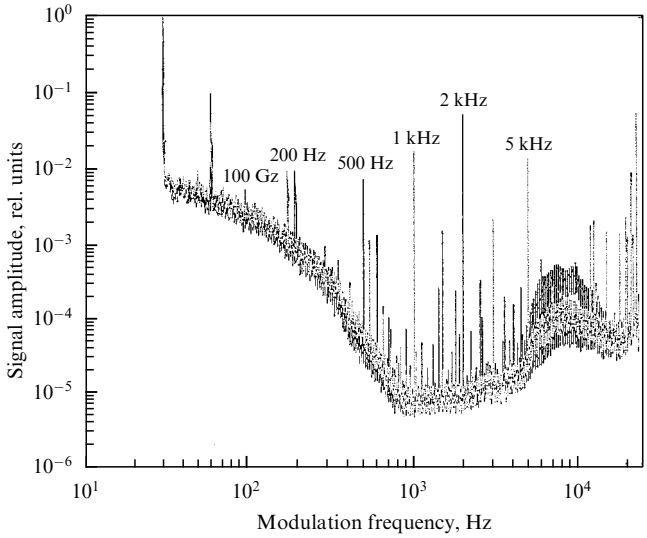

Figure 5. *Underground penetration of low-frequency radio waves generated by ionospheric detection*. Experiments were conducted in Alaska. Ionospheric disturbances were induced by the HIPAS station (see Fig. 8). Disturbing wave frequency was 2.85 MHz, transmitter effective power $PG \approx 80$ MW. Modulation frequency F ranged from 30 Hz to 20 kHz, modulation depth $\mu \approx 100\%$. Field amplitude of the detected ionospheric wave with frequency F was measured in a 20–25-meter deep underground tunnel 40 km from the transmitter. On the ordinate the signal amplitude inside the tunnel is plotted. The results and their comparison with the theory indicate that the detected signals produced by the more powerful HAARP station can be recorded under water several thousand kilometers apart (see Papadopoulos et al. *RF Ionosphere Interactions Workshop*, v. 1, p. 400, Santa Fe, 2001).

in these currents (almost linear or even quadratic) with decreasing modulation frequency F is illustrated in Fig. 4. The maximum amplitude of artificial magnetic-field disturbances amounts to $10\,\gamma$; it is especially high when the Earth's magnetic field is disturbed by magnetic storms (a moderate storm is associated with disturbances of the order of $100\,\gamma$, where $\gamma = 10^{-5}$ G $= 1$ nT). Certainly, these observations apply to magnetic disturbances at the Earth's surface.

It is known, however, that low-frequency electromagnetic radiation readily penetrates underground and underwater. By way of example, Fig. 5 demonstrates underground penetra-

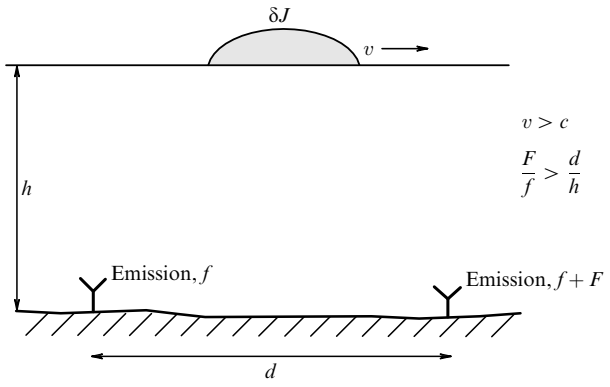

Figure 6. Superlight motion of current disturbance δJ in the current-carrying ionospheric layer (schematic of experiment [25]).

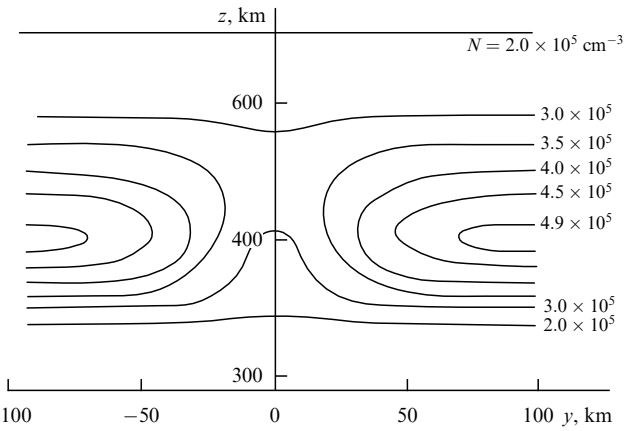

Figure 7. *Disturbance of ionospheric F-layer* (*theory*). Coordinate z — altitude, y — distance from the disturbing beam, and $N(z)$ — plasma number density; undisturbed ionosphere is flat-stratified. Maximum number density, $N_{\max} = 5 \times 10^5$ cm^{-3}, occurs in the undisturbed layer (night-time ionosphere) at $z \approx 400$ km. Emission by the ionospheric modification station with power $W = 200$ kW and frequency $f = 6$ MHz is guided vertically with an angular half-width of 6°. Effective emission power $PG \approx 40$ MW. Radio wave absorption in the lower layers of the night-time ionosphere is assumed to be absent. Electron heating in the powerful wave field results in a drop in plasma concentration near the layer's absorption maximum. The quasineutral plasma (electrons and ions) is forced out of the heated region. The curves depict steady distribution of a disturbed plasma. The powerful wave behaves as if it punches a 'hole' in the F-layer [27].

tion of radio waves observed in relevant experiments at the HIPAS facility in Alaska.

3.3 Superlight motion

The effect of superlight motion was also described for the first time by physicists (L F Mironenko and co-workers) based in the city of Gorky (now Nizhny Novgorod) (Fig. 6, Ref. [25]). Let us consider two high-power transmitters located at distance d from each other. If one of them emits waves of frequency f and the other emits waves of shifted frequency $f + F$, the interference picture will tend to move in the ionosphere with a speed depending on the frequency difference F and the ratio of scale d to a distance h between the Earth and the ionosphere (see Fig. 6). When the characteristic distance between the transmitters is $d = 200$ m and $h = 100$ km, a frequency shift $F > 0.01 f$ is sufficient for the interference picture to travel with speed v higher than the speed of light.

Because powerful radio waves give rise to the ionospheric current disturbance δJ, this latter could be expected to spread in the interference region with a superlight speed and thereby generate Cherenkov radiation. The very first experiments brought about positive results [25]. However, conclusive experimental evidence of Cherenkov radiation generated by ionospheric current disturbances traveling with a superlight speed remains to be found. It should be recalled that V L Ginzburg always showed great interest in superlight motion, emphasizing that a spot of reflected light can move with a superlight speed, and exemplified how such a motion might be achieved. Here, it is not a mere 'speckle' but one that disturbs the medium and generates real waves. However, such an ionospheric experiment is still a long way off.

4. Modification of ionospheric plasma

In the review dated 1960, Ginzburg and Gurevich [26] were the first to point out the possibility of disturbing not only the lower ionosphere but also the F-layer . Later on, this issue was considered in greater detail [27] (Fig. 7). The plenary lecture by the author at the URSI Congress in 1966 was met with keen interest and provoked a lot of comments. The author became aware of the reason for such interest much later: half an year before the URSI Congress, the US Government had decided to change its tracking station of launches of Soviet rockets in the North and offered all its equipment free to the Institute for Telecommunication Sciences in Boulder, Colorado. In this way, the institute found in its possession a great number of transmitters, receivers, and other radio equipment. Naturally, the administration of the institute sought to use the newly acquired equipment to solve an ambitious problem. The lecture provided such a problem.

The *Platteville* station near Boulder was built under the supervision of W Utlaut, Director of the Institute, and commissioned at the end of 1969. The first series of its reports appeared in *J. Geophys. Res.* in 1970 [28]. After a time, it became known that the most important data had been initially classified as secret and published only in 1974 [29].

Many new interesting nonlinear effects were observed. Therefore, similar studies were continued and are still underway at specialized stations in Russia (Sura), northern Norway (Tromsö), and Alaska (HAARP and HIPAS). Figure 8 shows the location of these facilities. One more, less powerful SPEAR station began to work at Svalbard. Furthermore, the powerful Arecibo station (Puerto Rico) is periodically at work. This station is known to have the world's most powerful incoherent scattering radar/radio telescope used to study in detail some important nonlinear effects. There were more stations, besides those listed in Fig. 8. In the Soviet Union, they were located near Murmansk, Gorky, Khar'kov, and Moscow, as well as in Tadzhikistan. These stations were operated for different periods; some results obtained were presented in Section 3.

4.1 Enhanced field-aligned scattering

One of the first effects recorded by the powerful Platteville station was called 'enhanced field-aligned scattering'. Formally, it allowed hearing at large distances signals of low-intense stations when this powerful facility was switched on. For example, the conversations of taxi drivers through transmitters having several watts of power at 50 MHz could be heard from New York to San Francisco — that is, over

· 1970: Platteville, Colorado
· 1975: Sura, Nizhny Novgorod, Russia
· 1980: Arecibo, Puerto Rico,
Tromsö, Norway; HIPAS, Alaska
· 1995: HAARP, Alaska
· 2003: SPEAR, Svalbard

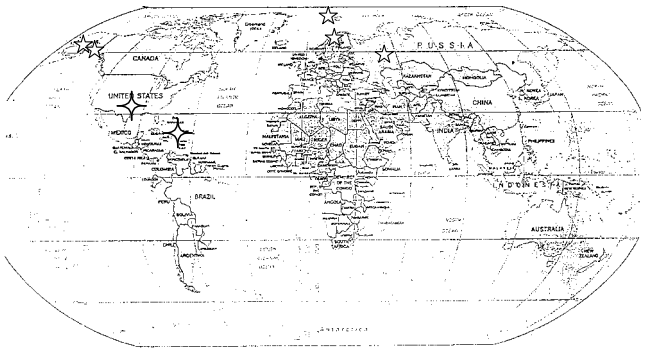

Figure 8. *Ionospheric modification stations*. The ionosphere plays an important role in the Earth's interaction with the flux of solar wind plasma traveling round the magnetosphere. Ionospheric properties vary essentially with latitude (to be precise, with 'geomagnetic' latitude, because the axis of the magnetic dipole responsible for the properties of the magnetosphere is deflected relative to the Earth's rotation axis). This fact accounts for the geographic disposition of ionospheric modification stations designed to study not only modification effects but also ionospheric properties. Thus, Tromsö, HAARP, and HIPAS stations are situated in subarctic regions or in the so-called auroral region, where the effects of magnetosphere–solar wind interactions are especially pronounced. The mid-latitude Sura station lies in the region of relatively quiet ionospheric conditions, whereas the new SPEAR facility occupies a 'polar cap', where the ionosphere adjoins regions directly affected by the solar wind.

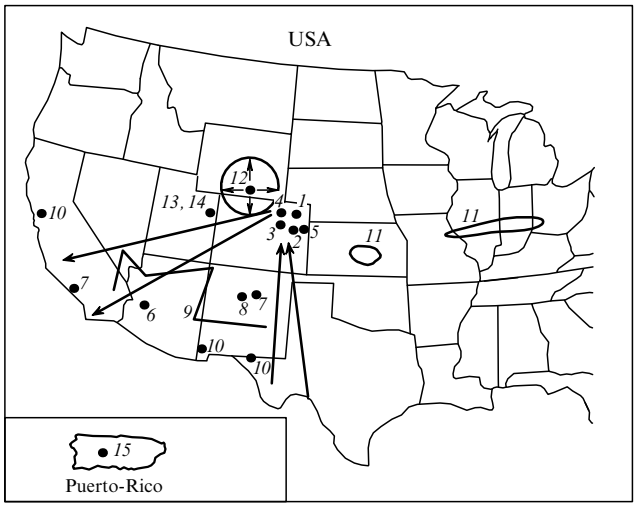

Figure 9. *Experiments on ionospheric modification by radio waves during the 1970–1974 campaign* (black dots — study areas): *1* — J C Carrol, E J Violette, "The Platteville high power facility" [29, p. 889]; *2* — W F Utlaut et al., "Ionosonde observations of ionospheric modification" [29, p. 889], [28, p. 6429]; *3* — M A Biondi et al., "Optical detection ($\lambda = 6300$ Å)" [28, p. 6421]; *4* — R Cohen, J D Whitehead, "Radioreflectivity detection of artificial modification" [28, p. 6439]; *5* — E M Allen et al., "HF phased array observations" [29, p. 905]; *6* — G D Thome, D W Blood, "First of RF backscatters from field-aligned irregularities" [29, p. 917]; *7* — P A Fialer, "Field-aligned scattering at HF and VHF" [29, p. 923]; *8* — J Minkoff et al., "VHF/UHF field-aligned and plasma line blackscatter measurements" [29, p. 941] (large arrows indicate directions of incident radar signals and those scattered by the disturbed ionosphere); *9* — J Minkoff et al., "Radio frequency scattering. Bistatic measurements using airplanes" [29, p. 957] (the zigzag line shows the plane's flight path); *10* — G B Carpenter, "VHF and UHF bistatic observations (radar frequencies 49.8 MHz, 157.5 MHz, 423.3 MHz, 435 MHz, 1200 MHz)" [29, p. 965]; *11* — V R Frank, "Observations of ion-acoustic wave scattering of long oblique paths" [29, p. 971] (closed loops — areas where scattered signals were recorded from mobile platforms); *12* — S A Bowhill, "Scattering from artificial spread-F. Studies from orbital and geostationary satellites" [29, p. 975] (circle with arrows — probing area); *13* — P B Rao, G D Thome, "Scattering models" [29, p. 987]; *14* — G H Barry, "HF-VHF communications and TV-communications using field-aligned scattering" [29, p. 1025], and *15* — W E Gordon, H C Carlson, "Arecibo heating experiments (incoherent scattering radar, instabilities, plasma line, ionograms, optics, electron heating, etc.)" [29, p. 1041].

thousands of kilometers. Normally, such devices transmit radio signals within sight, i.e., across a few dozen kilometers. Many such cases were documented. All of them implied that radio waves with frequencies much higher than those commonly reflected from the ionosphere propagated over unusually large distances. It looked as if a new ionosphere had been created. The frequency of the reflected waves was as high as 100–150 MHz, i.e., 5–6 times that of waves normally reflected from the ionosphere (Fig. 1b). The impression was that the newly commissioned powerful station provided a novel mode of long-range radio communication. The important practical implications of the new phenomenon attracted major resources to its investigation (Fig. 9). Extensive studies were conducted in 1970–1974.

Figure 10 illustrates field-aligned scattering. It was clear that a large group of strongly elongated field-aligned plasma irregularities existed over Platteville. They can be represented as a set of mirrors aligned strictly along the magnetic field but randomly oriented orthogonally to it. As a result, a radio wave incident on the ionosphere is scattered in the field-orthogonal directions, i.e., it undergoes aspect scattering. Specifically, a radio wave incident on the perturbed region orthogonally to the magnetic field, i.e., at an angle of 90°, scatters in all directions at 90° or along the entire 90° line shown in Fig. 10. Given a transmitting station located at the 88° line, its signal is heard at the 92° line, and vice versa (Fig. 10). This new mode of radio wave propagation through ionosphere was extensively studied in experiment. The cross section of field-aligned scattering turned out to be quite great, suggesting enormous ionospheric disturbances. It can be seen in Fig. 11 that the scattering cross section may be as large as 10^8 m^2, or equivalent to a 100 km^2 area of the reflecting radio wave.

It is worth noting that absorption is virtually absent because the case in point is that of high frequencies. The studies demonstrated the possibility of using field-aligned scattering for a long-range telecast. On the whole, it proved to be a very interesting physical phenomenon, even though it eventually failed to find practical application.

4.2 Phenomena in the modified ionosphere

Comprehensive Platteville studies demonstrated that new phenomena arise only under the effect of a powerful ordinary radio wave (O-wave) propagating in the vertical direction, or close to it. Such phenomena are referred to as '*ionospheric modification*' by powerful radio waves. They continue to be investigated at the aforementioned facilities. The following major phenomena are being observed, besides enhanced field-aligned scattering:

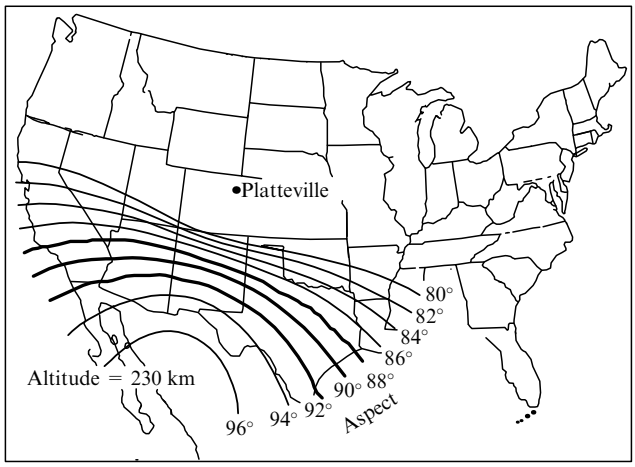

Figure 10. *Field-aligned scattering*. Radio emission of the powerful Platteville station induced a large number of plasma concentration irregularities in the ionosphere over it; they are strongly elongated parallel to the Earth's magnetic field. These irregularities are responsible for the field-aligned scattering of high-frequency radio waves (up to 100 – 150 MHz). The figure shows field-aligned scattering lines. The irregularities are supposed to be located 230 km over Platteville. Radio waves emitted by a high-frequency station situated at a certain place in the 90° line in the scattering region are orthogonal to the irregularities. This means that the waves are scattered along the entire 90° line and their radiation can be observed at any point in the 90° line. Given a station located in the 92° line, its emission is observed in the 88° line, and vice versa. The same refers to lines 94°, 86°, etc. (Fialer [29, p. 923]).

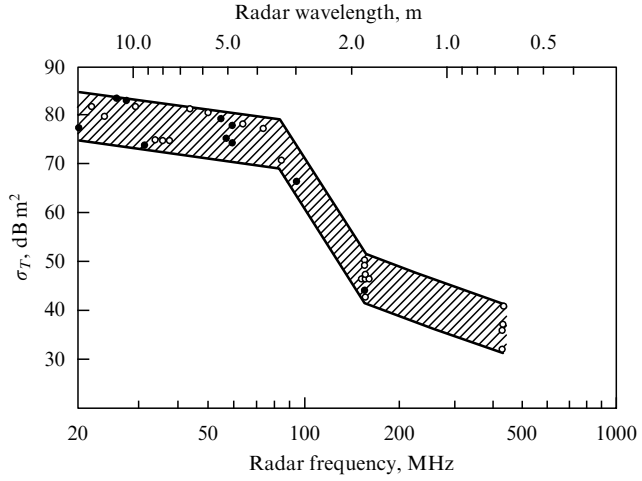

Figure 11. Cross section σ_T of field-aligned scattering as a function of the scattering signal frequency. Circles denote the observed values, the mean cross section is enclosed by lines. The maximum cross section amounts to 80 dB m^2. The cross section slowly diminishes as the frequency increases to ~ 100 MHz (the corresponding radio wavelength ~ 3 m) and then sharply decreases. However, its reduction slows down in the wavelength region below 2 m (Rao, Thome [29, p. 985]).

(1) *Structurization of ionospheric plasma*. Besides strongly elongated plasma irregularities (striations) governing field-aligned scattering and extending up to 10 km parallel to the Earth's magnetic field **B** and 5 – 10 m across it, there are other strong field-aligned irregularities having transverse dimensions from 100 – 200 m (group of striations) to 2 – 5 km (zone of striations). *Self-focusing* of the disturbing wave occurs in these structures. As a result, a powerful wave propagates along the Earth's magnetic field and is focused in the direction of the *magnetic zenith* (MZ).

(2) *Anomalous absorption*. A powerful wave is totally absorbed in the ionosphere (only $\sim 5\%$ is reflected), whereas normally, on the contrary, the night-time self-absorption does not exceed 5% of the total power. To put it otherwise, a drastic change in absorption of the ionosphere-disturbing radio wave occurs.

(3) *Broadband absorption*. There appears very strong absorption of other radio waves in the ionosphere within the 100 – 200 kHz frequency band close to the frequency of the powerful station.

(4) *Stimulated electromagnetic emission* (*SEE*). There appears strong radio emission from a perturbed ionospheric region at frequencies shifted by 100 – 300 kHz relative to the powerful station frequency.

(5) *Excitation of very strong natural oscillations of the ionospheric plasma*. The oscillations are recorded by incoherent scattering radars and other specialized powerful radars used in ionospheric research.

(6) *Effective acceleration of electrons in the ionospheric plasma*. Accelerated electrons are detected by incoherent scattering radars and by direct satellite measurements.

(7) *Strong stimulated optical ionospheric glow*. Glow is observed with the help of special spectroscopes, photodetectors, telescopes, and other photodiagnostic tools.

Ionospheric modification by high-power radio waves largely occurs in the F-layer. Similar phenomena are sometimes seen in the sporadic E_s-layer.

4.3 Physical nature of ionospheric modification

The ionosphere, like any plasma, undergoes natural oscillations and has eigenwaves. Of special interest for our discussion are electron Langmuir oscillations and closely related longitudinal Langmuir waves. The frequency ω_L of these oscillations grows with enhanced plasma density:

$$\omega_L(z_L) = \left(\frac{4\pi e^2 N(z_L)}{m}\right)^{1/2},$$

where e and m are the electron charge and mass, respectively, and $N(z_L)$ is the plasma number density at altitude z_L.

It follows from Fig. 1 that the plasma number density N in the ionosphere grows as altitude z increases to a maximum in the F-layer. The Langmuir frequency is augmented accordingly (Fig. 12). It is important that frequency ω of an ordinary radio wave propagating vertically upward coincides with the *Langmuir frequency* $\omega_L(z_L)$ at the reflection point. The frequency coincidence, $\omega = \omega_L(z_L)$, implies the possibility of *resonance interaction* of a powerful O-wave with natural oscillations and eigenwaves of the ionospheric plasma. It is resonance interaction between a powerful pump wave and natural plasma oscillations that are responsible for the principal features of an F-layer modification.

The Earth's magnetic field **B** has significant influence on the frequency of natural longitudinal oscillations of the ionospheric plasma. When the plasma oscillates along the magnetic field (to be precise, when the strength of the oscillation electric field **E** is oriented along **B**, i.e., $\mathbf{E} \parallel \mathbf{B}$), the eigenfrequency of oscillations coincides with the Langmuir frequency ω_L (see Fig. 12). If electric vector **E** is perpendicular to the magnetic field (i.e., $\mathbf{E} \perp \mathbf{B}$), the egienfrequency of oscillations equals the *upper-hybrid frequency* ω_{UH} (see Fig. 12):

$$\omega_{UH}(z_{UH}) = \left(\frac{4\pi e^2 N(z_{UH})}{m} + \omega_H^2\right)^{1/2},$$

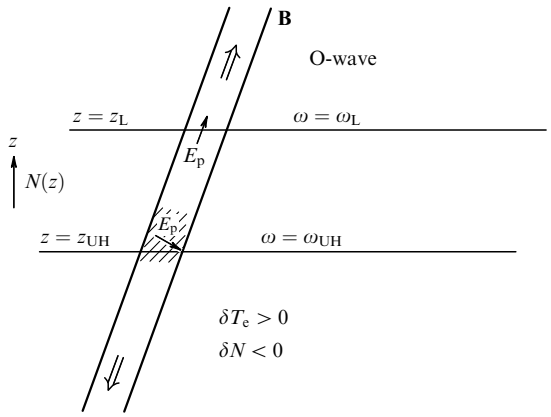

Figure 12. *Plasma resonance region*. At the reflection point, frequency ω of an ordinary (O) radio wave propagating vertically upward coincides with the eigenfrequency of longitudinal Langmuir plasma oscillations: $\omega = \omega_L$. The radio wave electric field $\mathbf{E}(z_L)$ at the reflection point is oriented parallel to the Earth's magnetic field **B**. The strength vector **E** of natural Langmuir plasma oscillations has the same direction. Radio waves are reflected below the F-layer maximum (see Fig. 1), therefore, plasma concentration $N(z)$ grows with altitude z in the vicinity of the reflection point z_L. The ionosphere is assumed to be flat-stratified $[N(z)]$, the Langmuir resonance region $z = z_L$ is shown by a horizontal line. At upper-hybrid resonance ($z = z_{UH}$), the radio wave frequency ω coincides with the UH-frequency: $\omega = \omega_{UH}$. The electric field **E** of UH-fluctuations is perpendicular to **B**. The UH-resonance region (z_{UH}) is depicted by a horizontal line, always lying below the Langmuir resonance. The layer between the resonances is as thick as $\Delta z = z_L - z_{UH} \approx (\omega_H^2/2\omega^2)/(\mathrm{d}N/\mathrm{d}z)$. It was taken into consideration that usually $\omega_L \sim (3-6)\,\omega_H$. Bearing in mind that the characteristic concentration gradient scale in the F-layer is $N/(\mathrm{d}N/\mathrm{d}z) \sim 30-100$ km, one finds $\Delta z \sim 2-10$ km. Note that the location and width of the resonance layer depend on the disturbing wave frequency ω and the number density distribution $N(z)$ in the ionosphere. The resonance regions become much wider near the F-layer maximum ($\mathrm{d}N/\mathrm{d}z \to 0$).

Resonance instability. In the presence of plasma irregularities in the UH-resonance region $z = z_{UH}$, the electric field of a powerful radio wave induces UH-waves. Negative irregularity, $\delta N < 0$, traps the UH-waves, giving rise to a standing wave. Such waves effectively heat electrons, $\delta T_e > 0$, which leads to plasma forcing out and enhances its irregularity. The resulting instability accounts for the appearance of numerous negative irregularities strongly elongated along the Earth's magnetic field. The electron heating zone in the UH-resonance region is shown by hatching; arrows indicate ejected plasma fluxes.

where $\omega_H = eH/mc$ is the gyromagnetic frequency. The difference between ω_L and ω_{UH} is 2–10% at one and the same plasma concentration N. Since ionospheric plasma number density N varies with altitude z, there must be an entire *resonance layer* for a powerful wave with a given frequency ω. This suggests *upper-hybrid resonance*, $\omega = \omega_{UH}(z_{UH})$, at the lower edge of the layer, and *Langmuir resonance*, $\omega = \omega_L(z_L)$, at its upper edge. The thickness of the resonance layer in the ionospheric F-region ranges 2–10 km (see Fig. 12 for details).

It should be emphasized that radio waves are also an eigenmode of the ionospheric plasma, but this mode is transverse. Eigenmodes of a homogeneous plasma are linearly independent. They propagate freely and are unrelated to one another. The resonance relation between modes results from *nonlinear processes*.

The following main features of the nonlinear impact of a powerful radio wave on the upper ionosphere are worth mentioning:

(1) Only an ordinary wave traveling in the vertical direction or close to it reaches resonance regions. An extraordinary wave always reflects below resonances.

(2) The radio wave amplitude significantly increases near the reflection point ([1, Sect. 17]) because the group velocity in the reflection region decreases. The amplitude growth intensifies nonlinear processes.

(3) Excitation of natural longitudinal plasma oscillations prevents electron collisions. Their frequency in the F-layer is very low: $\nu \sim 3 \times 10^2 - 10^3\ \mathrm{s}^{-1}$, i.e., many orders of magnitude smaller than the oscillation eigenfrequency $\omega_L \sim 10^7 - 3 \times 10^7\ \mathrm{s}^{-1}$, i.e., $\nu/\omega_L \approx 10^{-4} - 10^{-5}$. This makes possible intense nonlinear excitation of plasma eigenwaves by the action of pump waves.

(4) Moreover, collisional losses being small, there is the possibility of realizing a number of nonlinear interaction processes, mutual transformation of plasma waves, excitation of turbulence spectra, creation of plasma structures, and electron acceleration. Hence, there is a wide spectrum of physical phenomena associated with ionospheric modification.

5. Nonlinear effects at upper-hybrid resonance

5.1 Resonance instability

The moderate collision frequency in the F-layer is the source of one more important plasma property in the upper ionosphere. The point is that transport processes, such as diffusion and heat conductivity, strongly depend in magnetized plasma on the ratio of electron collision frequency ν to gyromagnetic frequency ω_H of their rotation. This ratio is very small in the F-layer: $\nu/\omega_H \sim 3 \times 10^{-5} - 10^{-4}$. As a result, particle and heat transfers along the magnetic field are several orders of magnitude greater than their transverse transport. In other words, longitudinal transport processes are rather strong. By this is also meant that any initial density or temperature disturbances tend to rapidly turn into strongly prolate field-aligned irregularities.

Imagine that such plasma irregularity occurs in the UH-resonance region for a radio wave emitted by a high-power station to modify the ionosphere. In other words, let $\omega = \omega_{UH}$, where ω is the radio wave frequency, and ω_{UH} is the UH-resonance frequency. What this means is that the powerful wave can excite upper-hybrid plasma waves. The excitation efficiency of plasma waves is proportional to the plasma concentration gradient $|\nabla N|$. Irregularities being strongly elongated along magnetic field **B**, the maximum concentration gradient $(\nabla N)_{max}$ is orthogonal to **B**. Therefore, a powerful wave most effectively pumps at UH-resonance upper-hybrid plasma waves with the wave vector $\mathbf{k} \parallel (\nabla N)_{max}$. These waves propagate orthogonally to the magnetic field, i.e., perpendicular to the axis of irregularity. In the case of a reduced plasma density, $\delta N < 0$ (see Fig. 12), they are trapped by irregularities and give rise to a standing UH-wave.

Collisions result in absorption of the UH-wave energy, leading to a rise in electron temperature T_e that in turn causes plasma forcing out, namely, enhances the negative disturbance of the plasma concentration. In this case, the absolute value of the density gradient, $|\nabla N|$, increases. Accordingly, both pumping and trapping of UH-waves by irregularities result in a new rise in T_e, decreased plasma concentration, enhanced wave pumping, etc. In a word, instability evolves

that leads to a rise in electron temperature, strengthening plasma forcing out from irregularities, and increasing the number of UH-waves trapped in them. This instability is termed *resonance instability*. Negative plasma irregularity strongly elongated parallel to the Earth's magnetic field plays the role of a resonator for this instability, in which the powerful radio wave field resonantly pumps UH-waves. The theory of resonance instability was developed in the works by Vas'kov and Gurevich [30] and Mjølhus [31].

Resonance instability explained the appearance of numerous strongly elongated irregularities (striations) in the ionosphere under the effect of a powerful O-wave; this, in turn, results in enhanced field-aligned scattering of radio waves. Processes proceeding in the UH-resonance region turned out important by themselves. Moreover, instability linking the collisionless generation of plasma waves with collisional processes (electron heating and plasma diffusion) was first discovered. Instability of this type arises only in strongly magnetized plasma ($\omega_H \gg \nu$), where the great difference between longitudinal and transverse transport processes exists, and serves as one of the main causes of plasma structurization.

5.2 Kelley's rocket experiment. Structurization of ionospheric plasma

Enhanced field-aligned scattering first observed in Platteville was thoroughly investigated in the 1980s at the Sura facility and other stations [6] in the USSR by Erukhimov et al. [32, 33] and Nasyrov [34], and at Arecibo by Noble and Djuth [35].

Plasma density perturbations were estimated at 1%, the length of irregularities at 1 – 10 km, and the transverse scale at several meters. Insight into their space and time-dependent patterns showed that irregularities tended to transfer with the ionospheric plasma in the case of presence in it drifts due to the action of the external electric field (Bernhardt et al. [36]). As this took place, the irregularities themselves remained stable — the scattering bandwidth was ~ 0.1 Hz.

Still, the scattering data did not produce a complete picture. Conclusive evidence was obtained in the direct rocket experiment performed by Kelley et al. [37] at Arecibo in 1995. Its results are presented in Fig. 13. The rocket crossed the region disturbed by the powerful Arecibo station emitting 5.1-MHz radio waves. The altitude of the reflection region was roughly 268 km. However, irregularities occurred both above and below it, from ~ 255 to 275 km, i.e., they were recorded over a scale height greater than 20 km. All irregularities showed only decreased plasma concentration. It appears from the inset to Fig. 13 that the irregularities were sharp but shallow solitonlike density dips, the depth of which did not exceed 10% of the electron concentration in the ionosphere. The rocket passed through several regions. Striations were practically absent in some of them but strongly manifested themselves in others. Data analysis revealed their stationary nature. They had a characteristic transverse dimension of 7 – 10 m, were clustered into groups with a transverse size of 100 – 200 m, and formed still larger zones with a radius of 1 – 3 km.

[6] Note that field-aligned scattering is observable on the Earth only at middle and low latitudes. The possibility of seeing it is determined by the tilt of the Earth's magnetic field **B**. The direction of **B** in high latitudes is close to vertical, so that high-frequency radio waves emitted from the Earth do not come back after field-aligned scattering.

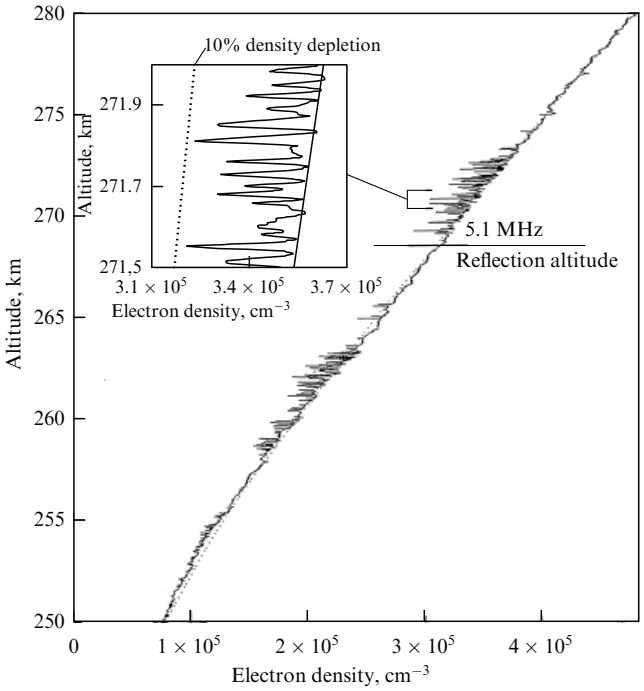

Figure 13. *Concentration distribution versus altitude z in the disturbed ionospheric plasma*, obtained in a rocket experiment (Kelley et al. [37]). Disturbance was effected at 5.2 MHz by the Arecibo station having effective power $PG = 40$ MW. Three zones containing concentration irregularities are readily distinguishable. The inhomogeneous region extends more than 20 km along altitude z, from 250 to 274 km. The inset shows detailed observational data for the segment $\Delta z \sim 0.5$ km. All irregularities are negative: $\Delta N = N - N_0(z) < 0$. They have a solitonlike shape and a characteristic size of 7 – 10 m. Plasma concentration disturbances in the irregularities do not exceed 10%: $|\Delta N|/N \leqslant 0.1$. All disturbances are allocated to three large zones measuring 2 – 5 km each. There are practically no perturbations between the zones, but 100 – 200 m groups of them can be seen within the zones.

Experiment [37] was preceded by a few similar attempts to study ionospheric regions disturbed by radio waves using rockets, but they failed to bring about valuable results. Kelley's experiment was successful because he used high-precision and high-speed measuring techniques. Measurements were made with an external Langmuir probe installed on the rod ahead of the rocket. Parameters measured by the 1.6 mm probe were read at a rate of 90,000 (!) times per second. Due to this, measurements of plasma concentration perturbations were available from every 1 – 2 cm of the rocket's path, and a highly detailed picture was obtained. Data analysis revealed stationary plasma concentration irregularities strongly elongated parallel to the Earth's magnetic field (for more than 10 km).

The theory of stationary striations was developed by Gurevich, Lukyanov, and Zybin [38] in 1995 almost simultaneously with the above rocket experiment. The theory is based on the resonance instability concept. Upper-hybrid waves excited by a powerful radio wave are trapped by negative inhomogeneities ($\Delta N = N - N_0 < 0$) and give rise to a standing UH-wave pattern in each of them. This leads to effective electron heating in the inhomogeneities and enhances resonance instability. Stabilization of instabilities is due to the fact that UH-waves are generated and trapped only in the vicinity of a UH-resonance, i.e., on scales of the order of 300 – 500 m, whereas irregularities in plasma density and electron temperature extend over distances of up to 10 km. In the unaffected region, perturbations are transferred and damped by virtue of collisional losses, resulting in strongly elongated stationary irregularity. Its scale and structure depend on the

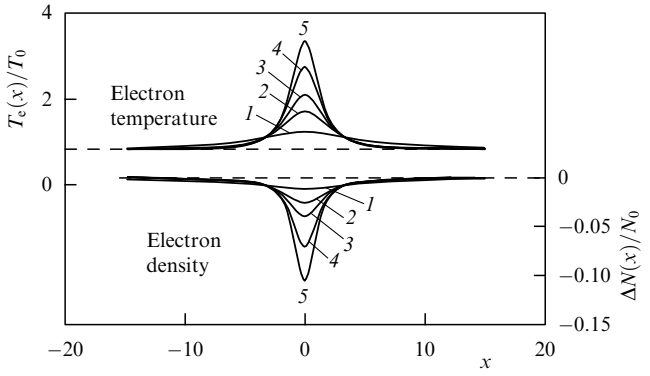

Figure 14. *Transverse distribution of electron temperature perturbations* T_e/T_0 *and plasma concentration perturbations* $\Delta N/N_0$ *in stationary striations* — plasma irregularities strongly elongated along the Earth's magnetic field (T_0 and N_0 — temperature and concentration of undisturbed plasma, $\Delta N = N - N_0$). On the abscissa the distance x from the axis of irregularity is plotted in units of $l_0 = (D_\perp^2 \varkappa_\parallel \tau / D_\parallel \delta \nu_e)^{1/4}$, where $D_\perp$ and $D_\parallel$ are the longitudinal and transverse coefficients of plasma ambipolar diffusion, $\varkappa_\parallel$ is the electron heat conductivity coefficient, ν_e and τ are the electron collision frequency and lifetime, respectively, and δ is the mean energy fraction lost by electrons in a single collision event. In the ionospheric F-layer, $l_0 \sim 5-10$ m. Curves are shown for different values of the relative amplitude of the pump-wave electric field E_0/E_c: *1* — $E_0/E_c = 1.15$; *2* — $E_0/E_c = 1.4$; *3* — $E_0/E_c = 1.8$; *4* — $E_0/E_c = 2.6$, and *5* — $E_0/E_c = 2.9$. Here, E_c is the critical field of excitation of stationary irregularities. Under conditions of the F-layer, $E_c \sim 30-100$ mV m^{-1}. Such a field is created in the F-layer by an ionosphere-modifying station with the effective emission power $PG \approx 10-100$ MW.

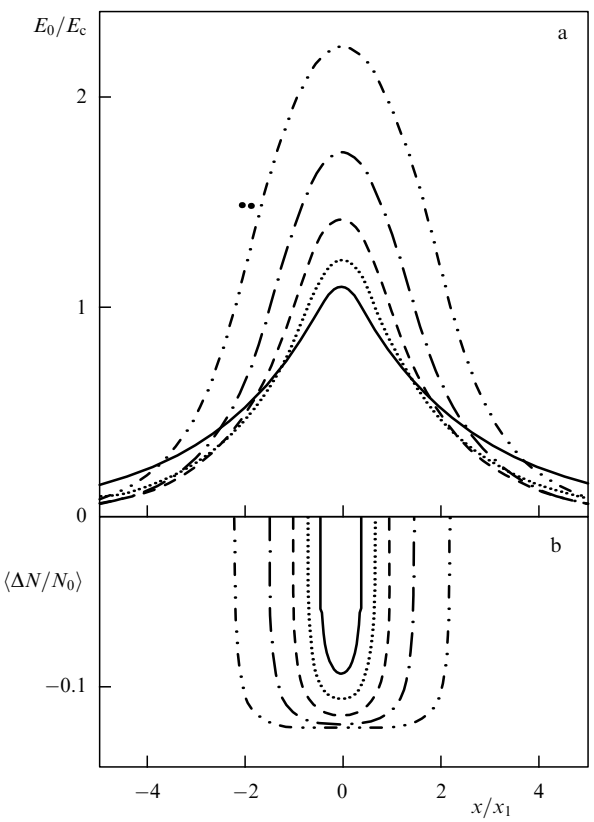

Figure 15. *Channeling of a powerful radio wave due to self-focusing on inhomogeneities strongly elongated along the Earth's magnetic field.* (a) Distribution of the powerful wave field amplitude in the direction x orthogonal to the magnetic field; the wave is trapped in the channel. (b) Distribution of plasma density perturbations $|\Delta N|/N_0$ averaged over a group of strongly prolate field-aligned inhomogeneities. The scale of the channel x is expressed in units of $x_1 = (\lambda/2\pi)[\langle(\Delta N/N_0)^2\rangle]^{-1/4}$, where λ — disturbing wavelength. In the ionospheric F-layer, $x_1 \sim 30-50$ m.

Evidently, when the focused field of a powerful radio wave in maximum, E_0^{max}, is only slightly greater than the critical field E_c, the small parabolic wave channels being formed take in only a small group of inhomogeneities. In the case of a stronger field $E_0^{max} \sim 2E_c$, the channel enlarges, acquires a rectangular shape, and almost entirely takes in the wave field.

effect of a powerful radio wave, resonance generation, and the trapping of UH-waves, on the one hand, and longitudinal and transverse transport processes in the plasma, on the other hand.

Theoretical predictions are illustrated in Fig. 14. Striations of different sizes are excited depending on the amplitude of the pump-wave electric field. Interestingly, relative density perturbations are on the order of 10%, in excellent agreement with experimental data. The transverse dimension of striations expressed in terms of plasma transfer parameters is 5–10 m. Although density perturbations are not very large, electron temperature within a striation may rise 2–4 times. This is the main prediction by the theory.

One more important feature exposed by the stationary striation theory is also worth noting. The point is that UH-waves resonantly excited by a pump wave in a given irregularity dissipate not only under the effect of electron heating but also as a result of direct transformation of UH-waves into electromagnetic ones, or to the so-called Z-mode [1, Sect. 29], [30, 31]. Z-mode waves have the same frequency as UH-waves and freely propagate across the magnetic field. Therefore, Z-mode waves emitted by one irregularity contribute to the pumping of UH-waves in other irregularities. As a result, they are absorbed by a sufficiently large group of 10^2-10^3 stationary irregularities. Due to this, excitation of a group of stationary irregularities by a pump wave is more efficacious than excitation of individual irregularities [38].

The critical excitation field of stationary striations is expressed as $E_c \approx E_T\sqrt{\delta v_T/c}$. Here, a characteristic value of the strong field, $E_T = (m\omega/e)\, v_T$, is singled out; in the pump wave field $E_0 \sim E_T$, the electron oscillation rate $eE_0/m\omega$ becomes equal to the thermal velocity v_T. Frequency ω being close to the Langmuir frequency, the pump-wave energy density $E_0^2/4\pi$ at $E_0 = E_T$ becomes equal to the thermal energy $N_0 T_e$ of plasma electrons. Evidently, radio wave propagation in the plasma is totally modified for $E_0 \geqslant E_T$, being determined by nonlinear processes.

Resonance nonlinear effects strongly manifest themselves even in $E_0 \ll E_T$ fields. For example, the critical field E_c is much weaker than E_T because δ and v_T/c are the small parameters. Under conditions of the ionospheric F-layer, $E_c \sim 30-100$ mV m^{-1}. Such a field is created by an ionospheric modification station with the effective emission power $PG \sim 10-100$ MW.

Self-focusing of a powerful radio wave. Excitation of a group of stationary irregularities is one of the causes governing self-focusing of a powerful radio wave. Indeed, a radio wave emitted by a high-power station has a scale an order of magnitude higher than the transverse scale of strongly elongated irregularities, and due to this its action encompasses a whole group of irregularities at a time. Because of reduced plasma density in each irregularity ($\Delta N < 0$), in the average the mean density for the pump wave is also lowered. As follows from Fig. 14, the fall in plasma density depends on the pump wave amplitude. It accounts for the nonlinear effect of self-focusing of the

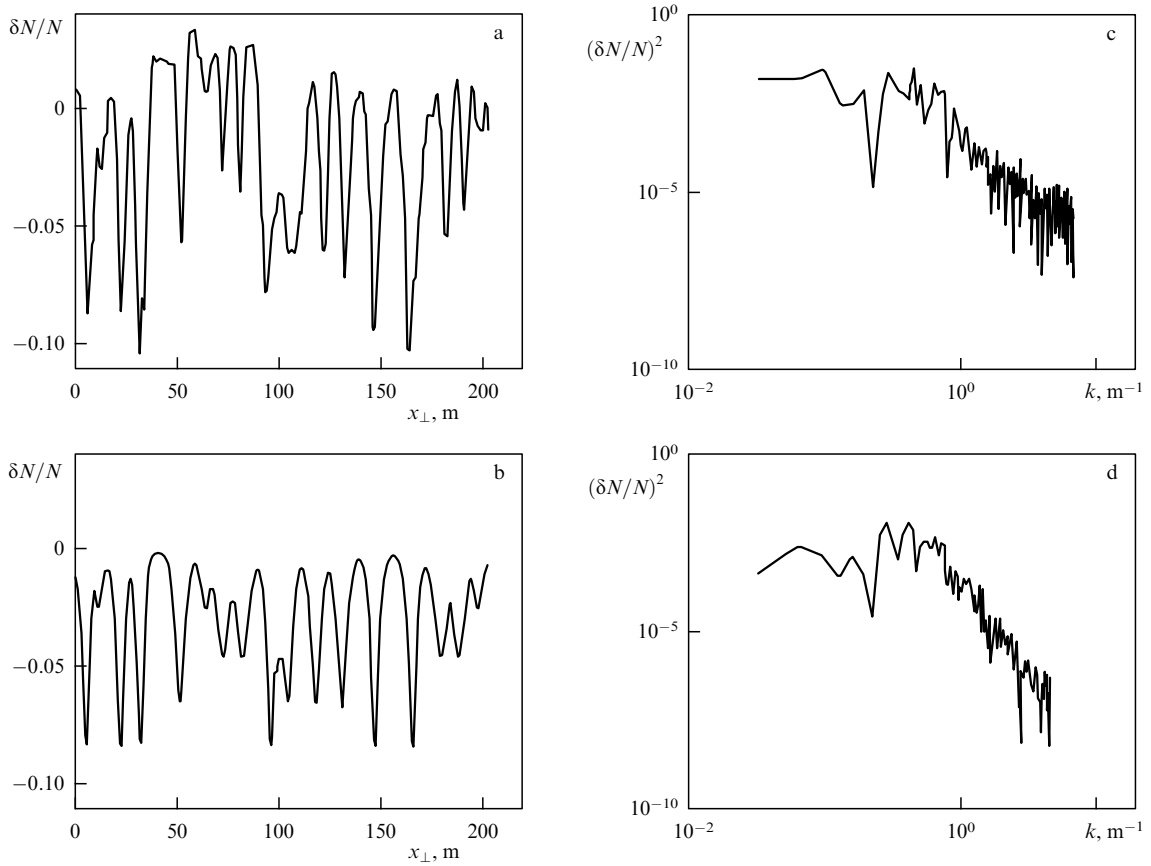

Figure 16. *Inhomogeneous structure spectrum of the disturbed ionospheric plasma.* Self-focusing results in a spectrum of structures across the magnetic field in the ionospheric plasma. Experimental and theoretical data were compared in Ref. [40] (Franz and co-workers). (a) Analysis of a rocket experiment [37]: results of direct observations are projected onto the plane perpendicular to the Earth's magnetic field. (b) Results of numerical computation of the spatial spectrum in accordance with theory [38] using maximum density fluctuation amplitude statistics derived from observations in Ref. [37]. Fairly good agreement between theory and experiment is evident. (c, d) The same data in the k-space. Experimental and theoretical spectra are completely conformable on scales from $k \approx 0.02$ m^{-1} to $k \approx 0.5$ m^{-1}. For $k > 0.5$ m^{-1}, the spectrum based on the theoretical model descends, always having a spectral index close to 4. The experimental spectrum has the same index only up to $k \approx 2$ m^{-1}; thereafter, the drop slows down.

powerful radio wave, and also for the formation of groups of irregularities exhibiting a parabolic solitonlike structure in terms of the amplitude of maximum density perturbations $\Delta N_{\max} < 0$ (Fig. 15). Due to the strong extension of irregularities along the Earth's magnetic field, self-focusing occurs only in the plane perpendicular to this field. It gives rise to forming the wave channels in the ionospheric plasma that trap the powerful pump wave itself, the latter spreading within a channel only parallel to the magnetic field (Fig. 15). This is the main feature of the self-focusing effect on strongly elongated irregularities [39].

A channel is formed by a group of striations with a transverse dimension on the order of 100 – 300 m. It is precisely these groups of irregularities of such scales that were observed in Kelley's experiments together with large groups containing many channels. Thus, the self-focusing process contributes to the formation of various structures in the ionospheric plasma that are extended along the Earth's magnetic field (Fig. 16). Simultaneously, self-channeling, trapping of the powerful wave, and its propagation along the magnetic field take place. This process underlies the so-called magnetic zenith effect.

To sum up, nonlinear self-focusing of a powerful radio wave on plasma irregularities created by the wave itself results in a variety of structures elongated along the Earth's magnetic field.

5.3 Magnetic zenith effect

The MZ effect is essentially described as follows. In the linear approximation, an ordinary radio wave guided vertically up must be deflected northward in the reflection region in the northern hemisphere [1, Sect. 35, Fig. 35d]). Surprisingly, Kosch et al. [41] as well as Pederson and Carlson [42] found out in ionospheric modification experiments that a vertical beam of powerful ordinary radio waves was deflected southward. Let us recall that the Earth's magnetic field also deviates from the vertical to the south toward the equator. In conformity with the above experimental results and theoretical considerations, a powerful wave may be trapped by a channel under the effect of nonlinear self-focusing and propagate along the magnetic field [43]. Moreover, the largest disturbance is brought about exactly in the direction of the magnetic field line passing through the modification station. This phenomenon is called the *magnetic zenith effect* [44 – 48]. As shown schematically in Fig. 17, there is a channel formed in the MZ direction in which a powerful wave propagates and electron temperature increases up to 3000 K, compared with 1000 K in the surrounding plasma.

The MZ effect was observed in experiments at all high-power facilities. A strong burst of radiation in the ionosphere was recorded at the HAARP station when a beam was directed to the magnetic zenith [44]. Figure 18 presents the results of investigations with the Oscar-27 satellite. The beam

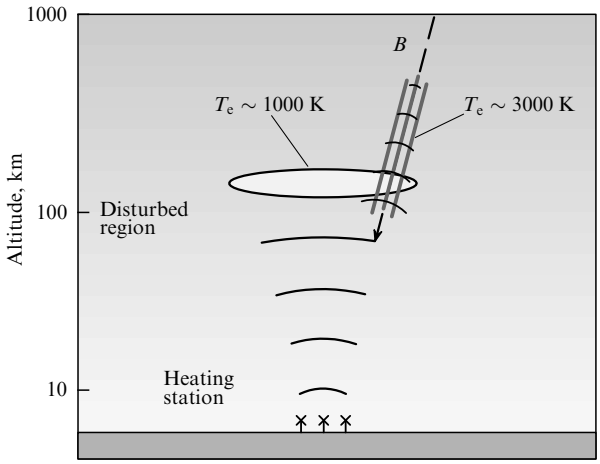

Figure 17. *Magnetic zenith effect* (*simulation*). A high-power station emits a beam of radio waves vertically upward. However, the strongest electron heating, glow, and disturbance of ionospheric plasma occur in the direction of the magnetic zenith (MZ) rather than in the vertical direction. Disturbance ascends as high as 400–600 km, i.e., much higher than the F-layer maximum. The MZ specifies the direction of the magnetic field vector at the location of a ground-based station. MZ deflection θ_z from the vertical is given by magnetic declination (tilt) of the axis of the magnetic dipole moment to the Earth's rotation axis and geographic latitude of the site. It is smaller for auroral facilities, such as HAARP ($\theta_z \approx 13°$) and Tromsö ($\theta_z \approx 9°$). Naturally, angle θ_z increases at lower latitudes, being $\theta_z \approx 19°$ for the Sura station.

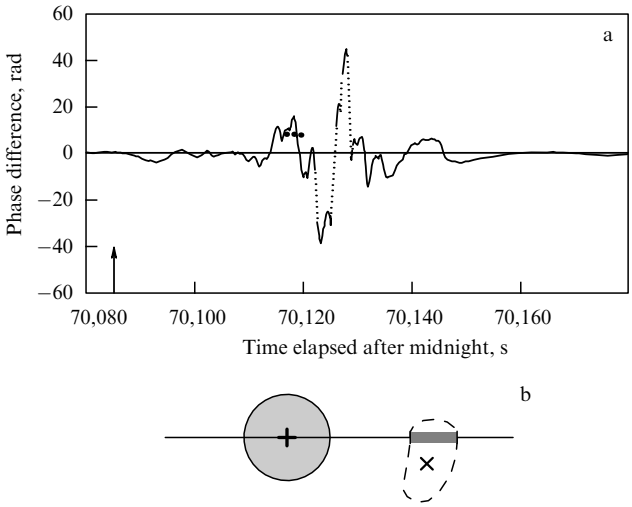

Figure 18. *The polar satellite Oscar-27* placed at the circular orbit altitude of 1000 km determined integral plasma-density perturbations in the ionosphere from the phase shift difference between two radio waves at frequencies $f_1 = 149.999$ MHz and $f_2 = 389.968$ MHz. Measurements were carried out by a network of ground-based receiving stations. Ionospheric disturbances were induced by the HAARP facility. A beam of powerful radio waves was emitted vertically upward. No marked plasma disturbances were apparent when the satellite was passing over the station. But, on the other hand, very strong disturbance was recorded 30 s later in the region whose projection coincided with the MZ direction. (a) Time-dependent plasma density perturbations in the ionosphere; arrow indicates the moment of satellite passage over HAARP. (b) Horizontal projection of the F-region disturbance; straight line depicts the satellite's path, the + symbol is the HAARP's location, the × symbol is the MZ location, and the dark circle is the beam projection. The region of observed strong disturbance in the satellite's trajectory is marked by a dark stripe. The magnitude of disturbances agrees with the theoretical prediction [49].

was guided vertically upward, and the maximum disturbance was observed souther in the direction close to the MZ. A major part of the wave power shifted southward, where the largest effect was revealed [49].

The MZ effect was first discovered by Leyser, Gustavsson, et al. [46, 48] at the Tromsö station. The facility, operating in a pulse-periodic regime, was programmed to switch on and off every 2 minutes. In the experiment, the directions of both the powerful beam and the measuring radar were gradually displaced from the vertical toward the magnetic field. No substantial plasma density or ion temperature perturbations were documented. In the beginning, electron temperature T_e did not significantly change, either. However, it sharply rose to $(3-4)\times10^3$ K as soon as the beam direction approached the MZ. The vertical size of the zone where plasma electrons underwent intense heating significantly increased too, with the zone itself being elevated to altitudes of 300–400 km. Figure 19 presents other observational results of the Tromsö experiment [48]. The tilt angles of the transmitter and the temperature-measuring radar were changed simultaneously. At angles in excess of 10° from the direction of the magnetic field, i.e., the MZ direction, electron temperature T_e was 1000 K, as in the undisturbed ionosphere. The temperature began to grow at an angle of 5° and rose to 3000 K when the beam was directed strictly to the zenith, thus suggesting a very narrow effect in terms of the angle of deflection from the strictly zenithward direction. [7]

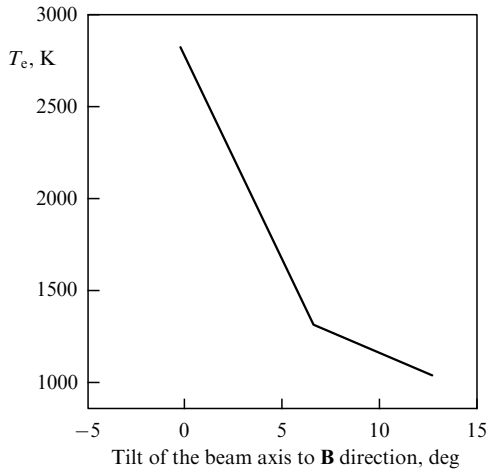

Figure 19. *Electron temperature perturbation recorded at Tromsö*. Electron temperature T_e at altitudes of 300–500 km depending on the angle between the powerful beam axis and the direction of the magnetic field **B** at Tromsö station. The disturbing wave frequency is 4 MHz, and effective power of the station $PG = 300$ MW. T_e was measured by an incoherent scattering radar coaxial with the disturbing beam.

According to the theory, the MZ effect should attenuate at lower latitudes for the station location. Nevertheless, the mid-latitude (56°) Sura station recorded substantial enhance-

[7] In 1995–1996, a group of theorists from the Lebedev Physical Institute worked at the Max-Planck Institut für Astronomie, owner of the Tromsö station. We many times tried to convince leaders of the experiment that the theory [38] predicted a marked rise in electron temperature in the F-layer under the effect of a powerful radio wave and that it needs to be examined. The experimenters always stated that observations regularly showed no more than a 20–30% increase and pointed to the absence of greater disturbances. It was true for almost any beam direction. It should be noted, however, that special observations made a few years later with a disturbing beam directed toward the MZ confirmed the theoretical prediction.

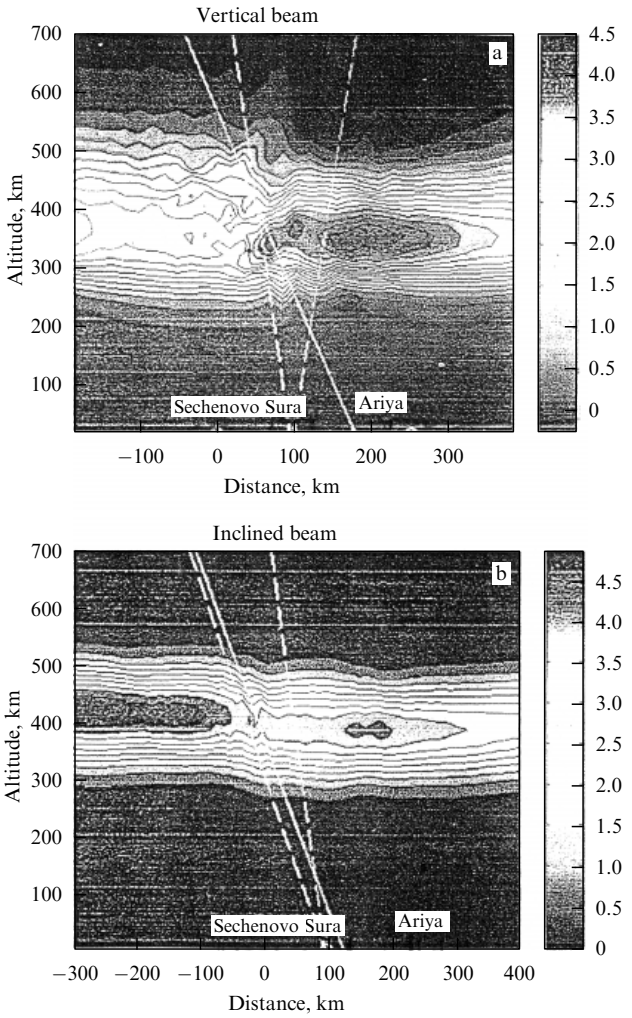

Figure 20. Plasma disturbances in the ionosphere excited by the Sura station. Powerful radio wave frequency is 4.3 MHz, and the effective emission power is 30 MW. The beams are shown by dashed straight lines: (a) vertical beam, (b) beam tilted through 12° in respect to the magnetic field. Direction of the magnetic field shown by the solid straight line deflects 19° from the vertical. Sechenovo and Ariya are the study sites. Concentration of ionospheric plasma was measured by the radiotomographic method from a Russian navigation satellite. It can be seen that the ionosphere is disturbed in the neighborhood of the MZ direction. The effect was heightened by tilting the transmitted beam. Prolonged heating prior to the satellite's passage (14 – 20 min) provoked wave type disturbances in a broad high-altitude area close to the F-layer maximum.

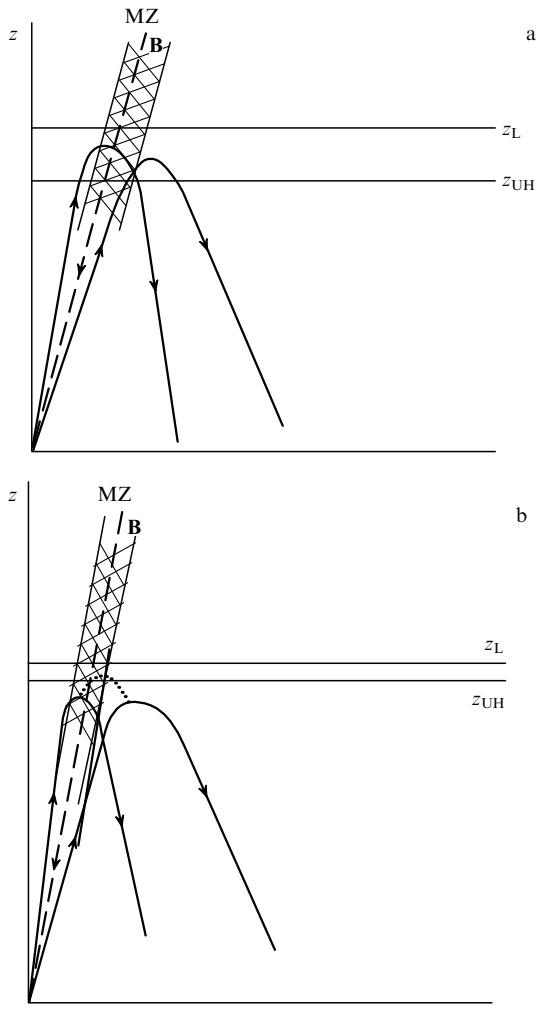

Figure 21. *MZ effect in the low- and high-frequency limits*. Dashed straight line — magnetic field direction (MZ direction). Solid curves — boundary rays of the disturbing radio-wave beam directed toward the MZ. Altitude z_{UH} corresponds to the UH-resonance region, and z_L to the Langmuir resonance region. (a) Low-frequency radio wave ($f \leqslant 4$ MHz). The wave beam directed toward the MZ freely reaches the UH-resonance region where resonance instability induces UH-turbulence that eventually leads to a strong plasma heating and formation of a channel in which the pump wave is trapped. As a result, the disturbing wave reaches both UH (z_{UH}) and Langmuir (z_L) resonance regions where electrons are effectively accelerated. The channel region is shown by hatching. (b) High-frequency radio wave ($f \geqslant 6$ MHz). In this case, the resonance region (between z_{UH} and z_L) is narrow. The radio wave directed towards the MZ reflects below the UH-resonance region. However, the plasma is gradually 'punched through' due to the ohmic heating of plasma electrons in the neighborhood of the reflection point (the heated region is shown by the dotted line). This enables the wave to reach the UH-resonance region. Thereafter, the process leading to the MZ effect proceeds in the same way as for a low-frequency wave. The difference is that the effect develops 20 – 30 s later. During this time, electrons are heated and the plasma is gradually forced out.

ment of the optical glow in the direction of the MZ. Figure 20 shows the distribution of plasma concentration perturbations in the ionosphere observed by Tereshchenko et al. [50] in a satellite experiment. Figure 20a demonstrates a case in which a disturbing beam of the Sura station is guided vertically upward. As evident from the plots, the plasma is strongly disturbed in the direction of the magnetic field despite the beam's vertical orientation. Figure 20b illustrates a case where the beam is deflected through 12° toward **B**. Here, perturbation in a narrow region in the MZ direction is much more apparent. Simultaneously, density perturbations were measured in irregularities having a scale length of some 100 m. They increased substantially with the tilt of the beam.

The above simple explanation of the MZ effect holds true only when the ionosphere is affected by low-frequency radio waves with $f \leqslant 4$ MHz. The picture at higher frequencies, $f \geqslant 5$ MHz, is more complicated; the point is that the UH-resonance region at low frequencies f lies much lower than the reflection point of a radio wave incident vertically on the ionosphere. For this reason, radio waves directed toward the MZ reach the UH-resonance region even at large tilt angles of the magnetic field with respect to the vertical ($\theta_z \leqslant 20°$) (Fig. 21a).

The picture changes at high frequencies f. In this case, the UH-resonance region is close to the reflection point for a

vertically incident wave. Therefore, a radio wave directed toward the MZ even at a rather small tilt angle of the MZ relative to the vertical ($\theta_z \leqslant 10^\circ - 15^\circ$) spreads obliquely and reflects below the UH-resonance region (Fig. 21b). In this case, the effect is achieved due to the ohmic heating of ionospheric electrons in the vicinity of the radio-wave reflection point. Electron heating in the reflection region results in plasma 'punching' (as shown in Fig. 7) and enables the wave to travel further up into the UH-resonance region. Thereafter, the process proceeds as in the low-frequency case [45, 51]. The preliminary electron heating is recorded in experiment as a delay of the MZ glow in the high-frequency limit [44] (because it needs much time, 20 – 30 s, to develop). It is therefore true that the MZ effect in a high-frequency case is in a sense analogous to 'punching a hole' in the ionosphere, predicted in Ref. [27], as a result of ohmic plasma heating. Certainly, the overall physical nature of the MZ effect associated with resonant processes is much more complicated.

5.4 Anomalous and broadband absorption

Strong excitation of natural plasma oscillations in the UH-resonance region inevitably leads to effective absorption of both the pump wave energy and energies of other radio waves propagating in the perturbed region. Only O-polarized waves like pump waves are absorbed. The absorption bandwidth (±200 kHz) depends on the width of the resonance region and the scale of strongly elongated irregularities (Erukhimov et al. [32, 33], Stubbe et al. [52 – 55]). Figure 22a demonstrates an example of anomalous absorption of the probing wave (PW) with a 70-kHz higher frequency than that of the pump wave. The ionospheric modification station (Fig. 22b) was programmed to alternatively switch on and off every minute. Evidently, switch-on sharply induced anomalous PW absorption that exceeded 20 dB. In other words, the received signal power dropped more than 100-fold! Let us recall that normal collisional absorption in the F-region is below 5 – 10%; this accounts for the well pronounced effect of anomalous and broadband absorption. The PW signal recovers for 10 – 20 s. This time characterizes the dispersal of strongly elongated irregularities. The point is that PW absorption is a result of excitation of UH-oscillations by the PW itself on strongly elongated irregularities created by the pump wave. The irregularities gradually disappear after cessation of pumping and absorption discontinues. It was the analysis of PW absorption at various frequencies that made it possible to estimate the longitudinal scale ($\sim$ 10 km) and the averaged density perturbation ($\sim$ 1%) of elongated irregularities much before rocket experiments [25, 54]. PW frequency dependence of anomalous absorption in the vicinity of the F-layer maximum is illustrated in Fig. 23.

Modulation transfer. Broadband anomalous absorption manifests itself in peculiar 'cross modulation' of radio waves in the F-layer. When emission of a high-power station is modulated with a certain low frequency F, it causes anomalous absorption of probing waves with different frequencies and their modulation with the same low frequency F. Such modulation 'transfer' is shown in Fig. 24. A powerful station operating at 5.75 MHz was programmed to be on for 1 s and off for 0.12 s (Fig. 24a). The modulation was imparted to a PW with a frequency of 5.85 MHz (Fig. 24b). The transferred modulation had the same basic frequency, but its shape or the frequency spectrum changed substantially. This is not surprising, since modulation transfer is related to the appearance and growth of irregularities created by the pump wave in the F-region. Therefore, characteristic times of their evolution and decay markedly affect modulation transfer. The result is 'hysteresis' and other interesting phenomena [32, 52, 56]. In-depth studies of modulation transfer are a source of data on nonstationary processes of the development of both the upper-hybrid and Langmuir turbulences. The latter is investigated via modulation with a very short disturbing pulse: $\Delta t \leqslant 0.1$ s [57].

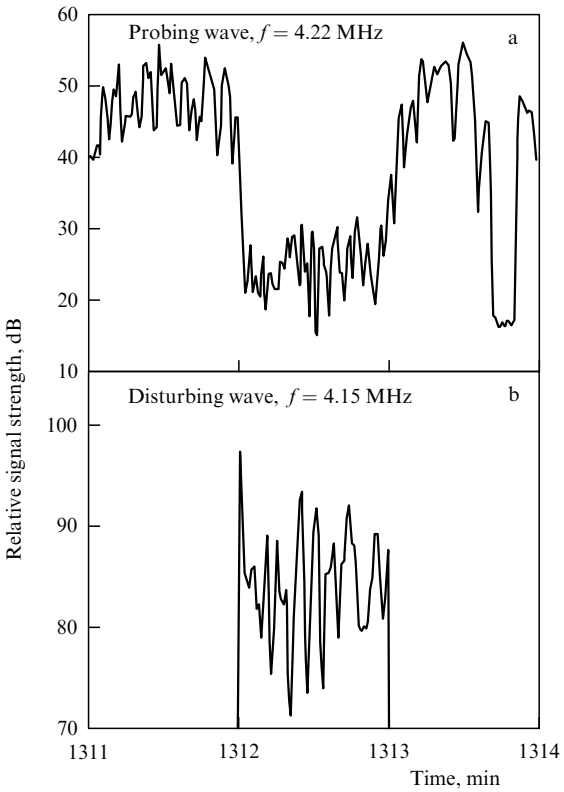

Figure 22. *Anomalous broadband absorption*. The ionosphere was disturbed by the high-power Tromsö station. Effective transmitter power $PG = 200$ MW. Disturbing wave frequency is $f = 4.15$ MHz. The transmitter operating in the pulse regime was programmed to switch on and off every minute. The intensity of the reflected wave is shown in Fig. 22b. The disturbing wave exhibits strong anomalous absorption ($\sim$ 20 dB). Figure 22a shows probing wave (PW) amplitude. PW frequency $f_p = 4.22$ MHz, or 70 kHz higher than the frequency of the disturbing station. It can be seen that anomalous PW absorption occurs very fast, i.e., within less than 10 s after turning the station on. Anomalous PW absorption is $\sim$ 20 dB. The disappearance of the effect after shutoff is much slower, taking some 20 s. This period is determined by the decay time of strongly elongated irregularities excited by a powerful radio wave in the region of the UH-resonance of the PW (Jones et al. [53]).

6. Stimulated electromagnetic emission

In the 1970s, Stenflo and co-workers [58] predicted that ionospheric modification by a powerful radio wave must induce backscattered radio emission from the ionosphere at frequencies distinctly different from the frequency of the disturbing station. This phenomenon, known as *stimulated electromagnetic emission* (SEE), was experimentally examined by Thidé, Kopka, and Stubbe [59] in 1982. SEE sources were shown to be located in a region perturbed by a powerful radio wave. The emission was described as continuous and

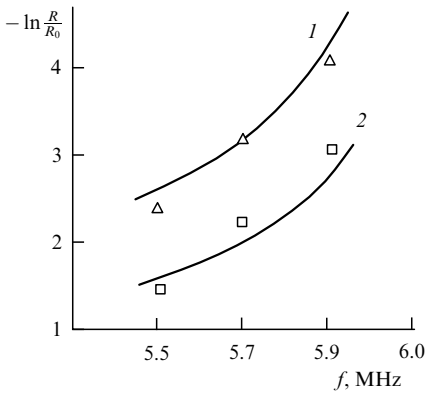

Figure 23. *Plot of anomalous absorption vs. probing wave frequency*. The disturbance was excited by a station with a relatively small maximum power ($PG = 20$ MW) and frequency $f = 5.75$ MHz, located at Zimenki (near Nizhny Novgorod). The critical frequency of the F-layer is $f_c \approx 6$ MHz (f_c — maximum frequency of radio waves reflected from the F-layer and propagating vertically). In other words, anomalous absorption was examined near the F-layer maximum (R, R_0 — coefficients of reflection for disturbed and undisturbed waves, respectively). Measurements were made at both maximum (△) and one-half (□) powers of the disturbing station. It can be seen that anomalous PW absorption occurred within a broad frequency band on the order of 400 kHz, and increased closer to the F-layer maximum, because the plasma density gradient dN/dz decreased as the layer maximum was approached and, correspondingly, the length of strongly elongated irregularities enlarged. Curves were obtained by calculation. Comparison of theoretical curves and experimental data made it possible to determine the mean concentration perturbation in irregularities on the assumption that they compactly fill up the entire disturbed region: $|\delta N/N| \approx 0.7\%$ and $|\delta N/N| \approx 0.5\%$ at maximum and half-maximum powers of the transmitter, respectively. It should be emphasized that anomalous absorption amounts to 15 dB, despite the relatively small power of the disturbing station (experiment — Getmantsev et al. [56], theory — Vas'kov, Gurevich [14]).

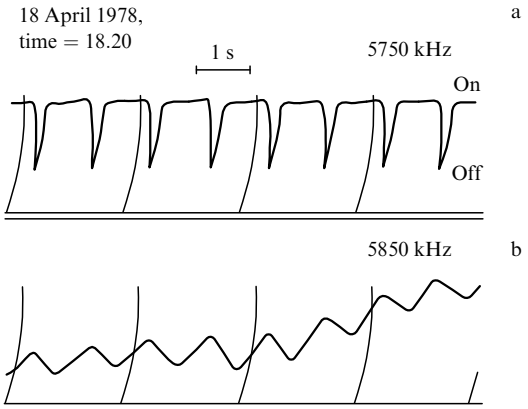

Figure 24. *Modulation 'transfer'*. The ionosphere was disturbed by a radio station with a relatively small maximum power $PG = 20$ MW (Zimenki). The station, operating at $f = 5.75$ MHz, was programmed to be turned on for 1 s and off for 0.12 s. (a) Recording of the reflected signal of a powerful radio wave; lines — time marks spaced at 2.24-s intervals. (b) Signal of a 5.85-MHz O-polarized probing wave received after reflection from the disturbed region. Due to anomalous absorption, the PW is modulated with the same frequency $F = (1.2\,\mathrm{s})^{-1}$, even though the emitted PW had a constant amplitude. Note that the shape of 'transferred' modulation is distinctly different from the modulation of the disturbing station. Also apparent is a marked shift of the modulation phase. Both the altered shape and the shifted phase of the modulation reflect the development and decay of strongly elongated irregularities generated by radio emission of the disturbing station and responsible for anomalous PW absorption resulting in modulation 'transfer' (Erukhimov et al. [32]).

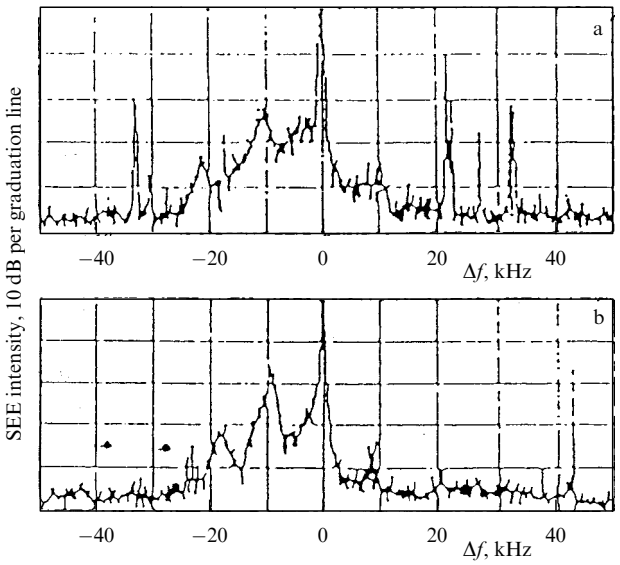

Figure 25. *Stimulated electromagnetic emission* (*SEE*). Characteristic SEE spectra obtained at Tromsö by Stubbe et al. [62]. The disturbing station power $PG = 210$ MW, radiation frequency: (a) $f = 5.3$ MHz, and (b) $f = 5.4$ MHz; $\Delta f = f_s - f$ — frequency shift of the received ionospheric radio emission f_s with respect to the disturbing station frequency. On the ordinate the relative signal intensity f_s (10 dB per graduation line) is plotted. It can be seen that the SEE frequency f_s is shifted down relative to the station frequency; this explicitly suggests the decay character of the processes generating the observed radiation.

UH-waves (ω_{UH}, k_{UH}) strongly excited by the pump wave decay into upper-hybrid (ω_{UH1}, k_{UH1}) and low-hybrid (LH) (Ω_{LH1}, K_{LH1}) waves: $\omega_{UH} = \omega_{UH1} + \Omega_{LH1}$, and $k_{UH} = k_{UH1} + k_{LH1}$. UH-waves are defined by natural oscillations of plasma electrons in the direction orthogonal to the magnetic field, and LH-waves by combined electron and ion oscillations. The frequency of UH-oscillations is high: $\omega_{UH} = (4\pi e^2 N(z_{UH})/m + \omega_{He}^2)^{1/2}$, i.e., close to the pump wave frequency: $\omega_{UH} = \omega = 2\pi f$. LH-oscillation frequency is low, close to $\Omega_{LH} = \omega_{UH}\sqrt{m/M}$, where m and M are the electron and ion masses, respectively. In the ionosphere, LH-frequency $F_L = \Omega_{LH}/2\pi \approx 8$ kHz. Note that F_L is the minimal LH-wave frequency or the 'cut-off' frequency. Spectrum of LH-waves set up in the decay process has characteristic frequencies $F_{LH} \sim (1.2-1.5)\,F_L$. Therefore, frequencies of UH-waves arising in the decay differ from the pump wave frequency by 10–12 kHz. It is these waves that are responsible for the well-apparent first peak of the radio signal (f_s) emitted by the ionosphere, referred to as the downshifted maximum (DM). Its height is only 15–20 dB lower than the amplitude of the reflected fundamental wave. The DM is the most prominent SEE structure. The second pronounced radiation peak results from secondary decay. Its frequency differs from f by 20–25 kHz. The well-developed UH-turbulence generates radio emission with a frequency shift of up to 100 kHz from the basic frequency.

incoherent. It occurred at lower frequencies than the disturbing wave frequency, barring the special cases discussed below.

Characteristic examples of the SEE spectrum are presented in Fig. 25. The total SEE bandwidth amounts to several dozen kilohertz. The first peak of backscattered emission is distinguished at a frequency shifted 10–15 kHz down from the disturbing wave frequency. Radiation intensity in the first peak is very high, being only 15–20 dB lower than the intensity of the reflected disturbing wave. This peak is the most typical SEE structure, referred to as the downshifted maximum (DM). Another less explicit maximum is also frequently observed, followed by a tail as long as a hundred of kilohertz.

Detailed analysis of SEE properties indicates that the DM completely develops within a few (up to 10) seconds after starting the modification station and disappears for several

milliseconds following shutoff. Investigations of these and other characteristics show that the DM and the following maximum are closely associated with processes in the UH-resonance region.

The theory predicts strong excitation of natural plasma oscillations in the UH-resonance region by virtue of resonance instability (see Fig. 12). Their frequency ω_{UH} coincides with the pump wave frequency ω, viz. $\omega_{UH} = \omega$. The length of the corresponding UH-waves or their wave vector k_{UH} are given by the transverse dimension of strongly elongated irregularities generated during the development of resonance instability. These are coherent oscillations where phase stability is due to the stability of both pump wave and strongly elongated irregularities.

However, small fluctuations of other waves are always present in the ionospheric plasma. When the amplitude of pumped UH-waves becomes sufficiently high and greatly exceeds the pump wave amplitude (resonance!), 'decay' instability develops. It can be essentially described as follows. There are such UH (ω_{UH1}, k_{UH1}) and LH (Ω_{LH1}, K_{LH1}) waves among plasma fluctuations that satisfy decay conditions $\omega_{UH} = \omega_{UH1} + \Omega_{LH1}$, and $k_{UH} = k_{UH1} + K_{LH1}$. Under these conditions, pulsation of two high-frequency waves exactly coincides both in frequency ($\omega_{UH} - \omega_{UH1}$) and space ($k_{UH} - k_{UH1}$) with a low-frequency wave with Ω_{LH1}, K_{LH1}. This makes possible energy pumping from the high-amplitude fundamental UH-wave with ω_{UH}, k_{UH} into very weak fluctuation waves (ω_{UH1}, k_{UH1} and Ω_{LH1}, K_{LH1}). Pumping is hampered by phase interruption resulting from electron collisions. Nevertheless, the electron collision frequency in the F-layer being small, $\nu/\omega_{UH} \sim 10^{-4} - 10^{-5}$, the phase interruption is overcome after the dominant wave amplitude becomes large enough; simultaneously, the decay process is initiated. For all that, radiation of waves generated in decay instability proves incoherent as a result of the regular interruption of phase synchronism, related to random electron collisions.

Further wave decay (ω_{UH1}, k_{UH1}) leads to the appearance of the second harmonic (ω_{UH2}, k_{UH2}), etc. That is how *upper-hybrid plasma turbulence* originates. Its development is influenced by other plasma processes, too. It is important that the decay processes are paramount for the development of UH-turbulence in a frequency region below the disturbing station frequency ω [60, 61].

Thus far, we have confined ourselves to the formation of the frequency spectrum of upper-hybrid plasma turbulence in the ionosphere. The question is: how does the ground-based SEE evolve? Both UH and radio waves are independent modes of the spatially uniform ionospheric plasma. The large number of elongated irregularities in our case makes the plasma strongly inhomogeneous. The process of conversion of UH-waves into radio waves in such a plasma proceeds via linear transformation (scattering) of UH-waves on stationary ionospheric irregularities. In this process, all peculiarities of the plasma turbulence frequency spectrum are preserved in the observed SEE spectrum. Specifically, the most pronounced SEE feature (characteristic peak of a downshifted maximum) reflects the frequency of the first decay mode (ω_{UH1}, k_{UH1}) of UH-turbulence (see Fig. 25). The DM frequency deviates from the disturbing station frequency by some 10 – 15 kHz; such a shift characterizes the LH-wave frequency Ω_{LH}. Similarly, the second peak reflects the second decay, i.e., its frequency shift is on the order of twice the LH-wave frequency.

Let us recall that the UH-wavelength coincides with the scale of ionospheric irregularities because they are generated simultaneously as a result of direct resonance pumping by a powerful radio wave; hence the equally efficacious reverse process of linear UH-wave transformation to radio waves on irregularities. The close association of SEE with UH-turbulence has been demonstrated in a series of experimental and theoretical studies [63 – 68].

Note that this section considered only the most characteristic properties of SEE. Detailed experiments have revealed its other interesting features [69 – 74], partly discussed in Sections 7, 8.

7. Multiple gyromagnetic resonance

7.1 Bernstein modes

Two resonance effects are simultaneously realizable in the ionosphere at certain frequencies of the disturbing wave ω. First is the ordinary resonance ($\omega = \omega_{UH}$) between ω and UH-frequency ω_{UH}. This resonance was considered in previous Section 6. It arises in the UH-resonance region at a certain altitude z_{UH} in the ionosphere, depending on frequency ω and altitude profile $N(z)$ of electron concentration (see Fig. 12). The second resonance has a frequency which is a multiple of the electron gyromagnetic rotation frequency: $\omega = n\omega_H$. In other words, double resonance occurs in those regions of the ionosphere where the following condition is satisfied:

$$\omega \approx n\omega_H \approx \omega_{UH}(z)\,. \qquad (1)$$

The multiple gyroresonance condition (1) in the ionospheric F-layer might be fulfilled at $n = 2, 3, 4, 5, 6$, and even greater, depending on the maximum electron concentration in this layer (Fig. 1a). Clearly, the double resonance conditions are met only at concrete frequencies ω of the disturbing wave [8] and given altitudes z, depending on the electron concentration profile $N(z)$.

All the phenomena evolving in the UH-resonance region under the action of a powerful wave on the ionosphere are substantially modified near double resonance. Specifically, the number of strongly elongated irregularities markedly decreases (to the point of disappearance). Enhanced field-aligned scattering along with anomalous and broadband absorption of radio waves change accordingly, and SEE is completely transformed as well. Moreover, the theory predicts the appearance of a system of new supersmall-scale strongly elongated irregularities accompanied by strong field-aligned scattering of ultrahigh-frequency (UHF) radio waves, up to 1 – 2 GHz.

The effect is due to the generation of a new type of waves, the so-called Bernstein modes, at double resonance. Physically, these waves are related to the gyromagnetic rotation of electrons about the magnetic field direction. The possibility of synchrotron acceleration of electrons by the wave's electric field with frequency ω coincident with the electron gyromagnetic rotation frequency, [9] $\omega = \omega_H$, was mentioned in Section 3.1. It turns out that phase synchronism of the wave's

[8] Here, we take into account that magnetic field variations in the subarctic and mid-latitude ionosphere are relatively small, so that the electron gyromagnetic rotation frequency may be approximately regarded as fixed: $\omega_H \approx 10^7$ s^{-1} (see Section 3.1).

[9] Notice that electron gyromagnetic rotation in the magnetic field is also referred to as Larmor rotation.

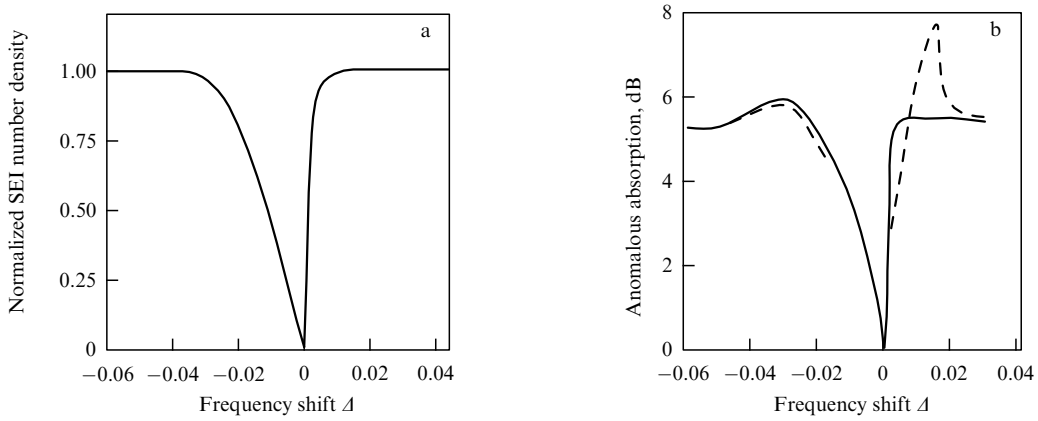

Figure 26. *Drop in number of striations near double gyroresonance*. Results of theoretical evaluation of the change in (a) the number of striations, (b) anomalous and broadband absorption depending on the disturbing wave frequency f at double gyroresonance near the third gyroharmonic [76]. On the abscissa the shift of f relative to resonance, $\Delta = f/3f_H - 1$, is plotted. On the ordinate in Fig. 26a the number density of striations normalized to the number density of striations excited far from the double resonance is plotted. As can be seen, the number of striations rapidly decreases as f approaches the resonance frequency $3f_H$. Striations totally disappear at $f = 3f_H$. Their number sharply increases again with growing $f > 3f_H$ and practically reaches the undisturbed level at $f - 3f_H = 0.01f$. Solid line in Fig. 26b shows anomalous absorption of the disturbing wave f, while dashed line shows absorption of the probe wave shifted by 70 kHz (broadband absorption). Variations in anomalous and broadband absorption are actually determined by the change in the number of striations. Both vanish at resonance $f = 3f_H$. A small peak of broadband absorption at $f - 3f_H \approx 0.02f$ arises from taking into account the upward (along z) shift of the UH-resonance point for the probe-wave frequency $f + 70$ kHz.

Theoretically, the nature of the marked change in the excited plasma state near double resonance is characterized as follows. Schematically, the system of equations describing excitation of UH-waves and strongly elongated irregularities (striations) may be represented in the form [38, 76]

$$-P_0 N_1 = E_1\left(\varepsilon_0(z) - N_1\right) + \overbrace{\frac{1}{1-\left[f/(2f_H)\right]^2}\frac{d^2E_1}{dx^2}} + \underline{\frac{\delta^2}{1-\left[f/(3f_H)\right]^2}\frac{d^4E_1}{dx^4}} + \underbrace{\frac{\delta^4}{1-\left[f/(4f_H)\right]^2}}\frac{d^6E_1}{dx^6} + \ldots, \tag{I}$$

$$N_1 = D_1(N_1, T_{e1}), \tag{II}$$

$$T_{e1} = E_1^2 + D_2(N_1, T_{e1}). \tag{III}$$

Equation (I) describes the excitation of UH-waves E_1 by the pump wave P_0. Here, N_1 is the relative (i.e., normalized to mean density) plasma density perturbation in strongly elongated irregularities, $\varepsilon_0(z)$ is the linear dielectric constant of UH-waves depending on altitude z, x is the coordinate across irregularities, normalized to their transverse scale l. Differential operators D_1 and D_2 describe transport processes N_1 and T_{e1} along and across the magnetic field. The set of equations (I)–(III) for the field of UH-waves E_1, plasma density perturbations N_1, and electron temperature T_{e1} describes strongly elongated irregularities N_1, T_{e1} and the UH-waves E_1 exciting them. The terms of Eqn (I) that are proportional to δ^2, δ^4, ... describe the effect of double gyroresonance for different gyroharmonics, $n = 3, 4, \ldots$. In the general case, they play but a minor role because $\delta = \rho_e/l$ is the small parameter: $\delta \sim 10^{-2}$ [here, ρ_e is the radius of gyromagnetic (Larmor) electron rotation in the Earth's magnetic field, $l \sim 5$ m]. However, their influence is much greater near double resonance where the wave frequency f approximates the multiple gyromagnetic frequency nf_H. For example, the third (underlined) term on the right-hand side of Eqn (I) gradually becomes predominant at $f \approx 3f_H$. Simultaneously, excitation of UH-waves decreases, and they are completely suppressed at resonance for $f = 3f_H$ together with striations. The same is observed near the fourth gyroresonance, where the fourth term on the right-hand side of Eqn (I) acquires the dominant role (lower brace), etc.

electric field oscillations with gyromagnetic rotation is also feasible at multiple gyroresonance, $\omega = n\omega_H$ [75]. This occurs if the plasma contains spatial irregularities, i.e., oscillations whose wavelengths are in a well-defined relation with the radius ρ_e of electron gyromagnetic rotation. It is these waves that are called Bernstein modes. Radius ρ_e is on the order of 1–2 cm under ionospheric conditions; it accounts for the small wavelength of Bernstein modes across the magnetic field: $\lambda_B \sim 2\pi\rho_e \sim 10-40$ cm. Length λ_B slightly decreases with increasing harmonic number n. Phase synchronism makes possible the effective pumping of the disturbing wave energy into Bernstein modes. Note that the modes can be excited only at frequencies not much higher than the resonance frequency, $\omega > n\omega_H$ [to be precise, at $\omega - n\omega_H \sim 2\pi \times (20-100)$ kHz].

7.2 Ionospheric modification in the double resonance region

Let us consider the development of ionospheric disturbances in the vicinity of double resonance, assuming that the disturbing wave frequency ω gradually approaches resonance at $n\omega_H$. In a region with $\omega < n\omega_H$, Bernstein modes are not yet excited. Meanwhile, processes in the UH-resonance region sharply subside closer to resonance, as appears from the altered excitation pattern of strongly elongated irregularities.

Figure 26 presents results of the theoretical evaluation of the excitation of strongly elongated irregularities and anomalous pump-wave absorption near the third gyroresonance ($n = 3$) [76]. The number of such irregularities falls considerably closer to resonance. They are totally absent at the resonance point ($\omega = 3\omega_H$) but grow in number even more sharply behind resonance. The total frequency width of the region where modification effects are grossly distorted is only 2–3% of the resonance frequency, viz. 100–200 kHz.

A change in the number of elongated irregularities naturally influences anomalous absorption of both the disturbing wave and the probing radio waves with a frequency shifted by 100 kHz or more that propagate in the disturbed region. This observation is illustrated by both

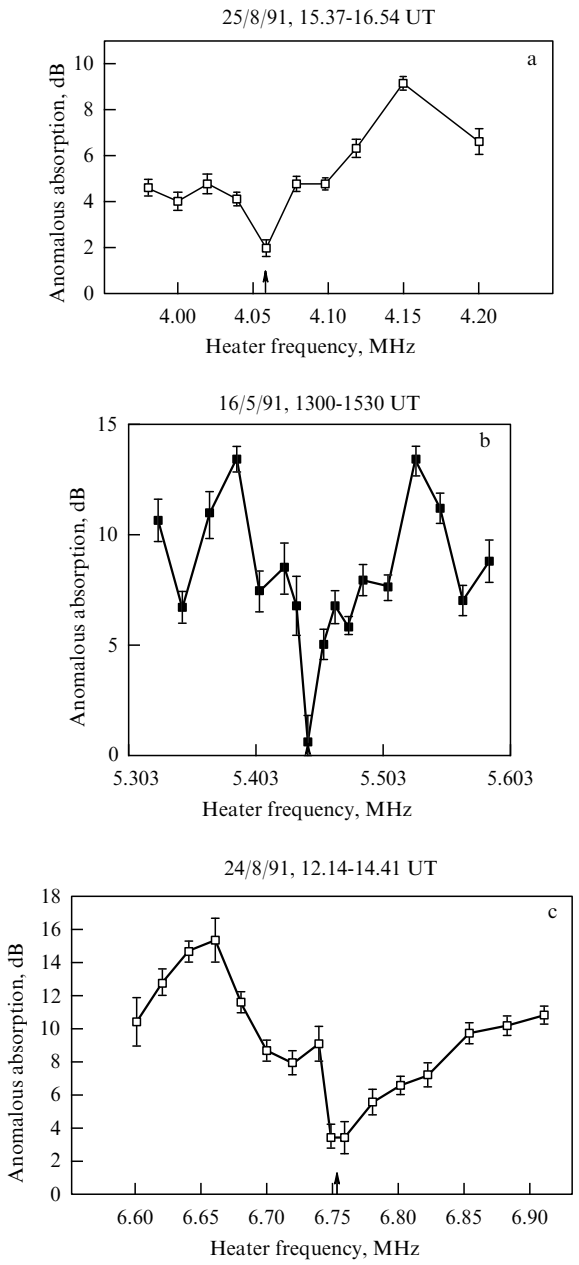

Figure 27. *Anomalous absorption of radio waves in the vicinity of double gyroresonance*. Observational results on anomalous absorption of radio waves in the vicinity of the third (a), fourth (b), and fifth (c) gyroresonances at the Tromsö station. Effective transmitter power $PG = 210-230$ MW. On the abscissa the disturbing wave frequency in the vicinity of the third gyroresonance $3f_H = 4.06$ MHz (a), fourth gyroresonance $4f_H = 5.443$ MHz (b), and fifth gyroresonance $5f_H = 6.76$ MHz (c) is plotted. The resonance point is shown by the arrow. On the ordinate the anomalous absorption of radio waves shifted 50–70 kHz relative to the disturbing station frequency is plotted. A sharp decrease in anomalous absorption near the resonance frequency is apparent. The bandwidth of the change in anomalous absorption in the neighborhood of resonance is ±50 kHz, i.e., 1% of the resonance frequency (results by Stubbe, Honary, Stocker, Robinson, and Jones [52, 62]).

Results of theoretical evaluation presented in Fig. 26b hold for the case of flat wave absorption in the stationary horizontally homogeneous ionosphere. The real ionosphere contains horizontal irregularities and alters with time, with the beam of probing radio waves being distinct from the flat wave. Moreover, normal (collisional) absorption of radio waves in the lower ionosphere can make a substantial contribution. It is therefore believed that the observational results presented are in excellent agreement with the theory (see Fig. 26b).

Fig. 26b presenting results of theoretical calculations and Fig. 27 showing experimental data. The two figures demonstrate that anomalous absorption is significantly reduced or totally disappears at the resonance point $\omega = n\omega_H$.

Naturally, field-aligned scattering of radio waves undergoes a similar change.

7.3 Broadband maximum of stimulated electromagnetic emission

Figure 28 presents results of experimental observations of the SEE spectrum at the varied disturbing station frequency in the neighborhood of gyromagnetic resonance [62]. To be concrete, SEE was measured near the fourth gyroresonance, $n = 4$. A totally similar picture was apparent near other resonances with $n = 3$, 5, 6, 7. The typical SEE picture described in Section 6 was observed at frequencies lower than the resonance frequency, $\omega < n\omega_H$. The emission spectrum was downshifted from the pump wave frequency; it had a well-apparent DM peak and a tail as long as 30–40 kHz. The picture changed as the pump wave frequency approached resonance, namely, the DM peak rapidly decreased. It disappeared at the moment of resonance, in good agreement with the disappearance of striations, and hence UH-turbulence.

At frequencies in excess of the resonance frequency, $\omega > n\omega_H$, the DM gradually recovers. However, the main feature here is the appearance of a new broad maximum in the SEE spectrum. This maximum lies *above the pump wave frequency* ω and thereafter shifts further forward as frequency ω increases. The effect of the broad upshifted maximum (BUM) in ionospheric radio emission spans approximately 100-kHz above-resonance frequency region. The BUM was discovered in 1983 by Thidé et al. [77] who immediately noticed that the ionospheric radio emission wave observed in the BUM could not be generated in a three-wave decay process because its frequency was higher than the pump wave frequency. A four-wave process was needed. The theory of this process was developed by several authors (S M Grach, Ya N Istomin, and some others) [78–80] and definitively formulated by J Huang, S Kuo, and H Zhou [81, 82]. The four-wave process includes interaction of a UH-wave (ω_1, k_1), the Bernstein mode (ω_2, k_2), powerful pump wave (ω, $k_0 = 0$), and a low-frequency electrostatic wave (ω_s, k). The principal relations of frequency and phase synchronism defining generation have the form

$$\omega_1 + \omega_s = \omega = \omega_2 - \omega_s\,, \qquad k_1 + k = 0 = k_2 - k\,. \qquad (2)$$

It can be seen that the frequency ω_2 of the Bernstein mode is always higher than that (ω) of the powerful pump wave. Critical fields shown in Fig. 29 fairly well correspond to experimental ones. Other peculiarities of BUM behavior also found an explanation. The UH-wave ω_1 generates a newly appeared downshifted maximum above resonance, while the BUM is determined by the Bernstein mode ω_2 alone (see Fig. 28).

7.4 Supersmall-scale elongated irregularities

It was shown in Section 7.3 that the BUM is given by generation of the Bernstein mode. The theory being in good agreement with experiment, all seems to be correct.

There is a problem, however. The theory considers the excitation of Bernstein modes, i.e., longitudinal waves as long as dozens of centimeters, whereas ground-based facilities record ionospheric radio emission or transverse electromag-

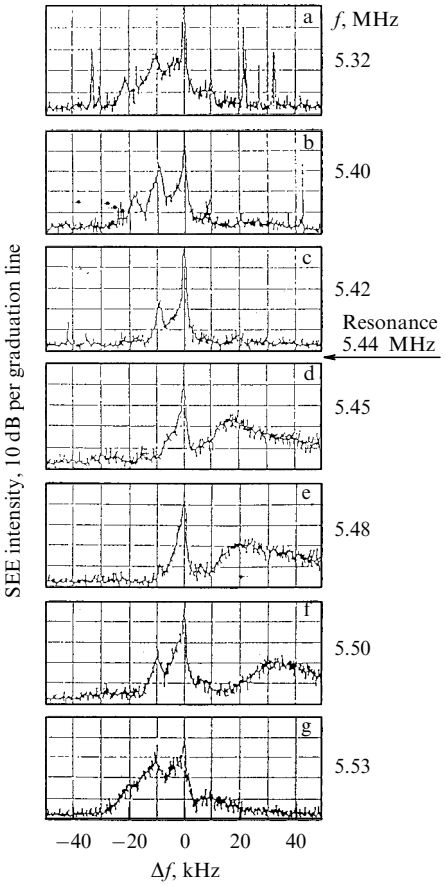

Figure 28. *Stimulated electromagnetic emission. Broad upshifted maximum* (*BUM*). Variations in the SEE spectra with alteration of the disturbing station frequency f in the vicinity of gyromagnetic resonance $f \sim 4f_H$ were examined in Tromsö experiment by Stubbe and co-workers [62]. Disturbing station power was $PG = 210$ MW, forth gyroharmonic frequency $4f_H \approx 5.44$ MHz. SEE spectra at different frequencies f of the disturbing station are presented. On the abscissa the SEE frequency shift $\Delta f = f_s - f$ relative to the station frequency is plotted. On the ordinate the intensity of the received signal (10 dB per graduation line) is plotted. Station frequencies f are shown on the right. At an f value lower than the resonance frequency, $f < 4f_H$ (a, b), peaks of intensity of only those signals being received that have a downshifted frequency, $f_s < f$, are pronounced. Both the first and the second downshifted maxima (DMs) can be seen. This radiation depends on the decay process alone (see Section 6 and Fig. 25). The DM sharply decreases close to resonance (c), totally disappears at the resonance point $f = 4f_H \approx 5.44$ MHz, and grows gradually again as the disturbing wave frequency f increases (d–f). Worthy of note is a new *broad* maximum of ionospheric radio emission that appears for $f > 4f_H$ and has a frequency higher than that of the disturbing station, $f_s > f$; this is the so-called broad upshifted maximum (d). The BUM further broadens and shifts up with a rise in the disturbing wave frequency f, that is, $f_s - f$ increases (e, f). However, the BUM begins to decrease for $f - 4f_H \geqslant 80$ kHz and gradually vanishes (g). The BUM appears as a result of the ionospheric excitation of the Bernstein mode during the four-wave decay process in the vicinity of a multiple gyroresonance. The frequency of the Bernstein wave is always higher than that of the disturbing station. The four-wave decay is essential near the resonance frequency nf_H in a range of $\delta f/f \leqslant 2\%$, where $\delta f = f - nf_H$.

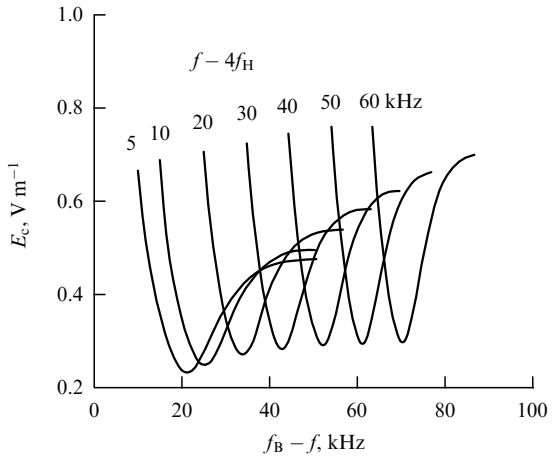

Figure 29. *Threshold electric field of excitation of the four-wave process.* Results of theoretical evaluation of threshold electric fields of four-wave parametric instability [82]. Instability occurs near multiple gyromagnetic resonance as a result of the double nonlinear decay process. This process involves two quanta (photons) of a powerful pump radio wave leading to simultaneous generation of a UH-wave (UH-'plasmon'), the Bernstein mode (Bernstein 'plasmon'), and two low-frequency LH-waves (LH-'plasmon').

On the abscissa the frequency shift of the Bernstein wave f_B relative to the pump wave frequency f is plotted. On the ordinate the threshold pump-wave field intensity for the four-wave decay process is plotted. The decay occurs only for $f_B > f$ and in a frequency region of $20 \leqslant f_B - f \leqslant 80$ kHz. The Bernstein mode is apparent in the SEE spectrum in the form of a broad upshifted maximum.

Threshold field intensities of four-wave instability are given for different $f - 4f_H$ shifts of the pump wave frequency from gyromagnetic resonance. The Bernstein mode appears only for $f > 4f_H$. Evidently, a rise in $f - 4f_H$ entails an increase in frequency $f_B - f$ at which the threshold field of generation of the Bernstein mode is minimal. In other words, the growth of $f - 4f_H$ is accompanied by a shift in the BUM location with respect to the pump wave frequency. These events are in excellent agreement with the observations shown in Fig. 28.

netic waves 50 – 60 m in wavelength — something of another kind. Therefore, the Bernstein mode should be one way or another transformed into such observable waves. The maximum of the observed radiation being very high (Fig. 28), transformation must be highly efficient. Meanwhile, its mechanism remains obscure. The matter is that strongly elongated ionospheric irregularities have a large scale, $d \sim 7-10$ m, while that of Bernstein waves is much smaller, $\lambda_B \sim 10-40$ cm. Hence, the Bernstein waves propagate adiabatically through irregularities, so that the linear transformation is exponentially small. This issue has recently been settled in the framework of the theory elaborated by Gurevich and Zybin [83]. The UH-wave plays an important role in the four-wave interaction generating Bernstein mode [see relations (2)]. It is not free but is trapped by an elongated irregularity. In other words, it is a standing wave with a stationary phase (Fig. 30), which is made up of two waves propagating in opposite directions. [10] Either of them, rightward or leftward, generates a Bernstein mode in the course of the linear four-wave decay process. Due to this, the Bernstein mode also produces a standing wave inside an irregularity. The standing Bernstein wave, similar to a UH-wave, has a large amplitude. Therefore, it forces out plasma from the regions of electric field maximum through the striction effect and thus creates plasma irregularities with a transverse scale of $\lambda_B/2$, and a longitudinal scale (along the magnetic field) of order 1 km. These are *supersmall-scale* (SSS) elongated irregularities measuring dozens of centimeters in the transverse direction. The linear transformation (scattering) of the Bernstein waves on SSS irregularities is responsible for the appearance of the broad upshifted maximum in stimulated electromagnetic emission. The observed intensity of the

[10] Notice that this fact is equally important in the three-wave decay process generating DM of ionospheric radio emission [68].

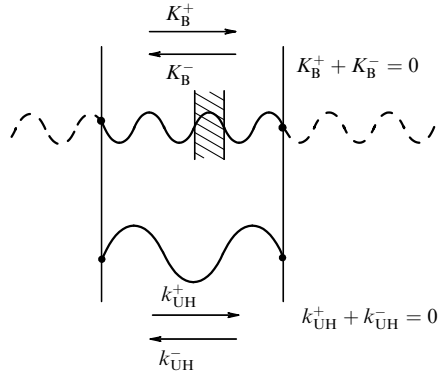

Figure 30. *Trapped waves in strongly elongated ionospheric irregularities.* A UH-wave is shown at the bottom. Trapping of UH-waves by irregularities plays an important role in *resonance instability* (see Section 5.1) at which UH-waves are intensely excited concurrently with the generation of strongly elongated ionospheric irregularities. In steady-state irregularities (Section 5.2), summation of two UH-waves traveling in opposite directions with wave vectors k_{UH}^+ and k_{UH}^- gives rise to a standing wave. The field vanishing condition at the boundaries $x = 0$ and $x = d$ of the irregularity: $E_{UH}^+|_{x=0} + E_{UH}^-|_{x=0} = 0$, $E_{UH}^+|_{x=d} + E_{UH}^-|_{x=d} = 0$, $d = 2\pi/|k_{UH}|$, specifies a strictly determinate relationship between wave phases with k_{UH}^+ and k_{UH}^-, and thereby creates the trapped standing UH-wave shown in the figure.

Generally speaking, Bernstein waves presented at the top of the figure propagate unobstructed in the ionospheric plasma. They are not trapped by irregularities. In our case, however, they are generated in the four-wave decay process where UH-waves play an important role. Each UH-wave with k_{UH}^+ and k_{UH}^- generates its own Bernstein mode (K_B^+ and K_B^-). Note that UH-waves are excited only within irregularities. This means that Bernstein modes also arise only inside irregularities. Both the relation between UH-wave vectors, $k_{UH}^+ + k_{UH}^- = 0$, and their phase ratio are transferred to the Bernstein waves: $K_B^+ + K_B^- = 0$, $E_B^+|_{x=0} + E_B^-|_{x=0} = 0$, $E_B^+|_{x=d} + E_B^-|_{x=d} = 0$. As a result, a standing Bernstein wave appears in a strongly elongated ionospheric irregularity, as shown by the solid line at the top of the figure. Plasma is forced out from the region of the maximum of the Bernstein wave field modulus, giving rise to SSS irregularities (one of them is shown by hatching).

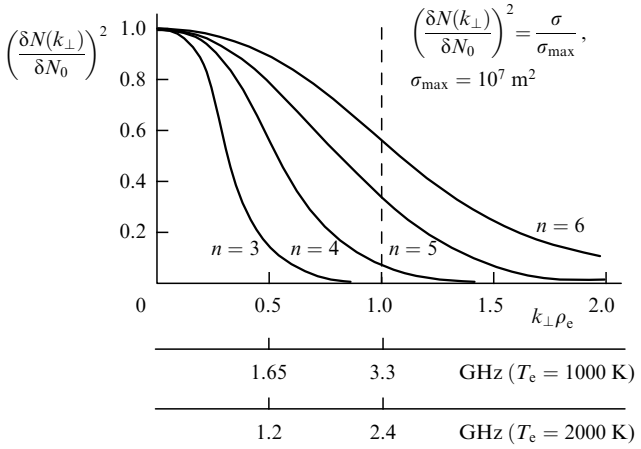

Figure 31. *Spectrum of supersmall-scale (SSS) fluctuations and scattering of UHF radio waves.* The figure shows a spectrum of SSS fluctuations and a cross section of UHF wave scattering on them. Here, $k_\perp = 2\pi/d_\perp$ is the wave vector of SSS fluctuations, $d_\perp$ is the scale of fluctuations across the Earth's magnetic field, and $\rho_e = \sqrt{T_e/m\omega_{He}} = \sqrt{T_e c/eH}$ is the Larmor electron rotation radius. $\delta N(k_\perp)$ is the magnitude of fluctuations, and $\delta N_0 = \delta N(k_\perp = 0)$. The curves correspond to different gyromagnetic resonances whose numbers n are given in the figure. It can be seen that the SSS fluctuation spectrum stretches towards smaller scales as n increases. SSS irregularities may result in effective scattering of radio waves, including UHF waves ($f > 300$ MHz). Scattering cross section $\sigma(k_\perp)$ is proportional to quantity $(\delta N_1(k_\perp)/\delta N_0)^2$ on the ordinate axis. Maximum scattering cross section σ_{max} is achieved as $k_\perp \to 0$. It is estimated that $\sigma_{max} \sim 10^7$ m^2. Additional abscissa axes show scattering frequencies of UHF radio waves. Because the scale of irregularities and, accordingly, scattering depend on the Larmor electron rotation radius $\rho_e \sim \sqrt{T_e}$, the figure has two additional abscissa axes for electron temperatures in the ionosphere, $T_e = 1000$ K and $T_e = 2000$ K. This shows that SSS irregularities may result in efficacious scattering of radio waves with a very high frequency of up to 1–3 GHz. The frequency of the scattered waves increases with an increase in the number n of multiple gyroresonance.

scattered signal was used to estimate plasma density fluctuations in SSS irregularities: $\Delta N/N \sim 10^{-3}$ or $\Delta N \sim 3 \times 10^2$ cm^{-3}. These values are consistent with the estimate of the Bernstein mode amplitude excited in the four-wave interaction.

7.5 Field-aligned scattering of ultrahigh-frequency radio waves

Supersmall-scale elongated irregularities responsible for certain peculiarities of SEE near multiple gyroresonance may cause other effects, too. The main one is a strong field-aligned scattering of UHF radio waves. The results of relevant computations are presented in Fig. 31. They show that radio waves of very high frequency, up to 1–3 GHz, may undergo strong scattering whose maximum cross section σ_{max} is derived from the estimates of small-scale fluctuations in plasma density, $(\Delta N/N)^2 \sim 10^{-5}$, as described in the previous Section 7.4. The estimation gives very strong scattering: $\sigma_{max} \sim 10^7$ m^2. Nevertheless, it is much weaker than the enhanced field-aligned scattering of UHF radio waves on stationary strongly elongated ionospheric irregularities. At the same time, the frequency range of this effect is an order of magnitude higher. Other features of the effect predicted in Ref. [83] are listed below.

(1) SSS irregularities arise inside strongly elongated irregularities that result from heating electrons by resonantly excited UH-waves. Therefore, electron temperature inside the irregularities is 2–3 times higher than its mean value. Temperature gradients are responsible for the appearance of the quasistationary electric field. Small-scale irregularities drift in this field with a speed of 30–100 m s^{-1}. This speed determines the Doppler width of the frequency spectrum of radio waves scattered on SSS irregularities.

(2) A sharp switch-on of the disturbing station makes SSS irregularities grow together with strongly elongated irregularities. Hence, their growth times are of the same order (1–10 s). In contrast, a sharp shutoff makes SSS irregularities, due to striction processes, disappear within 50 ms or faster, whereas strongly elongated irregularities live as long as 10 s or even more. This accounts for hysteresis effects showing themselves in UHF scattering during manipulation with 'on' and 'off' periods of the disturbing station.

7.6 Field-aligned scattering of high-frequency radio waves near multiple gyroresonance

Field-aligned scattering of high-frequency (HF) radio waves near the multiple gyroharmonic, illustrated in Fig. 32, was calculated based on the theory [83]. It must contain two components: one of which is determined by stationary strongly elongated irregularities, and the other by SSS irregularities. Their properties may be quite different, as shown in Section 7.5.

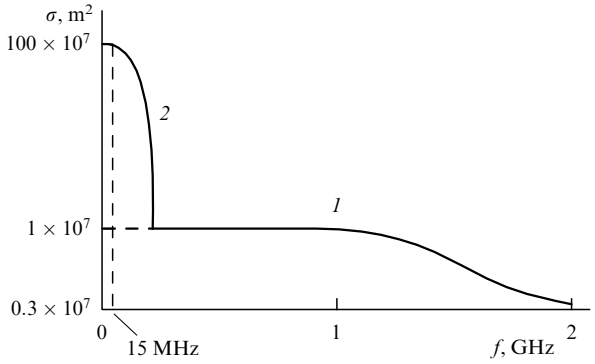

Figure 32. *Field-aligned scattering of HF radio waves near multiple gyroresonance*. Field-aligned scattering of HF radio waves in the vicinity of a gyroharmonic depends on two processes: scattering on stationary strongly elongated irregularities, and scattering on supersmall-scale (SSS) irregularities. Shown in the figure are cross sections σ of both processes as a function of the scattered wave frequency f. Curve *1* corresponds to standard scattering on striations, curve *2* to scattering on SSS irregularities. The characteristic frequency of HF radio waves (15 MHz) is denoted by the dashed line. Obviously, standard scattering of HF radio waves on striations predominates. However, an additional scattering component arises due to the presence of SSS irregularities. Its interesting features are a broader Doppler spectrum, rapid disappearance after the station is turned off, etc. They help to distinguish this component and to examine it separately.

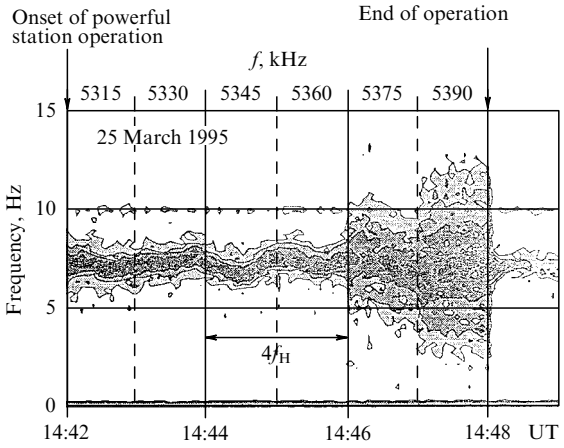

Figure 33. *Doppler spectrum of an HF signal scattered in the vicinity of the fourth gyroresonance*. Time-dependent changes in the Doppler spectrum of a 15-MHz signal undergoing aspect scattering [84]. The ionosphere was disturbed by the Sura station with the effective emission power $PG = 150$ MW. The powerful transmitter was programmed to be 'on' for 6 min, and 'off' for 1 min. Its frequency was varied simultaneously. A 15-MHz HF radio wave was continuously transmitted from Moscow, and the spectrum of the signal scattered in the disturbed ionosphere over Sura (aspect scattering spectrum) was analyzed with the world's largest UTR-2 radiotelescope in Khar'kov. The abscissa axis shows the exact time of one working cycle of the transmitter: switched on at 2:42 pm, switched off at 2:48 pm. The upper scale depicts variations in the transmitter frequency f, which increased at a rate of 15 kHz per min. The frequency passed through the fourth gyroresonance region ($4f_H \approx 5.35$ MHz) at a time close to 2:45 pm. The ordinate axis shows a dopplerogram of the radio signal obtained with the radio telescope. Signal power levels spaced 12 dB apart are depicted by color gradation. The overall shift (7 Hz) of the signal is due to the general drift of the disturbed ionospheric region. The width of the Doppler spectrum of the scattered signal is not very large at frequencies of the disturbing station below the gyroresonance frequency. It increases considerably (5-fold and more) after passage through the resonance at 2:46-2:48 pm. At the end of transmitter operation (2:48 pm), the signal width sharply decreases; only a narrow signal remains for a minute, during which its intensity gradually drops.

The first experimental study on field-aligned scattering of HF radio waves in the fourth gyroresonance region was reported by Ponomarenko, Leyser, and Thidé [84] in 1999. The ionosphere was disturbed by the Sura station, and the scattered 15-MHz radio signal was analyzed with the world's largest UTR-2 HF radiotelescope (Khar'kov). The observational results are presented in Figs 33, 34. The frequency of the disturbing Sura station grew slowly near the fourth gyroresonance. Figure 33 displays the Doppler spectrum of the scattered signal. Its half-width below resonance (for $f < nf_H$) is 0.1 – 0.2 Hz, meaning that field-aligned scattering occurs on highly stable, quasistationary, strongly elongated irregularities. However, the Doppler spectrum markedly enlarges to 2 – 3 Hz, as gyroresonance ($f > nf_H$) is passed. This suggests an important contribution to field-aligned scattering from irregularities, the speed of which amounts to dozens of meters per second. Analysis of the above observations leads to the conclusion that two components of field-aligned scattering arise in the region with $f > nf_H$ (see Fig. 34). The narrow one is produced by strongly elongated irregularities, as usual, while the wide component has a smaller amplitude (by approximately 10 dB) but an almost 5 times broader spectrum. Spectrum broadening is in line with the velocity of motion of SSS irregularities. The 10-dB difference of intensities is also consistent with the maximum scattering cross section ratio: 10^8 m^2 for quasistationary irregularities (see Section 4.1, Fig. 11), and 10^7 m^2 for SSS irregularities (see Section 7.5, Fig. 31). The two components fall at totally different rates after the disturbing station is sharply turned off (Fig. 33). The wide component rapidly vanishes (within the limits of sensitivity of the measurements, 70 ms), whereas the narrow one lives dozens of seconds longer as befits components conditioned by strongly elongated irregularities. Similar phenomena were observed by Frolov, Yampol'sky, Vertogradov et al. [85] in a study of field-aligned scattering after ionospheric disturbance by the Sura station in 2004. The scattering was measured at two frequencies and in two locations: Rostov-on-Don (10 MHz), and Khar'kov (15 MHz). Thus, excitation of SSS irregularities was confirmed not only by observation of the BUM component in the SEE spectrum, but also by direct measurements of field-aligned scattering of HF radio waves in the multiple gyroresonance region. For all that, *direct experimental evidence of HF-wave scattering* is needed to prove conclusively the existence of this interesting physical phenomenon.

7.7 Electron acceleration at multiple gyroresonance

There is little doubt that strong cyclotron acceleration of electrons at major resonance at $\omega = \omega_H$ took place when the powerful wave of the Moscow pulse facility reached the ionospheric F-layer at nighttime (see Section 3.1) [14, 19]. However, no observable evidence of electron acceleration was obtained for the lack of necessary diagnostic tools. [11]

Early experimental studies of the effects of powerful radio emission at the second harmonic, $f = 2f_H$, were conducted at the Platteville station. P Fialer was the first to demonstrate substantial strengthening of enhanced field-aligned scattering near the second gyroresonance [29]. In 2004, extensive studies at $f = 2f_H$ were initiated by Djuth et al. [86] based at HAARP

[11] Artificial glow was seen in the D- and E-layers [16], probably due to direct heating of electrons in the ionosphere.

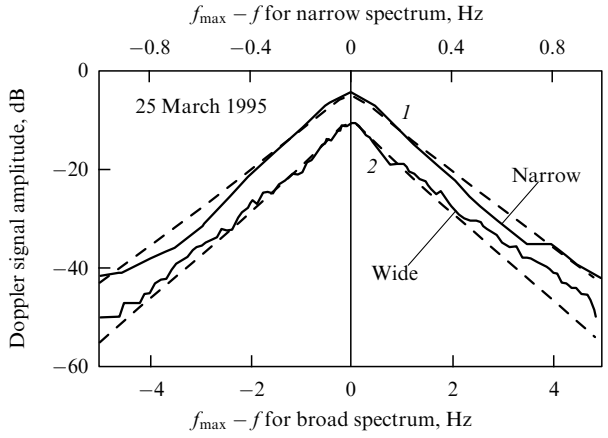

Figure 34. *Graphical shape of two Doppler spectrum components of a scattered signal*. The shapes of Doppler spectrum lines of two scattered signal components near the fourth gyroresonance are presented (taken from Ref. [84]). The ionosphere was disturbed by the Sura station at frequencies close to the frequency of the fourth gyroresonance, $f \approx 4f_H \approx 5.35$ MHz. A 15-MHz radio wave underwent resonance scattering. Two components are clearly distinct in the scattered signal spectrum for $f > 4f_H$. The spectrum shape of either component is deduced by a 60-s averaging of the observed signal for $f < 4f_H$ and $f > 4f_H$. For $f < 4f_H$ ($f = 5.13$ MHz), the spectrum is represented by a narrow line (curve *1*); for $f > 4f_H$ ($f = 5.390$ MHz), the wide component is also apparent (curve *2*). Dashed curves demonstrate exponential filtering of both signals. Lower and upper abscissa axes show the frequency shift $f_{max} - f$ from the scattered signal maximum for wide and narrow components, respectively. On the ordinate the relative amplitude of the scattered radio signal normalized to the maximum amplitude of the broad spectrum is plotted. The spectrum lines are similar in shape, but the wide line is 5 times broader than the narrow one. The amplitude of the narrow line in the maximum ($f_{max} - f = 0$) is almost 10 times higher than that of the wide line. Nevertheless, the wide line is well apparent on the dopplerogram (see Fig. 33), whereas the narrow one sharply (exponentially) decreases with frequency, in agreement with theoretical predictions [83] (see Fig. 32). It is therefore supposed that the observed wide spectral component in the signal from aspect scattering of an HF radio wave is due to the scattering on supersmall-scale irregularities.

station. The authors observed strong electron acceleration and resonant excitation of UH-waves.

These data agree with theoretical predictions: both resonant enhancement of UH-wave excitation and electron acceleration must take place near the second harmonic [38, 87] (see also the caption to Fig. 26, where the term in Eqn (I) responsible for the resonance amplification of UH-waves near the second gyroharmonic is labelled by the upper curly bracket). For higher harmonics, $\omega/\omega_H = 3, 4, 5, \ldots$, the theory predicts acceleration of electrons by Bernstein waves [87, 88]. The magnitude of this effect strongly depends on the presence of SSS irregularities. Experimental data on the electron acceleration effect at multiple gyroresonance remain to be obtained. Further detailed studies of this phenomenon are needed, both in theory and experiment.

8. Nonlinear phenomena at Langmuir resonance

8.1 Langmuir turbulence

As mentioned above (Section 4.3), Langmuir resonance $f = f_L = \omega_L/2\pi$ is achieved near the reflection point of an ordinary radio wave of frequency f directed vertically up to disturb the ionosphere. Let us recall that the Langmuir frequency f_L is identified with the frequency of natural electron oscillations of the plasma, directed along the Earth's magnetic field **B** (see Fig. 12). The electric field of a powerful radio wave **E** in the vicinity of the reflection point is parallel to field **B**. It was shown that *parametric* instability can be induced in such a field [Silin [89, 90] (1965), DuBois and Goldman [91] (1965)]. This instability is a combined aperiodic and periodic three-wave process. Two electron plasma waves (k^+ and k^-) traveling from opposite directions, $k^+ + k^- = 0$, are generated in the aperiodic process; in fact, a standing plasma wave is set up. In periodic decay instability, both electron and ion plasma waves are generated simultaneously. The downward shift of the electron plasma wave frequency relative to that of the pump wave is compensated for by the ion wave frequency.

Excitation of plasma waves in the ionosphere is easily observable with the help of incoherent scattering radars. The first nonlinear oscillation spectra of plasma waves were obtained at Arecibo by W Gordon and co-workers [28, 29] in 1971. Figure 35 exemplifies the observations made at Tromsö. The first peak corresponds to excitation of the standing Langmuir wave with a frequency strictly equal to the plasma frequency ω_L. It results from the aperiodic component of instability. The second peak is due to the periodic instability component. Here, the plasma wave frequency is shifted downwards as much as the ion oscillation frequency. Also shown are the subsequent decay processes: the first harmonic appears followed by the second one, etc. Each time, the decay occurs into plasma and ion-acoustic waves. A plasma wave resulting from the first decay has a very large amplitude. The peak is higher by 20 dB, i.e., a hundred times, than the neighboring minimum. The width of the peak increases in subsequent decays, but its height above the minimum lowers. The cascade spectrum of Langmuir waves, shown in Fig. 35a, is characteristic of the so-called 'weak' turbulence. Other spectra are also observed but they have no cascade structure (Fig. 35b). They correspond to 'strong' turbulence [92, 93].

Certain features of the time evolution of Langmuir turbulence are worthy of note. Sharp switching of the disturbing station causes rapid excitation of Langmuir waves, accompanied by very efficacious pump wave absorption. Simultaneously, it induces strong stimulated electromagnetic emission. However, this strong Langmuir effect is of short duration; it lasts some 100 ms. The fact is that the Langmuir layer is underlain by the UH-resonance region where the developing strongly elongated irregularities begin to gradually (after 0.5 – 5 s) govern anomalous absorption of radio waves. This leads to a decrease in pump wave intensity in the Langmuir resonance region and a consequent attenuation of Langmuir turbulence processes. Effects at the initial stage of evolution of ionospheric turbulence have been experimentally investigated by many authors [57, 63, 70 – 74, 94 – 96].

8.2 Cavitons

Very strong excitation of plasma waves at the Langmuir resonance due to nonlinear processes may be accompanied by perturbations of the distribution of mean plasma concentration and the formation of so-called cavitons.

The process of caviton formation is fully analogous to the formation of strongly elongated irregularities described in Section 5.1. The difference is the pump-wave electric field and the plasma oscillation field at Langmuir resonance are

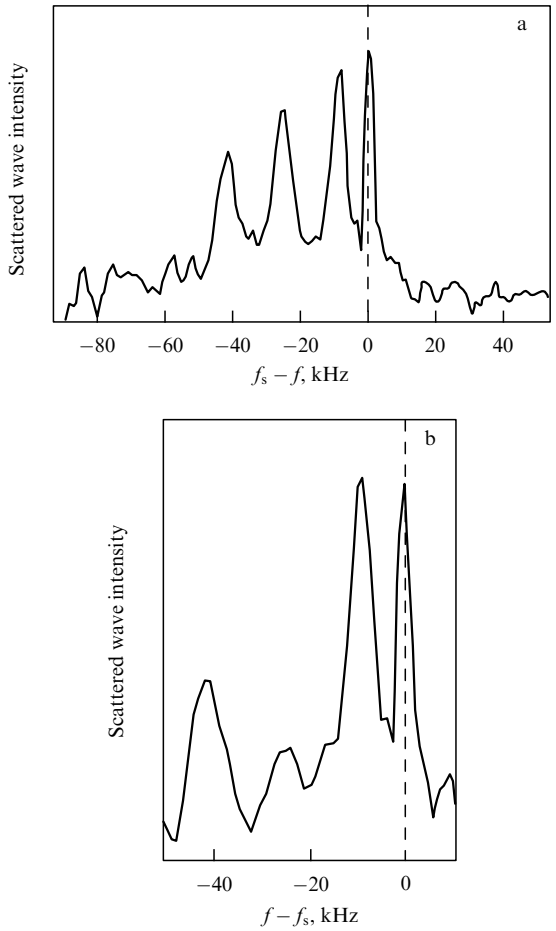

Figure 35. *Langmuir turbulence*. (a) Spectrum of plasma waves excited in the ionosphere in the reflection region of the disturbing O-wave emitted by the Tromsö station [92]. Transmitter effective power $PG = 200$ MW, and frequency $f = 5.7$ MHz. Plasma waves were recorded by incoherent scattering radar. On the abscissa the quantity $f_s - f$ is plotted, i.e., shift of the scattered signal frequency f_s with respect to the pump wave frequency f. On the ordinate the intensity of the scattered wave is plotted. It can be seen that the main scattering peak maximum corresponds to the zero frequency shift shown by the dashed line. This peak is produced by standing plasma waves excited as a result of aperiodic parametric instability. They have a frequency identically coinciding with the frequency of Langmuir oscillations: $f_s = f_L = f$. The next peak results from the decay into electron and ion waves. It arises due to periodic parametric instability and is downshifted as much as the ion-sound wave frequency. Other pronounced peaks are produced by a cascade of second and third decays. They are followed by a smeared tail. It is evident that plasma oscillations excited in the Langmuir resonance region in this example of 'weak' turbulence have a cascade structure: it has well-apparent peaks and extends downwards over a frequency range of 100 kHz. (b) Example of 'strong' turbulence spectrum from the Tromsö experiment. Only first peaks of aperiodic and periodic parametric instabilities are pronounced here. The spectrum exhibits a broad plateau with random excursions instead of a regular cascade structure.

polarized along the magnetic field in contrast to the situation at UH-resonance. Consider a case of producing plasma density irregularity in the form of a density dip in the plane perpendicular to the magnetic field. The pump field then excites plasma oscillations in this irregularity. In other words, the density dip or caviton at Langmuir resonance functions as a resonator in which the electric field of a powerful radio wave resonantly pumps plasma waves. Striction forces deepen the density dip, and pumping gains. The process of caviton generation and growth is a sequel to 'modulation' instability [97, 98] described by Zakharov equations in the hydrodynamic approximation [99].

Cavitons are layers of plasma density irregularities across the magnetic field. The transverse scale of these inhomogeneities is on the order of ten Debye radii, i.e., some 10 cm under conditions of the ionospheric F-layer. According to the strong turbulence theory in the *hydrodynamic* approximation, cavitons gradually evolve under the effect of the pump wave field and accumulate plasma waves; this process is accompanied by plasma forcing out. Cavitons become deeper, shrink, and finally collapse [100]. This process is known as Zakharov collapse.

8.3 Caviton stabilization

The nonlinear *kinetic* theory of evolution of plasma turbulence at the Langmuir resonance is based on the results of both analytical and numerical approaches [101 – 106]. It is important that the total thickness L of the Langmuir resonance region in the ionospheric F-layer is on the order of the disturbing wave length near the reflection point, which is around 100 m and smaller than the electron mean free path. Therefore, particle collisions may be neglected in the description of electron and ion kinetics in the Langmuir resonance layer in the first approximation. Figures 36, 37 present the results of numerical solutions to the compatible system of collisionless kinetic equations for electrons and ions and the equation for the electric field [106]. As evident from Fig. 36, the parametric instability induced by the external electric field of the pump wave leads to an exponential growth of the electric field energy ε_f of plasma oscillations. Simultaneously, the kinetic energy ε_e of electron oscillations increases and becomes equal to a large part of their thermal energy (up to 30 – 50%). The exponential field growth stops after characteristic time $t \sim 1/\gamma_m$ inverse to the increment γ_m of modulation instability [98]. The instability causes density dips or cavitons to appear (Fig. 37). The figure shows strong plasma disturbance in cavitons, on the order of $(0.2-0.4)\,N$. The cavitons are quasineutral, since electron and ion number densities in them are very similar. They have a width $a \approx 15-20\,\lambda_D$, and the characteristic distance between them is $d \approx 50\,\lambda_D$. Here, $\lambda_D = v_T/\omega_L$ is the Debye radius, $v_T = \sqrt{2T_e/m}$ is the electron thermal velocity, and $\omega_L = 2\pi f_L$ is the angular frequency of Langmuir oscillations. Naturally, regions of most strongly excited cavitons and of the maximum pump-field amplitude $E_0(x)$ overlap. There is a strong correlation between plasma density dips and the mean energy of plasma oscillations trapped in cavitons (see Fig. 37). The caviton-trapped wave is a standing one, i.e., it has a fixed oscillation phase. However, various cavitons are significantly different in terms of oscillation phases. This fact ensures effective transfer of oscillation energy to fast plasma electrons.

The caviton depth sharply increases at the initial period (up to $t \approx 2/\gamma_m$). Thereafter, the growth of cavitons slows down; at $t \sim (5-10)\,\gamma_m^{-1}$, the system of cavitons gives rise to a sort of ion-acoustic density wave with an amplitude of 0.2 – 0.3. Density minima are filled up with plasma oscillations having a high enough amplitude (E^2) of electric field oscillations (see Fig. 37). Thus, cavitons stabilize rather than collapse in the kinetic problem under consideration, because accelerated electrons absorb the energy of plasma oscillations excited by the pump wave in density dips. The process of electron acceleration and electron interaction with cavitons is described at greater length in Section 8.4.

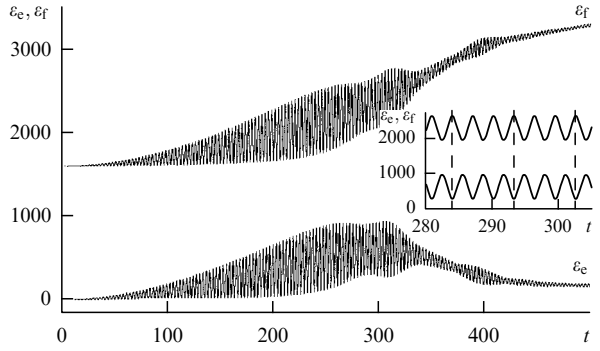

Figure 36. *Evolution of parametric instability* (*kinetic theory*). Variations in electric field energy ε_f and kinetic energy ε_e of electron oscillations with time t during development of parametric instability in plasma. On the abscissa the time t in units of ω_L^{-1} is plotted, where ω_L is the Langmuir frequency of plasms oscillations. On the ordinate the total electric field energy ε_f and kinetic energy ε_e of oscillations are plotted. The field energy is the sum of the energies of the external pump field, oscillations, and cavitons. It can be seen that the energy of plasma oscillations and the kinetic energy of electron oscillations grow exponentially with the onset of parametric instability (instant $t = 0$). The inset shows that rapid field (ε_f) and electron (ε_e) fluctuations are strictly in antiphase. By the time $t_c \sim 250/\omega_L$, corresponding to the characteristic increment of modulation instability [98, 99], $t_c \sim \gamma_m^{-1}$, the exponential growth of ε_f and ε_e first slows down; thereafter, they settle at a certain (rather low) level.

Solution of the compatible system of collisionless kinetic equations for electrons and ions with the Poisson equation for the electric field in the accelerating plasma layer of scale L was obtained [106] by the particle-in-cells method using some 10^7 particles. The external field $\mathbf{E}(x)\sin\omega t$ exciting plasma instability was taken as a given. The boundary conditions for the external field in the layer L were assumed to be periodic. The scale of the layer $x = 1000\,\lambda_D$, where λ_D is the Debye radius. Conditions at the boundaries of the accelerating layer for the electron distribution function were found by solving the kinetic equation outside the layer. This solution takes into account the electron collisions with neutral molecules and ions outside the layer. Collisions repeatedly return fast electrons back into the accelerating layer, as apparent from the considerable pumping of their energy into the high-energy tail of the distribution function. The altered character of growth of ε_f and ε_e oscillations for $t > t_c$ is related to the appearance and evolution of cavitons; the gradual decrease in oscillations to the lower quasistationary level is due to the formation of a quasi-stationary ion-acoustic wave (see Section 8.4).

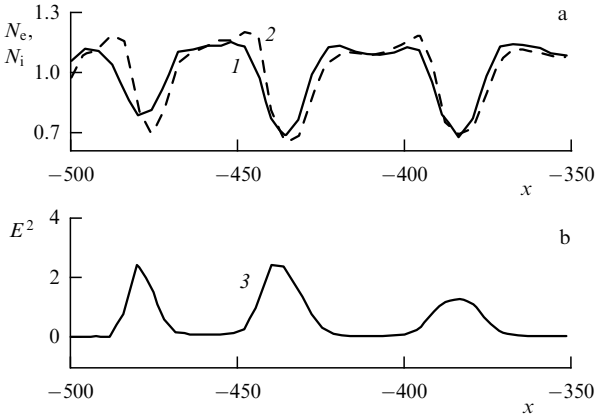

Figure 37. *Caviton structure*. Results of the simultaneous numerical solution of a system of kinetic equations and the equation for the electric field in the accelerating layer in the developed nonlinear phase $\omega_L t \sim 300-400$. (a) Distribution of electron (solid line) and ion (dashed line) concentrations normalized to average plasma number density N over a section $-500 \leqslant x/\lambda_D \leqslant -350$ of the accelerating layer at instant $\omega_L t = 350$. (b) Energy distribution of the electric field of plasma oscillations at the same section and time instant.

Modulation instability that developed by the time $\omega_L t = 350$ resulted in forming a system of cavitons (plasma density dips) in the accelerating layer. Density disturbances in cavitons are as deep as 30–40% of the mean plasma density. In this case, the cavitons are quasineutral, since electron and ion densities in them are very similar. They have an average size of $15\,\lambda_D$, and the mean distance between them is $40-50\,\lambda_D$.

There is a strong correlation between energy density peaks E^2 of electric field oscillations and caviton location. Plasma oscillations are resonantly pumped in density dips by the powerful pump-wave field $E_0(x)$. Plasma oscillations are trapped in cavitons, and the oscillation electric field in each caviton has a fixed phase. However, field oscillations in different cavitons occur independently, and their phase relations are random. This fact influences the acceleration of fast electrons by the electric field of plasma waves trapped in cavitons.

It should be noted that calculations were also made with allowance for thermal electron collisions in the Langmuir layer. Their results testify to the fact that taking account of collisions leads to electron heating and damping of plasma oscillations (a decrease in caviton amplitude). Heating results in a substantial loss of energy by the pump wave, up to 30% under ionospheric conditions.

8.4 Multiple electron acceleration

As shown above, the electric field of plasma oscillations is sharply strengthened in each caviton. Meanwhile, it is well known that plasma waves can transfer their energy to electrons by the Landau damping mechanism. Local acceleration occurs as traveling electrons cross cavitons; it has a diffusive character. The magnitude of acceleration is determined by a correlator of the plasma oscillation electric field (Fig. 38). It is obvious that the correlator has pronounced maxima at caviton locations. An important feature of this acceleration mechanism is an involvement of only those electrons that have a sufficiently high velocity v, for which the length $\lambda = v/\omega_L$ is greater than the scale a of a caviton. In other words, only electrons in the tail of the distribution function are accelerated. On the other hand, slow (thermal) electrons adiabatically oscillate in cavitons and do not absorb the field energy. The borderline between fast and slow electrons is given by the effective caviton width $a \approx 15-20\,\lambda_D$.

However, the acceleration process under ionospheric conditions does not stop at this stage. As mentioned above, the accelerating plasma layer is thinner compared to the electron mean free path. Due to this, electrons accelerated in this layer and underwent scattering by collisions outside it may enter accelerating layer anew and increase their energy as they pass through it. This process repeats itself a number of times. The energy of fast electrons grows until its fraction lost in collisions equals that acquired in the accelerating layer. Repeated passage of electrons through the Langmuir turbulence layer significantly strengthens the acceleration effect, and the size of the region occupied by the accelerated electrons increases many times, amounting to dozens of kilometers [107, 108].

The result of the numerical solution taking account of electron multiple scattering is presented in Fig. 39. It appears that the initial Maxwellian distribution of electrons is rapidly distorted (the tail of fast electrons lengthens). It may be characterized by an effective temperature T_{eff} 50–100 times higher than the initial temperature T_{e0}: $T_{eff} = 5-10$ eV at $T_{e0} = 0.1-0.2$ eV [107]. The number of such strongly accelerated electrons is small (1% or even less of the total number of particles). Nevertheless, their total

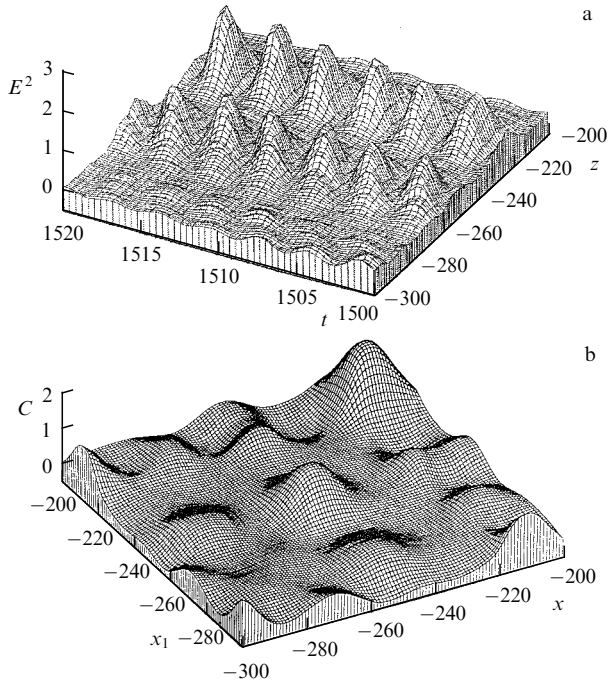

Figure 38. *Steady-state energy and correlator of plasma oscillation electric field.* (a) Spatial (x) and temporal (t) distributions of the electric field energy of steady-state electron plasma oscillations. On the abscissa the spatial scale x normalized to the Debye radius λ_D and time t normalized to ω_L^{-1} are plotted. On the ordinate the electric field energy of plasma electron oscillations, normalized to the plasma thermal energy, is plotted. The electric field fluctuates in time with the Langmuir, viz. electron (plasma), frequency. In space x, field fluctuations are trapped by the system of cavitons, forming a quasistationary ion-acoustic wave with a characteristic length of about $50\,\lambda_D$. (b) Correlator $C(x; x_1; t) = \langle E(x, t_1)\, E(x_1, t + t_1)\rangle_{t_1}$ of electric field oscillations. Averaging is over the ensemble of field E oscillations. The correlator has pronounced maxima at caviton locations. It determines diffusive electron acceleration by plasma electron oscillations trapped in the cavitons. Only fast electrons are accelerated. In steady-state conditions, the distribution function of accelerated electrons for $\varepsilon \gg T_{e0}$, where T_{e0} is the thermal electron temperature in the plasma, may be roughly presented in the form [106, 108]

$$f \approx f_0 \exp\left(-\int_{\varepsilon_0}^{\varepsilon} \frac{d\varepsilon}{T_{\rm eff}(\varepsilon)}\right), \qquad f_0 = f(\varepsilon_0), \qquad \varepsilon_0 \gg T_{e0},$$

where

$$T_{\rm eff}(\varepsilon) = \frac{e^2}{\sqrt{\delta}} \sqrt{\frac{2\varepsilon}{m}} \int_0^L dx\, D\left(\sqrt{\frac{2\varepsilon}{m}}; x, t\right),$$

$$D\left(\sqrt{\frac{2\varepsilon}{m}}; x, t\right) = \int_{-\infty}^{t} dt_1 C\left[x; x - \sqrt{\frac{2\varepsilon}{m}}\,(t - t_1); t_1\right].$$

Evidently, the distribution function of fast electrons over energy ε has a quasi-Maxwellian character. Effective electron temperature $T_{\rm eff}$ in the tail of the distribution function is given by the electric field correlator averaged over the entire accelerating layer L. The multiple acceleration process is also of importance. It reflects small parameter δ (mean energy loss by an electron colliding with neutral molecules or ions outside the accelerating layer L of the ionospheric plasma) in the relationship for $T_{\rm eff}$. Under characteristic conditions of Langmuir turbulence excited in the ionosphere by powerful radio waves, one finds $T_{\rm eff} \sim 5-10$ eV. To compare, thermal electron temperature $T_{e0} \sim 0.1-0.2$ eV. In other words, the number of fast electrons in the perturbed region of ionospheric plasma exponentially increases due to their acceleration in the cavitons.

energy is comparable to the total energy of thermal particles.

Because the scale a of a caviton is an important parameter determining the total number of accelerated particles, it is also

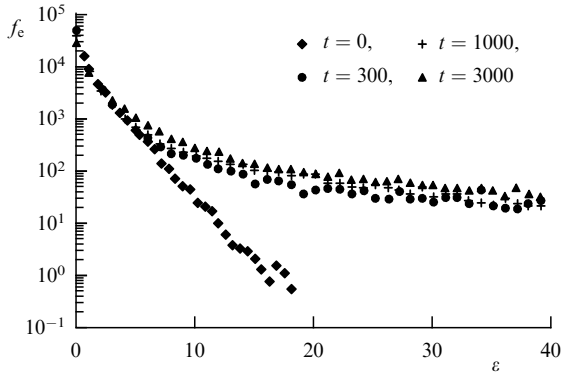

Figure 39. *Electron energy distribution function.* Results of numerical calculation of electron distribution function f_e in Langmuir turbulence [106]. On the abscissa the electron energy ε normalized to initial temperature T_{e0} is plotted. On the ordinate the f_e values at the logarithmic scale are plotted. Symbol ◆ is the initial distribution function, ●, +, ▲ correspond to the instants of time t shown in the figure in units of ω_L^{-1}. It is evident that effective electron acceleration in cavitons causes rapid extension of the distribution function tail. Effective electron temperature in the tail is 50 – 100 times higher than the initial temperature T_{e0}.

related to the general balance between energies spent to excite plasma oscillations in cavitons by the pump wave and to heat and accelerate electrons during plasma oscillations in cavitons. It is this balance that determines the effective scale a of a caviton. Thus, structural features of nonlinear Langmuir turbulence depend on a variety of processes proceeding both inside the accelerating layer and outside it in an extensive region of the surrounding collisional plasma.

Figure 40 exhibits results of direct observations of accelerated electrons in the ionosphere with the help of the unique Arecibo radar [109, 110]. It is the sole facility with which it is possible to directly observe fast electron pulses by recording the excited plasma waves (Fig. 40a). Figure 40b illustrates the energy dependence of the electron flux. The energy amounted to 18 – 20 eV. The measuring method used and the technical characteristics of the radar did not allow measurements outside the 9 – 18 eV range. The spatial scale of the region in which fast electrons were recorded was several dozen kilometers (Figs 40a, c). Fast electrons could be seen both above and below the accelerating layer, in excellent agreement with the multiple acceleration theory. Notice that electrons accelerated by a powerful station rather far from the affected region were observed for the first time by Carlson and co-workers in 1972.

8.5 Artificial ionospheric glow

Red (630 nm) and green (557 nm) lines are the most prominent features of optical emission from the ionosphere disturbed by powerful radio waves. Both lines are produced by excitation of atomic oxygen: $O(^1D_2)$ (red), and $O(^1S_0)$ (green). The red line is remarkable for the very low minimal level of excitation by an electron impact (1.96 eV). At the same time, red line emission corresponding to the $^1D_2 - {}^3P_2$ transition is delayed by $t_1 \approx 130$ s. Therefore, quenching of excited atoms by collisions with other atoms and molecules in the ionosphere becomes important. Hence the strong altitude dependence of the intensity of red line emission. For example, quenching is not very strong in the F-layer ($z \sim 300$ km) but practically eliminates red glowing in the E-layer ($z \sim 110-130$ km).

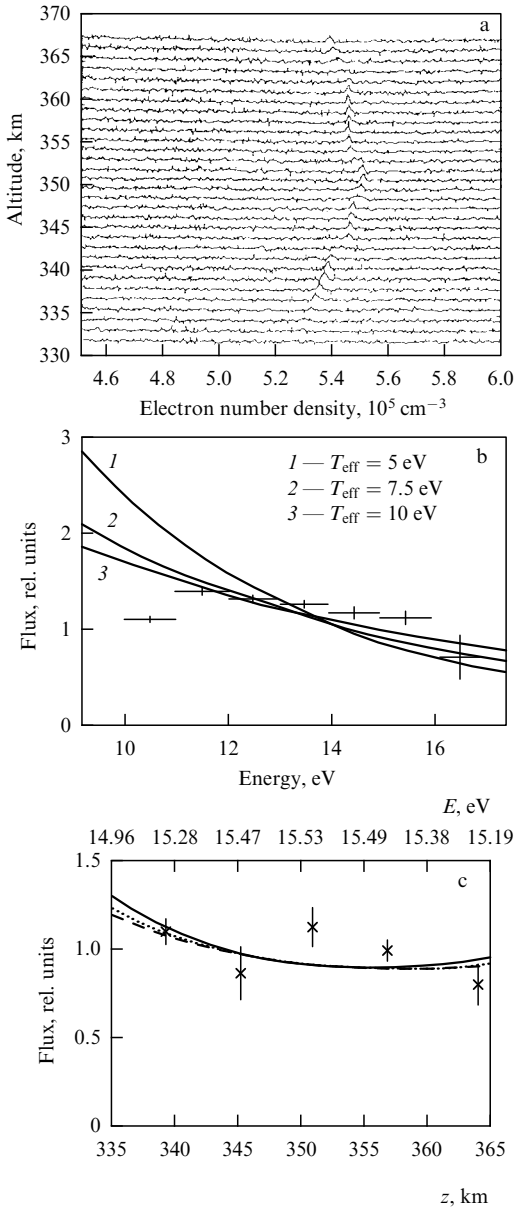

Figure 40. *Energetic electrons.* Results of direct observation of accelerated electrons in the ionosphere affected by a powerful radio wave. Observations were made with the Arecibo incoherent scattering radar with the wavelength $\lambda_r \approx 70$ cm (frequency 430 MHz). The radar permitted resolving plasma waves in a signal scattered by the ionosphere. The main scattered signal came from the waves with a vector directed toward the radar; wavelength λ_p satisfied the condition of spatial synchronism at the radar wavelength: $\lambda_p = (1/2)\,\lambda_r$. Assume that

$$\lambda_p = \frac{v_p}{f_p},$$

where v_p is the phase velocity of a plasma wave, and

$$f_p = \omega_L/2\pi = \sqrt{\frac{e^2 N(z)}{\pi m}}$$

is its frequency, and the wave is excited by a fast electron moving with the velocity v, i.e., $v_p = v$. Then, one obtains

$$v = v_p = f_p \lambda_p = \frac{1}{2}\,\lambda_r \sqrt{\frac{e^2 N(z)}{\pi m}}, \qquad \varepsilon = \frac{mv^2}{2} = \frac{\pi e^2}{m}\, N(z) \lambda_r^2 .$$

The radar determined plasma number density $N(z)$ with a high resolution in z.

(a) Observation of a scattered signal depending on altitude z in the ionosphere from which it comes. On the abscissa the ionospheric plasma density is plotted. The resonance signal from fast electrons is readily distinguishable through the noise. It is possible to find the energy of fast electrons at point z from the above relations, and their flux density from the amplitude of the main scattered signal. Figures (b) and (c) are plots of relative flux density versus energy (experiment [110]) and altitude (experiment [109]), respectively. The curves are calculated using formulas from [107, 108] (see caption to Fig. 38) for T_{eff} values shown in the figure. Clearly, the region exhibiting accelerated electrons is dozens of kilometers in altitude. The plasma line of fast electrons was observed immediately after shutoff of the powerful station. The signal gradually attenuated within 10–20 ms, in excellent agreement with the theory. The Langmuir turbulence region, i.e., the main region where electrons were accelerated while the transmitter was 'on', lay at the altitude $z = 285$ km in experiment [109], and $z = 295$ km in experiment [110]. Fast electrons (Figs 40a, c) could be detected dozens of kilometers from the acceleration region.

The green line is attributed to a higher minimal excitation potential (4.17 eV) and has a very small time delay. Therefore, its luminosity depends on collisional electron excitation alone.

Both emission lines excited when powerful radio waves affected the ionospheric F-layer were observed many times at all high-power facilities starting from the Platteville station [41, 42, 111–115]. Green line emission intensity is lower than the red one. Figure 41 exemplifies red- and green-line ionospheric glow observed at HAARP [44]. The results are on the whole consistent with the theory. Specifically, the scale of the emission region (some 10–30 km according to observations [46]) agrees with the estimates of the multiple acceleration theory.

Analysis of observational data and comparison with theoretical predictions reveal that red emission lines visible after disturbance of the ionosphere by low-frequency radio waves, $f \leqslant 4$ MHz, result from intense electron heating at UH-resonance, i.e., they appear as a sequel to a marked rise in electron temperature [45, 116, 117], whereas the green line emerges only in the case of electron acceleration at Langmuir resonance [103–106, 111, 114]. The same refers to red line luminosity under the effect of high-frequency radio waves, $f > 5$ MHz [45]. Improvement in the resolving power and sensitivity of photo cameras allowed other lines to be identified, having higher minimal excitation potentials, viz. 9 eV (777.4 nm), 11 eV (3436 nm), 19 eV (4278 nm) [86, 118]. Appearance of these lines suggest the presence of high-energy ionospheric electrons resulting from their multiple acceleration at Langmuir resonance. The most intense green line emission was observed in the E-sporadic layer (Kagan et al. [119]). It attained an extremely high level (up to 4000 rayleighs) and could be seen with the naked eye when the ionosphere is excited by radio waves from HAARP guided towards the magnetic zenith [120, 121].

It may be hoped that further development of optical techniques and detailed comparison of observational data with the theory will provide a deeper insight into electron acceleration processes in Langmuir turbulence.

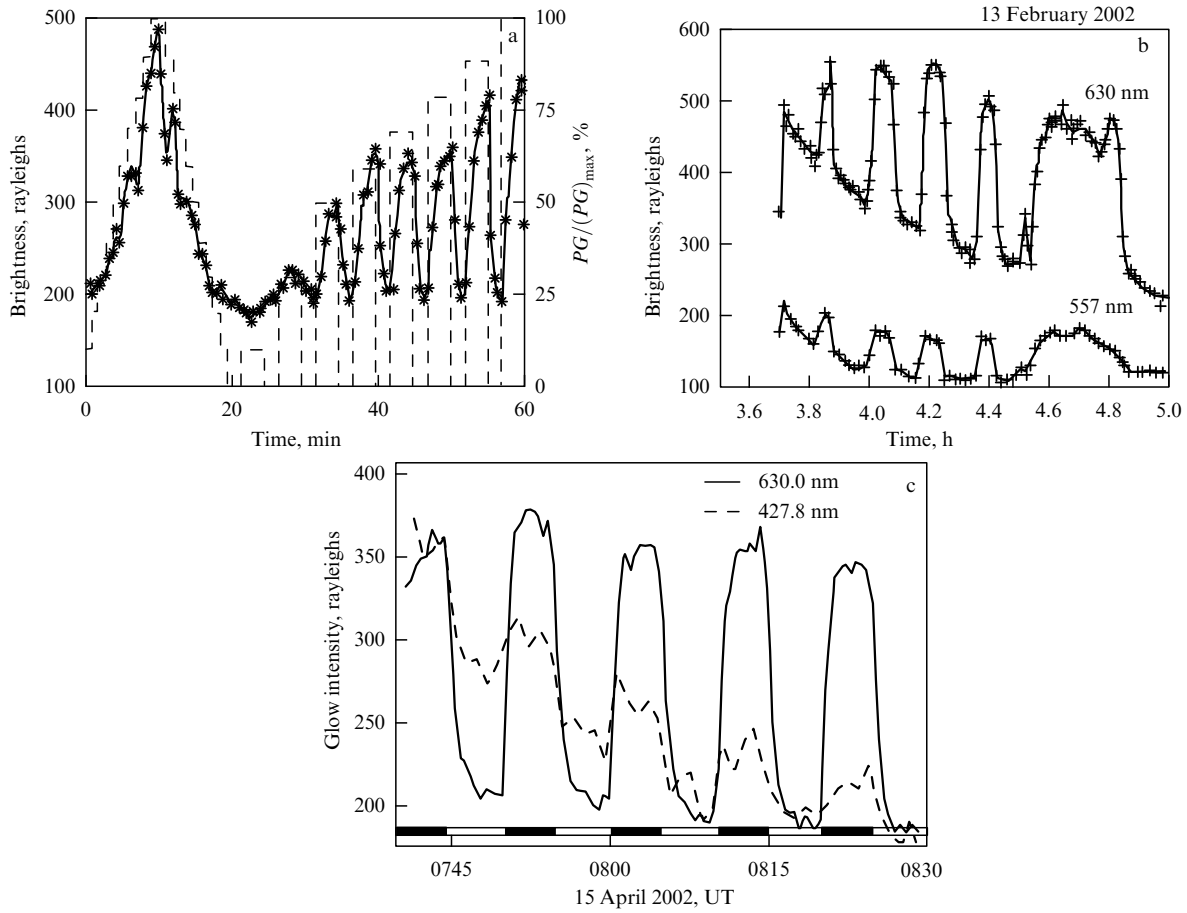

Figure 41. *Optical emission from a perturbed ionospheric region.* Examples of optical luminescence of the disturbed ionosphere observed at HAARP in 2002 by Pedersen et al. [44] and Gerken et al. [118].

(a) Red line ionospheric glow (630 nm). The frequency of the power wave was only 3.3 MHz, maximum effective emission power $(PG)_{max} = 20$ MW. *PG* uniformly increased to a maximum during the first 20 min and fell thereafter. The power dependence of brightness was estimated when the station operated in a periodic regime (switched on for 3 min, and off for 2 min), while its power progressively increased from 10 to 100% of $(PG)_{max}$ (dashed lines). On the ordinate the observed red line glow in rayleighs (1 rayleigh is 1 mln light photons emitted in all directions per cm^2 of the receiver area for 1 s) is plotted. The glow intensifies in proportion to the emission power *PG*. However, its further growth slows down at maximum powers. The observed red line emission under the effect of low-frequency radio waves is consistent with the theory [45, 51] explaining its increase with power *PG* by the effective heating of ionospheric plasma in the UH-resonance region (see Sections 5.3, 8.4).

(b) Red (630 nm) and green (557 nm) line ionospheric glow. The frequency of the power wave was high (7.8 MHz). Green line emission (against the background) was almost 1/3 of the red line glow. Such intense luminosity suggests that it is due to electrons accelerated in the Langmuir turbulence region. This inference is confirmed by a marked delay (~ 20 s) in the appearance of green line glow after the onset of operation of the powerful transmitter. The theory accounts for this delay by the necessity of preliminary heating of the ionospheric plasma by a powerful wave field; the heating permits the powerful pump wave to reach the Langmuir resonance region (see Section 5.3, Fig. 21).

(c) Simultaneous measurement of red (630 nm) and violet (427.8 nm) line emission. The high minimal excitation potential (19 eV) for the violet line explicitly indicates that the effective temperature of accelerated electrons is extremely high, $T_{eff} \sim 10$ eV, in excellent agreement with the predictions of the theory of multiple electron acceleration at Langmuir resonance.

9. Conclusions

The ionosphere is a natural laboratory for physical studies of plasma. Its properties in laboratory facilities depend to a large extent on the plasma generation methods and plasma interaction with the chamber walls. This especially relates to strongly rarified plasma. Its mobility and active interaction with electric and magnetic fields give rise to instability and turbulization. Taken together, these factors account for the extreme difficulty of plasma experiments and the theoretical interpretation of their results. A variety of nonlinear plasma states necessitates an evaluation of its properties in each concrete case; in other words, experiments with any new device require a special theory to be analyzed.[12] It is not without reason that it proved so difficult to create a long-lived plasma isolated from the walls of a thermonuclear reactor and investigate its physical properties.

The aforesaid explains the importance of physical experiments in a free natural plasma, such as the ionosphere. Its properties are highly diverse due to exponentially rapid altitudinal variations in neutral molecule concentration in the atmosphere and the effects of the Earth's magnetic field. This opens up the possibility of studying linear and nonlinear plasma phenomena, the excitation of turbulent states, the generation of various plasma structures, mechanisms of electron acceleration, and a variety of plasma and gyromagnetic resonances. Results of experiments are in good agreement with the theory, which allows the observed phenomena

[12] This does not mean that detailed laboratory experiments are of little value as a source of useful information. See, for instance, recent data in Ref. [122].

to be interpreted not only qualitatively but in many cases quantitatively, too.

Of course, investigations into nonlinear phenomena in the ionospheric plasma are far from complete. Some of them, for example, a detailed study of nonstationary processes of stimulated ionospheric emission (see Section 6) have not yet received an acceptable theoretical interpretation. On the other hand, the predicted supersmall-scale stratification of the ionosphere remains to be observed in direct experiments (Sections 7.4, 7.5). Doubtlessly, optical emission studies will be intensified. Generally speaking, further improvements in the spatial and temporal resolution of diagnostic tools open up new prospects for the in-depth analysis of perturbations in the ionospheric plasma.

At the same time, investigations of nonlinear effects provide important material for the characteristic of ionospheric processes, such as diffusive and heat transfer, field-dependent drifts and winds of neutral molecules, ionospheric plasma fluxes, and chemical composition at varying altitudes and in different latitudinal zones of the ionosphere. Extensive studies of these issues are underway. The method of scattering on artificial periodic irregularities [123] may be mentioned by way of example.

Of special interest is the possibility of using nonlinear impacts on the ionosphere for the study of the magnetosphere and the relationship between magnetospheric and ionospheric processes. It is an extremely broad field of research, including the propagation of Alfvén and whistle waves in the magnetosphere after they are generated by modulation of the electric current in the ionosphere under the action of a powerful radio wave (the Getmantsev nonlinear detection effect). It should be emphasized that this method permits obtaining a very broad frequency spectrum of electromagnetic oscillations (Section 3.2). Another method consists in direct observation of upward nonlinear fluxes of plasma and fast electrons generated by ionospheric modification stations operating at frequencies close to the critical frequency of the F-layer. Of special importance are nonlinear investigations of the ionosphere and magnetosphere in auroral and subarctic areas. Recent measurements at HAARP demonstrated that low-frequency (1 Hz) disturbances induced in the resonance region of the F-layer propagated over large distances (up to 5000 km). Their amplitude was four orders of magnitude greater than that of disturbances generated earlier in the E-layer by the action of powerful radio waves on the current region (Fig. 4). Simultaneously, marked disturbances developed in the upper ionosphere (700 km) that spread horizontally as far as 600 km [124]. Also, it proved possible to affect the Earth's radiation belts by a powerful VLF wave in the whistle range (10–20 kHz) [125]. In this way, the global current system could be explored by resonant action on the ionosphere and magnetosphere for the creation of small transient disturbances. A global network of observation stations and satellites would be necessary to detect such disturbances.

To conclude, the launch of the first Soviet Earth-orbiting satellite in 1957 began the practical exploration of near space, i.e., the ionosphere and magnetosphere. This activity has been increasingly intense during the last few decades. Hundreds of artificial satellites are launched annually, many of them as components of specialized systems, such as GLONASS (Global Navigation Satellite System), NAVSTAR GPS (Navigation Satellite Time and Ranging Global Positioning System), Galileo, NAVSAT (Navy Navigation Satellite), NIMS (Navy Ionospheric Monitoring System), Globalstar, and some others. They constitute the basis of other global systems, including the *Internet, mobile telephone systems, global TV networks and visual communications, global navigation and positioning systems, etc*. In other words, the practical use and exploration of the ionosphere and magnetosphere are now among the major factors that drive the process of *globalization*. Radio communication plays a key role in this process through ultralong-range communication systems between artificial satellites, satellites and Earth, ground-based stations, etc. [126, 127]. Its further development requires continuation and extension of ongoing research on physical phenomena in the ionosphere and magnetosphere, related to the propagation of various radio waves, including powerful ones.

Acknowledgments. This work was supported by a grant from the RF President's Program of Support for Leading Scientific Schools and EOARD grant 067004 (ISTC 3641 p). The author is grateful to M O Ptitsyn for valuable assistance in preparing this review, and K P Zybin for fruitful long-term collaboration.

References

1. Ginzburg V L *Rasprostranenie Elektromagnitnykh Voln v Plazme* (The Propagation of Electromagnetic Waves in Plasmas) 2nd ed. (Moscow: Nauka, 1967) [Translated into English (Oxford: Pergamon Press, 1970)]
2. Al'pert Ya L *Rasprostranenie Radiovoln i Ionosfera* (Radio Wave Propagation and the Ionosphere) (Moscow: Izd. AN SSSR, 1960) [Translated into English (New York: Consultants Bureau, 1963)]
3. Kelley M C *The Earth's Ionosphere: Plasma Physics and Electrodynamics* (San Diego: Academic Press, 1989)
4. Tellegen B D H *Nature* **131** 840 (1933)
5. Bailey V A, Martyn D F *Philos. Mag.* **18** 369 (1934)
6. Vilenskii I M, Zykova N A *Izv. Vyssh. Uchebn. Zaved. Radiofiz.* **2** 543 (1959); **5** 221 (1962)
7. Ratcliffe J A, Shaw I J *Proc. R. Soc. London Ser. A* **193** 311 (1948)
8. Huxley L G H, Foster H G, Newton C C *Proc. Phys. Soc. London* **61** 134 (1948)
9. Hibberd F H *J. Atm. Terr. Phys.* **6** 268 (1955); **8** 120 (1956)
10. Ginzburg V L *Izv. Akad. Nauk SSSR, Ser. Fiz.* **12** 293 (1948)
11. Fejer J A *J. Atm. Terr. Phys.* **7** 322 (1955); **32** 597 (1970)
12. King J W *J. Atm. Terr. Phys.* **10** 166 (1957); **14** 41 (1959)
13. Gurevich A V, Shvartsburg A B *Nelineinaya Teoriya Rasprostraneniya Radiovoln v Ionosfere* (Nonlinear Theory of Radio Wave Propagation in the Ionosphere) (Moscow: Nauka, 1973) §§ 5.5
14. Gurevich A V *Nonlinear Phenomena in the Ionosphere* (New York: Springer, 1978) §§ 2.5.5, 2.5.6
15. Bailey V A *Nature* **139** 68, 838 (1937)
16. Adeishvili T G et al. *Fiz. Plazmy* **4** 1293 (1978) [*Sov. J. Plasma Phys.* **4** 721 (1978)]
17. Gurevich A V *Zh. Eksp. Teor. Fiz.* **30** 1112 (1956) [*Sov. Phys. JETP* **3** 895 (1957)]; *Radiotekh. Elektron.* **1** 706 (1956); *Radiofiz.* **1** (4) 21; (6) 17 (1958)
18. Gurevich A V, Shlyuger I S *Izv. Vyssh. Uchebn. Zaved. Radiofiz.* **18** 1237 (1975)
19. Shlyuger I S *Pis'ma Zh. Eksp. Teor. Fiz.* **19** 274; **20** 722 (1974) [*JETP Lett.* **19** 162; **20** 334 (1974)]
20. Gurevich A V, Milikh G M, Shlyuger I S *Zh. Eksp. Teor. Fiz.* **69** 1640 (1975) [*Sov. Phys. JETP* **42** 835 (1975)]
21. Getmantsev G G et al. *Pis'ma Zh. Eksp. Teor. Fiz.* **20** 229 (1974) [*JETP Lett.* **20** 101 (1974)]
22. Kotik D S, Trakhtengerts V Yu *Pis'ma Zh. Eksp. Teor. Fiz.* **21** 114 (1975) [*JETP Lett.* **21** 51 (1975)]
23. Kapustin I N et al. *Pis'ma Zh. Eksp. Teor. Fiz.* **25** 248 (1977) [*JETP Lett.* **25** 228 (1977)]
24. Barr R, Stubbe P *Radio Sci.* **19** 1111 (1984); Barr R et al. *Nature* **309** 534 (1984); *J. Geophys. Res.* **90** 2861 (1985); **91** 4451 (1986); *Radio*

Sci. **22** 1073 (1987); **23** 379 (1988); Barr R, Stubbe P *Geophys. Res. Lett.* **18** 1035, 1971 (1991); **20** 2243 (1993); Dowden R L et al. *Ann. Geophys.* **8** 765 (1990)
25. Mironenko L F et al. *Izv. Vyssh. Uchebn. Zaved. Radiofiz.* **41** 298 (1998) [*Radiophys. Quantum Electron.* **41** 196 (1998)]
26. Ginzburg V L, Gurevich A V *Usp. Fiz. Nauk* **70** 201, 393 (1960) [*Sov. Phys. Usp.* **3** 115, 175 (1960)]
27. Gurevich A V *Geomagn. Aeron.* **5** 70 (1965); **7** 291 (1967)
28. *J. Geophys. Res.* **73** 6402 (1970) (Collection of papers)
29. *Radio Sci.* **9** (11) 881 (1974) (Collection of papers)
30. Vas'kov V V, Gurevich A V *Zh. Eksp. Teor. Fiz.* **69** 176 (1975) [*Sov. Phys. JETP* **42** 91 (1975)]; **73** 923 (1977); *Geomagn. Aeron.* **24** 350 (1984)
31. Mjølhus E *J. Plasma Phys.* **29** 195 (1983); *J. Atm. Terr. Phys.* **55** 907 (1993); Dysthe K B et al. *Phys. Scr.* **T2B** 548 (1982)
32. Erukhimov L M, in *Teplovye Nelineinye Yavleniya v Plazme* (Executive Ed. V Yu Trakhtengerts) (Gor'ky: Izd. IPF AN SSSR, 1981) p. 3
33. Erukhimov L M et al. *Izv. Vyssh. Uchebn. Zaved. Radiofizika* **30** 208 (1987) [*Radiophys. Quantum Electron.* **30** 156 (1987)]
34. Nasyrov A M *Rasseyanie Radiovoln Anizotropnymi Ionosfernymi Neodnorodnostyami* (Scattering of Radio Waves by Anisotropic Ionospheric Inhomogeneities) (Kazan': Izd. Kazansk. Univ., 1991)
35. Noble S T, Djuth F T *J. Geophys. Res.* **95** 15195 (1990)
36. Bernhardt P A, Duncan L M, Tepley C A *Science* **242** 1022 (1988)
37. Kelley M C et al. *J. Geophys. Res.* **100** 17367 (1995)
38. Gurevich A V, Zybin K P, Lukyanov A V *Phys. Rev. Lett.* **75** 2622 (1995); Gurevich A V, Lukyanov A V, Zybin K P *Phys. Lett. A* **206** 247 (1995)
39. Gurevich A et al. *Phys. Lett. A* **239** 385 (1998)
40. Franz T L, Kelley M C, Gurevich A V *Radio Sci.* **34** 465 (1999)
41. Kosch M J et al. *Geophys. Res. Lett.* **27** 2817 (2000)
42. Pedersen T R, Carlson H C *Radio Sci.* **36** 1013 (2001)
43. Gurevich A V, Carlson H, Zybin K P *Phys. Lett. A* **288** 231 (2001)
44. Pedersen T R et al. *Geophys. Res. Lett.* **30** 1169 (2003)
45. Gurevich A V et al. *Phys. Lett. A* **305** 264 (2002)
46. Gustavsson B et al. *J. Geophys. Res.* **106** (A12) 29105 (2001)
47. Leyser T B et al. *Adv. Polar Atm. Res.* **14** 1 (2000)
48. Rietveld M T et al. *J. Geophys. Res.* **108** (A4) 1141 (2003)
49. Gurevich A et al. *Phys. Lett. A* **301** 307 (2002)
50. Tereshchenko E D et al. *Phys. Lett. A* **325** 381 (2004)
51. Gurevich A V, Zybin K P, Carlson H C *Izv. Vyssh. Uchebn. Zaved. Radiofiz.* **48** 772 (2005) [*Radiophys. Quantum Electron.* **48** 686 (2005)]
52. Stubbe P *J. Atm. Terr. Phys.* **58** 349 (1996)
53. Jones T B et al. *J. Atm. Terr. Phys.* **46** 147 (1984)
54. Robinson T R *Phys. Rep.* **179** 79 (1989)
55. Jones T B et al. *Radio Sci.* **18** 835 (1993)
56. Getmantsev G G et al. *Pis'ma Zh. Eksp. Teor. Fiz.* **18** 621 (1973) [*JETP Lett.* **18** 364 (1973)]
57. Cheung P Y et al. *Phys. Plasmas* **8** 802 (2001)
58. Stenflo L S *Eos. Trans. AGU* **60** 595 (1979); Stenflo L, Trulsen J *J. Geophys. Res.* **83** (A3) 1154 (1978); Stenflo L, Yakimenko I P *Phys. Scr.* **18** 151 (1978); Dysthe K B et al. *J. Geophys. Res.* **82** 717 (1977)
59. Thidé B, Kopka H, Stubbe P *Phys. Rev. Lett.* **49** 1561 (1982)
60. Stubbbe P et al. *J. Geophys. Res.* **89** 7523 (1984)
61. Leyser T B *Geophys. Res. Lett.* **18** 408 (1991)
62. Stubbe P et al. *J. Geophys. Res.* **99** (A4) 6233 (1994)
63. Leyser T B et al. *J. Geophys. Res.* **99** (A10) 19555 (1994)
64. Sergeev E N et al. *Izv. Vyssh. Uchebn. Zaved. Radiofiz.* **42** 619 (1999) [*Radiophys. Quantum Electron.* **42** 544 (1999)]
65. Zhou H L, Huang J, Kuo S P *Phys. Plasmas* **1** 3044 (1994)
66. Shvarts M M, Grach S M *J. Atm. Solar-Terr. Phys.* **59** 2421 (1997)
67. Mjølhus E *J. Geophys. Res.* **103** (A7) 14711 (1998)
68. Gurevich A V et al. *Phys. Lett. A* **231** 97 (1997)
69. Bernhardt P A et al. *Phys. Rev. Lett.* **72** 2879 (1994)
70. Frolov V L et al. *Izv. Vyssh. Uchebn. Zaved. Radiofiz.* **40** 1091 (1997) [*Radiophys. Quantum Electron.* **40** 731 (1997)]
71. Frolov V L et al. *Geophys. Res. Lett.* **24** 1647 (1997)
72. Frolov V L et al. *Phys. Rev. Lett.* **81** 1630 (1998)
73. Frolov V L, Kagan L M, Sergeev E N *Izv. Vyssh. Uchebn. Zaved. Radiofiz.* **42** 635 (1999) [*Radiophys. Quantum Electron.* **42** 557 (1999)]
74. Sergeev E N et al. *Izv. Vyssh. Uchebn. Zaved. Radiofiz.* **45** 214 (2002) [*Radiophys. Quantum Electron.* **45** 193 (2002)]
75. Akhiezer A I et al. *Elektrodinamika Plazmy* (Plazma Electrodynamics) (Ed. A I Akhiezer) (Moscow: Nauka, 1974)
76. Gurevich A V, Lukyanov A V, Zybin K P *Phys. Lett. A* **211** 363 (1996)
77. Thidé B et al. *Radio Sci.* **18** 851 (1983)
78. Bud'ko N I, Vas'kov V V *Geomagn. Aeron.* **32** 80 (1992) [*Geomagn. Aeron.* **32** 63 (1992)]
79. Grach S M, Thidé B, Leyser T *Izv. Vyssh. Uchebn. Zaved. Radiofiz.* **37** 617 (1994) [*Radiophys. Quantum Electron.* **37** 392 (1994)]
80. Istomin Ya N, Leyser T B *Phys. Plasmas* **2** 2084 (1995)
81. Huang J, Kuo S P *J. Geophys. Res.* **99** (A10) 19569 (1994)
82. Huang J, Kuo S P, Zhou H L *J. Geophys. Res.* **100** (A2) 1639 (1995)
83. Gurevich A V, Zybin K P *Phys. Lett. A* **358** 159 (2006)
84. Ponomarenko P V, Leyser T B, Thidé B *J. Geophys. Res.* **104** (A5) 10081 (1999)
85. Kagan L M et al. *Radio Sci.* (in press)
86. Djuth F T et al. *Phys. Rev. Lett.* **94** 125001 (2005)
87. Kuo S P, Rubinrant M, in *Proc. RF Ionospheric Interactions Workshop, Santa Fe, NM, April 25 – 28, 2006*
88. Dimant Ya S, Gurevich A V, Zybin K P *J. Atm. Terr. Phys.* **54** 425 (1992)
89. Silin V P *Zh. Eksp. Teor. Fiz.* **48** 1679 (1965) [*Sov. Phys. JETP* **21** 1127 (1965)]
90. Silin V P *Parametricheskoe Vozdeistvie Izlucheniya Bol'shoi Moshchnosti na Plazmu* (Parametric Effect of Powerful Radiation on the Plasma) (Moscow: Nauka, 1973)
91. DuBois D F, Goldman M V *Phys. Rev. Lett.* **14** 544 (1965)
92. Stubbe P, Kohl H, Rietveld M *J. Geophys. Res. A* **97** (A5) 6285 (1992)
93. DuBois D F et al. *J. Geophys. Res.* **98** (A10) 17543 (1993)
94. Nordling J A et al. *Radio Sci.* **23** 809 (1988)
95. Cheung P Y et al. *Phys. Rev. Lett.* **79** 1273 (1997)
96. Sergeev E N et al. *Izv. Vyssh. Uchebn. Zaved. Radiofiz.* **41** 313 (1998) [*Radiophys. Quantum Electron.* **41** 206 (1998)]
97. Vedenov A A, Rudakov L I *Dokl. Akad. Nauk SSSR* **159** 767 (1964) [*Sov. Phys. Dokl.* **9** 1073 (1965)]
98. Litvak A G, Fraiman G M, in *Vzaimodeistvie Sil'nykh Elektromagnitnykh Voln s Besstolknovitel'noi Plazmoi* (Interaction of Powerful Electromagnetic Waves with Collisionless Plasma) (Executive Ed. A G Litvak) (Gor'ky: Izd. IPF AN SSSR, 1980) p. 50
99. Zakharov V E *Zh. Eksp. Teor. Fiz.* **62** 1745 (1972) [*Sov. Phys. JETP* **35** 908 (1972)]
100. DuBois D F, Rose H A, Russell D *Phys. Rev. Lett.* **61** 2209 (1988); *J. Geophys. Res.* **25** (A12) 21221 (1990); *Phys. Rev. Lett.* **66** 1970 (1991)
101. Morales G J, Lee Y C *Phys. Rev. Lett.* **33** 1534 (1974)
102. Kovrizhnykh L M, Sakharov A S, in *Vzaimodeistvie Sil'nykh Elektromagnitnykh Voln s Besstolknovitel'noi Plazmoi* (Interaction of Powerful Electromagnetic Waves with Collisionless Plasma) (Executive Ed. A G Litvak) (Gor'ky: Izd. IPF AN SSSR, 1980) p. 117
103. DuBois D F, Russell D, Rose H A *Phys. Plasmas* **2** 76 (1995)
104. Wang J G, Newman D L, Goldman M V *J. Atm. Solar-Terr. Phys.* **59** 2461 (1997)
105. Mjølhus E, Helmersen E, DuBois D F *J. Geophys. Res.* **106** (A9) 18525 (2001)
106. Gurevich A V et al. *Fiz. Plazmy* **30** 1071 (2004) [*Plasma Phys. Rep.* **30** 995 (2004)]
107. Vas'kov V V, Gurevich A V, Dimant Ya S *Zh. Eksp. Teor. Fiz.* **84** 536 (1983) [*Sov. Phys. JETP* **57** 310 (1983)]
108. Gurevich A V et al. *J. Atm. Terr. Phys.* **47** 1057 (1985)
109. Gurevich A V et al. *Geophys. Res. Lett.* **27** 2461 (2000)
110. Carlson H C, Wickwar V B, Mantas G P *J. Atm. Terr. Phys.* **44** 1089 (1982)
111. Gordon W E, Carlson H C *Radio Sci.* **9** 1041 (1974)
112. Sipler D P, Enemark E, Biondi M A *J. Geophys. Res.* **79** 4276 (1974)
113. Haslett J C, Megill L R *Radio Sci.* **9** 1005 (1974)
114. Bernhardt P A, Tepley C A, Duncan L M *J. Geophys. Res.* **94** 9071 (1989); Bernhardt P A, Duncan L M, Tepley C A *Science* **242** 1022 (1988)
115. Bernhardt P A et al. *Geophys. Res. Lett.* **18** 1477 (1991)

116. Mantas G P, Carlson H C *J. Geophys. Res.* **101** (A1) 195 (1996)
117. Gurevich A V, Milikh G M *J. Geophys. Res.* **102** (A1) 389 (1997)
118. Gerken E et al., in *Proc. RF Ionospheric Interaction Workshop, Santa Fe, NM, April, 2005*
119. Kagan L M et al. *Phys. Rev. Lett.* **85** 218 (2000)
120. Pedersen T D, Gerken E A *Nature* **433** 498 (2005)
121. Kagan L M et al. *Phys. Rev. Lett.* (2008) (in press)
122. Starodubtsev M V, Nazarov V V, Kostrov A V *Phys. Rev. Lett.* **98** 195001 (2007)
123. Belikovich V V et al. *Ionospheric Research by Means of Artificial Periodic Irregularities* (Berlin: Copernicus GmbH, 2002)
124. Papadopoulos D et al., *Doklad na Mezhdunarodnom Nauchnom Forume*: *"Kosmos i Nauka XXI Veka, Oktyabr' 2007, Moskva*" (Report to International Scientific Forum 'Cosmos and Science in 21st Century' October 2007, Moscow)
125. Polyakov S V et al., in *Proc. of VIIth ISS Suzdal Symp. on Ionosphere Modification, Moscow, 16–18 October 2007* (Troitsk: IZMIRAN, 2007) p. 54
126. Gurevich A V, Tsedilina E E *Sverkhdal'nee Rasprostranenie Korotkikh Radiovoln* (Long Distance Propagation of HF Radio Waves) (Moscow: Nauka, 1979) [Translated into English (Berlin: Springer-Verlag, 1985)]
127. Roddy D *Satellite Communications* (McGraw-Hill Telecommunications, 2001)